DETERMINATION OF THERMAL DECOMPOSITION KINETICS FOR Fe/KCIO$_4$ BINARY MIXTURES   UTILIZING ANALYTICAL AND NUMERICAL METHODS

Fe/KCIO$_4$ İKİLİ KARIŞIMLARININ ISIL BOZUNMA KİNETİĞİNİN ANALİTİK VE NÜMERİK YÖNTEMLERLE TAYİN EDİLMESİ

ANIL ALKAN

PROF. DR. SELMA MUTLU

Supervisor

Submitted to Graduate School of Science and Engineering of Hacettepe University

as a Partial Fulfillment to the Requirements

for the Award of the Degree of Master of Science

in Chemical Engineering

2018

This work named **"Determination of Thermal Decomposition Kinetics for Fe/KClO$_4$ Binary Mixtures Utilizing Analytical and Numerical Methods"** by **ANIL ALKAN** has been approved as a thesis for the Degree of **MASTER OF SCIENCE IN CHEMICAL ENGINEERING** by the below mentioned Examining Committee Members.
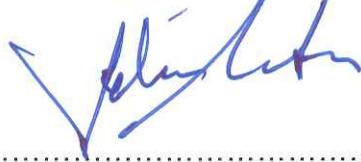
Prof. Dr. Nuray YILDIZ

Head

....

Prof. Dr. Selma MUTLU

Supervisor

....

Prof. Dr. Tülay DURUSOY

Member

....

Assoc. Prof. Dr. Görkem KÜLAH

Member

....

Assoc. Prof. Dr. Selis ÖNEL

Member

....

This thesis has been approved as a thesis for the Degree of **MASTER OF SCIENCE IN CHEMICAL ENGINEERING** by Board of Directors of the Institute for Graduate School of Science and Engineering.

Prof. Dr. Menemşe GÜMÜŞDERELİOĞLU

Director of the Institute of

Graduate School of Science and Engineering

YAYINLAMA VE FİKRİ MÜLKİYET HAKLARI BEYANI

Enstitü tarafından onaylanan lisansüstü tezimin/raporumun tamamını veya herhangi bir kısmını, basılı (kağıt) ve elektronik formatta arşivleme ve aşağıda verilen koşullarla kullanıma açma iznini Hacettepe üniversitesine verdiğimi bildiririm. Bu izinle Üniversiteye verilen kullanım hakları dışındaki tüm fikri mülkiyet haklarım bende kalacak, tezimin tamamının ya da bir bölümünün gelecekteki çalışmalarda (makale, kitap, lisans ve patent vb.) kullanım hakları bana ait olacaktır.

Tezin kendi orijinal çalışmam olduğunu, başkalarının haklarını ihlal etmediğimi ve tezimin tek yetkili sahibi olduğumu beyan ve taahhüt ederim. Tezimde yer alan telif hakkı bulunan ve sahiplerinden yazılı izin alınarak kullanması zorunlu metinlerin yazılı izin alarak kullandığımı ve istenildiğinde suretlerini Üniversiteye teslim etmeyi taahhüt ederim.

☐ **Tezimin/Raporumun tamamı dünya çapında erişime açılabilir ve bir kısmı veya tamamının fotokopisi alınabilir.**
(Bu seçenekle teziniz arama motorlarında indekslenebilecek, daha sonra tezinizin erişim statüsünün değiştirilmesini talep etseniz ve kütüphane bu talebinizi yerine getirse bile, tezinin arama motorlarının önbelleklerinde kalmaya devam edebilecektir.)

☒ **Tezimin/Raporumun 13.06.2023 tarihine kadar erişime açılmasını ve fotokopi alınmasını (İç Kapak, Özet, İçindekiler ve Kaynakça hariç) istemiyorum.**
(Bu sürenin sonunda uzatma için başvuruda bulunmadığım taktirde, tezimin/raporumun tamamı her yerden erişime açılabilir, kaynak gösterilmek şartıyla bir kısmı ve ya tamamının fotokopisi alınabilir)

☐ **Tezimin/Raporumun .... tarihine kadar erişime açılmasını istemiyorum, ancak kaynak gösterilmek şartıyla bir kısmı veya tamamının fotokopisinin alınmasını onaylıyorum.**

☐ **Serbest Seçenek/Yazarın Seçimi**

13/06/2018

Ahıl ALKAN

ETHICS

In this thesis study, prepared in accordance with the spelling rules of Institute of Graduate Studies in Science of Hacettepe University,

I declare that

- all the information and documents have been obtained in the base of academic rules
- all audio-visual and written information and results have been presented according to the rules of scientific ethics
- in case of using other Works, related studies have been cited in accordance with the scientific standards
- all cited studies have been fully referenced
- I did not do any distortion in the data set
- and any part of this thesis has not been presented as another thesis study at this or other university.

1/6/2018

Anıl ALKAN

ÖZET

Fe/KClO$_4$ İKİLİ KARIŞIMLARININ ISIL BOZUNMA KİNETİĞİNİN ANALİTİK VE NÜMERİK YÖNTEMLERLE TAYİN EDİLMESİ

Anıl ALKAN

Yüksek Lisans, Kimya Mühendisliği Bölümü

Tez Danışmanı: Prof. Dr. Selma MUTLU

Haziran 2018, 132 sayfa

Önerilen tez, birincil pil teknolojilerinden ısıl pilde kullanılan ısı tabletinin kinetik dinamiklerinin araştırılması ve modelleme ile doğrulanmasını amaçlamaktadır. Tez kapsamında, farklı kütlesel karışımlarında Fe/KClO$_4$ için sıcaklık taramalı termal analiz yöntemiyle ısı (Q) – sıcaklık (T) verileri elde edilmiştir. Isı (Q) – sıcaklık (T) verileri, MATLAB™ (R2014A)'da yazılan veri işleme yazılımı kullanılarak dönüşüm (reaksiyonun ilerleme oranı, α) – sıcaklık (T) verisine çevrilmiştir. Her ısı tabletinin ısıl bozunma reaksiyonunun görünür aktivasyon enerjisi (E$_a$) Starink'in izodönüşüm yöntemiyle belirlenmiştir ve bu aktivasyon enerjisi kullanılarak Malek kinetik prosedürüyle reaksiyon modeli (f(α)) belirlenmiştir. Analitik yöntemlerle elde edilen reaksiyon parametreleri (görünür aktivasyon enerjisi, E$_a$, reaksiyon modeli, f(α), frekans faktörü, A), COMSOL Multiphysics yazılımında oluşturulan deneysel veri ile model verisi arasındaki farkı iteratif yöntem ile minimuma indirgeyen paket programında sınır koşulu olarak kullanılmış ve optimum reaksiyon parametreleri elde edilmiştir. Son olarak; nümerik yöntemle elde edilen optimum kinetik parametreler COMSOL Multiphysics'de tanımlanan ısı tableti yanma modelinde

çalıştırılarak yanma hızı sonuçları hesaplanmıştır. Bu sonuçlar literatürdeki yanma hızı sonuçları ile karşılaştırılmış ve böylece kinetik parametrelerin doğrulaması gerçekleştirilmiştir.

Tez çalışmasının ilk aşamasında farklı kütlesel karışımlarda (a/a) (82/18, 84/16, 86/14 ve 88/12) hazırlanan ısı tabletlerinin görünür aktivasyon enerjisi değerleri Starink izodönüşüm yöntemi kullanılarak sırasıyla 208, 210, 218 ve 222 kJ/mol bulunmuştur. Yüzde $KClO_4$ oranı arttıkça aktivasyon enerjisi azalmaktadır. Bu durum, tablet içerisindeki $KClO_4$ miktarı arttıkça, Fe molekülü ile reaksiyon gerçekleşme ihtimalinin artmasına bağlanmıştır. Ayrıca, Starink yöntemiyle elde edilen dönüşüme karşı aktivasyon enerjisi değerleri, dönüşüm değeri 0.4 olana dek $KClO_4$ bozunması ve Fe oksitlenme reaksiyonlarının aynı anda gerçekleştiğini göstermiştir.

Farklı ısı tabletleri için ortalama aktivasyon enerjisi değerleri ve Malék prosedürü kullanılarak, ısı tabletinin ısıl bozunma reaksiyonunun Šesták-Berggren reaksiyon modeline uyduğu belirlenmiştir. Malék prosedürü kapsamında ısı tableti bozunma reaksiyonu için oluşturulan y(α) ve z(α) eğrileri bozunma reaksiyonunun çekirdeklenme (İng. Nucleation) sürecine göre gerçekleştiğini göstermiştir.

Elde edilen kinetik parametreler kullanılarak farklı ısı tabletleri için zamana (t) karşı dönüşüm (α) eğrileri hesaplanmış ve deneysel verilerle karşılaştırılmıştır. Karşılaştırma, hesaplanan zamana karşı dönüşüm ve deneysel zamana karşı dönüşüm eğrilerinin yeterince örtüşmediğini göstermiştir. Bu sebeple, kinetik parametrelerin optimizasyonu için COMSOL Multiphysics yazılımında iterativ prosedürü kullanan deneysel ve model arasındaki farkı minimize etmeye dayalı program yazılmıştır. Programın çıktısı olan optimize kinetik parametreler kullanılarak hesaplanan zaman (t) – dönüşüm (α) ve deneysel zaman (t) – dönüşüm (α) eğrilerinin örtüşme oranı korelasyon faktörü cinsinden (r) 0.98 – 0.99 aralığında bulunmuştur.

Optimize edilmiş kinetik parametreler ısı tabletinin yanma modelinde kullanılmıştır. 82/18, 84/16, 86/14 ve 88/12 kütle karışım oranlarındaki ısı tabletleri için yanma

hızı sırasıyla 26.0, 15.7, 11.5 ve 10.7 cm/s olarak hesaplanmıştır. Yüzde $KClO_4$ oranı arttıkça yanma hızının eksponensiyel olarak arttığı görülmüştür. Bu durum, ısı tabletlere ait kinetik parametrelerle de örtüşmektedir. Buna ek olarak, hesaplanan yanma hızının literatürdeki değerlere çok yakın olduğu görülmüştür. Bu örtüşme elde edilen kinetik parametrelerin doğruluğunu teyit etmektedir.

Isıl pilin aktifleşme ve çalışma süreçlerinin doğru modellenemebilmesi için doğruluğu teyit edilmiş ısı tableti bozunma kinetik parametrelerinin elde edilmesi gerekmektedir. Sonuç olarak; ısıl pilin modellemeye dayalı tasarım süreçleri için kritik öneme sahip olan ısı tabletinin bozunma reaksiyonuna ait kinetik parametreler elde edilmiştir.

Anahtar Kelimeler: Isıl pil, ısı tableti, reaksiyon kinetiği, aktivasyon enerjisi, termal analiz, reaksiyon modeli, optimizasyon, piroteknik, modelleme.

ABSTRACT

DETERMINATION OF THERMAL DECOMPOSITION KINETICS FOR Fe/KClO$_4$ BINARY MIXTURES   UTILIZING ANALYTICAL AND NUMERICAL METHODS

Anıl ALKAN

Master of Science, Department of Chemical Engineering

Supervisor: Prof. Dr. Selma MUTLU

June 2018, 132 pages

The proposed thesis aims to investigate the kinetic dynamics of heat pellets used in thermal batteries which is a type of a primary battery. For this purpose, heat (Q) – temperature (T) curves for Fe/KClO$_4$ mixtures with different weight compositions were obtained using non-isothermal thermal analysis. Heat (Q) – temperature (T) curves were then converted to conversion (α) – temperature (T) curves utilizing a data processing script that was developed with MATLAB™ (R2014A). For thermal decomposition of each heat pellet with different weight composition, the apparent activation enery (E$_a$) was determined using Starink's isoconversional method. Malek's kinetic procedure was followed to determine the reaction model, (f(α)) with the obtained activation energy. The kinetic parameters that were analytically was used as the initial values for the program that was developed with the COMSOL Multiphysics that aims to minimize the difference between experimental and calculated values in a iterative fashion. Lastly, the optimized kinetic parameters that were calculated using numerical methods were used in the heat pellet burning

simulation which was defined with COMSOL Multiphysics to calculate the burn rate of heat pellets. These burn rate values were compared with the literature values to validate the obtained kinetic parameters.

In the first part of the study, for heat pellets with different weight compositions (w/w) (82/18, 84/16, 86/14, 88/12) apparent activation energies were determined as 208, 210, 218, 222 respectively using the Starink isoconversional method. The activation energy decreases with the increasing % content of $KClO_4$. The reason for this increasing trend is the increased probability of oxidation reaction with increasing % content of $KClO_4$. Additionally, activation energy values with respect to conversion revealed that multi-step decomposition ($KClO_4$ decomposition and Fe oxidation) takes place until the overall conversion reaches 0.4.

The reaction model for the thermal decomposition of heat pellets was found to follow Šesták-Berggren's reaction model that was found by using the apparent activation energies obtained for different heat pellets together with the Malék's kinetic procedure. The master plots, $y(\alpha)$ and $z(\alpha)$ revealed that the thermal decomposition of heat pellets takes place according to the nucleation model.

The obtained kinetic parameters were used to calculate the conversion (α) vs. time (t) to compare with the experimental values. Comparison showed that there was no overlapping between calculated and experimental values. Therefore, for the optimization of kinetic parameters the iterative approach that was designed with COMSOL Multiphysics to minimize the difference between model and experimental values was employed. The optimized kinetic parameters obtained from optimization tool was used to calculate the time (t) – conversion (α) curve which was compared with the experimental time (t) – conversion (α) curve. Correlation factor (r) between these curves were calculated as 0.98 – 0.99.

The optimized kinetic parameters were used in the simulation of burning process of heat pellets. For the heat pellets with weight compositions of 82/18, 84/16, 86/14 and 88/12 the burn rates were calculated as 26.0, 15.7, 11.5 and 10.7 cm/s, respectively. With increasing % content of $KClO_4$, the burn rate increases

exponentially. This behavior is supported with the obtained kinetic parameters for heat pellets. Additionally, the calculated burn rate values were found to be close to the literature values. This correlation verifies that the obtained kinetic parameters are accurate.

In order to accurately model the activation and operation processes of thermal batteries, accurate kinetic parameters of the thermal decomposition of heat pellets should be determined. Consequently, the kinetic dataset of the thermal decomposition of heat pellets which is crucial for the design processes relying on modelling are obtained within the scope of this study.

Keywords: Thermal battery, heat pellet, reaction kinetics, activation energy, thermal analysis, reaction model, optimization, pyrotechnic, modelling.

ACKNOWLEDGEMENTS

TABLE OF CONTENTS

LIST OF FIGURES

LIST OF TABLES

LIST OF ABBREVIATIONS AND ACRONYMS

(w:w)	Percent by mass or mass fraction
A	Pre-exponential factor of frequency factor (s^{-1})
Al_2O_3	Alumina, aluminium oxide
BPP	Boron/Potassium perchlorate pyrotechnic mixture
C	Concentration (mol/m^3)
C_0	Initial concentration of reactant (mol/m^3)
C_p	Heat capacity (J/g.K)
D	Diffusion coefficient (m^2/s)
d_{pellet}	Apparent density of heat pellet (g/cm^3)
DSC	Differential Scanning Calorimetry
DTA	Differential Thermal Analysis
$d_{theo.}$	Theoretical density of heat pellet (g/cm^3)
dα/dt	Conversion rate, as a function of time (s^{-1})
dα/dT	Conversion rate, as a function of temperature (s^{-1})
E_a	Apparent activation energy (kJ/mol)
E_{avg}	Mean value of apparent activation energy (kJ/mol)
$f(T)_α$	Mathematical function to express that the conversion is specified
f(α)	Differential reaction model dependent on the reaction mechanism
Fe	Iron
FEM	Finite Element Method
FeS_2	Iron disulfide, pyrite
F_{fb}	Fraction of heat that is lost to the surruonding during propagation
FPP	Iron/Potassium perchlorate pyrotechnic mixture
FWO	Flynn-Wall-Ozawa isoconversional method
g(α)	Integral reaction model that was used in isoconversional methods
k(T)	Reaction rate constant as a function of temperature
KAS	Kissinger-Akahira-Sunose isoconversional method

KClO$_4$	Potassium perchlorate
Li(Si)	Lithium silicon
m	Śesták-Berggren reaction model parameter
m$_0$	Initial sample mass (g)
m$_f$	Final sample mass (g)
m$_T$	Remaining sample mass at temperature, T (g)
n	Śesták-Berggren reaction model parameter
p(x)	Temperature integral function that is used in isoconversional method
PDE	Partial Differential Equation
PP	Potassium perchlorate
Q$_{released}$	Amount of heat release from decomposition of heat pellet per mass (W/mg)
R	Universal gas constant (8.314x10^3 kJ/mol)
r	Correlation factor
RH	Relative Humidity
RSS	Objective function in the non-linear regression
SDT	Simultaneous Differential Technique
SEM	Scanning Electron Microscope
SNOPT	Sparse Nonlinear Optimizer
T	Absolute temperature (K)
t	Time (s)
t$_f$	The time when last surface of heat pellet decomposes (s)
TGA	Thermogravimetric Analyzer
t$_i$	The time when the first surface of heat pellet starts to decompose (s)
V	Voltage (V)
x	Cartesian coordinate axis, x
x=E/RT	Reduced form of activation energy
XRD	X-Ray Diffraction
y	Cartesian coordinate axis, y
y(α)	Master plot function used in malek's procedure
y$_{calc.}$	Calculated conversion dataset for non-linear regression

y_{exp}	Experimental conversion dataset for non-linear regression
z	Cartesian coordinate axis, x
z(α)	Master plot function used in malek's procedure
ZPP	Zirconium/Potassium perchlorate pyrotechnic mixture
α	Degree of conversion
β	Heating rate, dT/dt (°C/min)
ΔH$_r$	Heat of reaction (kJ/g)
ΔT	Temperature difference (K)
λ	Thermal conductivity (W/m.K)

1. INTRODUCTION

Thermal batteries are mostly used for military application which require high power outputs such as in guidance kits, fuses, cruise missiles, emergency ejection seats, space vehicles and in the nuclear warheads [1-4]. Thermal batteries are designed according to the requirements of the system that it will be used in. Operation time of a thermal battery varies from few seconds to one hour which makes it a versatile electrical source for military applications. Main advantages of thermal batteries over conventional batteries are its endurance to the harsh environment conditions and its low or none self-discharge under storage conditions. This low/none self-discharge feature gives thermal battery the ability to withstand high/low temperatures under storage conditions over 15 years without losing its electrical capacity [1]. Solid-state electrolyte pellet is the main reason for the low/none self-discharge characteristic. Thermal battery is activated by melting the solid electrolyte with the carefully amount of thermal energy.

In a conventional thermal battery, pellets of iron powder (Fe) and potassium perchlorate ($KClO_4$) binary mixtures are used as a heat source which supplies thermal energy necessary for melting the eutectic salt. Melted eutectic salt permits ionic migration between anode and cathode. Consequently, thermal battery starts to provide desired voltage output within a certain amount of time. Activation time is a critical design parameter to be adjusted for the system that the battery is implemented in can perform its mission successfully [2, 3]. Understanding of heat generation mechanism and the rate which this heat is generated is critical for the activation phase of the battery. For this purpose, thermal decomposition mechanism and kinetic parameters needs to be evaluated.

The main objective of this Master's Thesis is to develop a kinetic dataset for thermal decomposition of Fe/$KClO_4$ heat pellets that are used as the heat source for thermal batteries. In addition, this thesis also evaluates the effect of weight compositions to the decomposition kinetics of heat pellets.

For this purpose, a self-validating analytical and numerical path of kinetic analysis method was engineered compiling the methods that are used commonly in literature.

Although the kinetic analysis of stoichiometric mixture of Fe/$KClO_4$ powder was studied previously [4], the novelty is introduced by the study of kinetic analysis in pellet form and validation of the kinetic parameters by simulation studies.

Heat pellets with varying weight compositions were prepared and thermal analysis was conducted. Kinetic parameters for heat pellets were extracted from thermal analysis data utilizing analytical methods (isoconversional method and malek's procedure). Analytically obtained kinetic parameters showed that with decreasing $KClO_4$ content, reactivity of heat pellet was decreased. Furthermore, decomposition mechanism of heat pellets were determined. It was showed that thermal decomposition of heat pellets obeys nucleation model. Fine-tuning of the analytically obtained kinetic parameters were performed with COMSOL Multiphysics's optimization tool. Model data obtained using optimized kinetic parameters gave good fitting with the experimental data. Correlation factors, (r) were in the range of 0.98 – 0.99. Accountability of the obtained kinetic parameters were proven by modelling the burning process with obtained kinetic parameters. With increasing $KClO_4$ content, burn rate showed an increasing trend which was in the range of 10.7 – 26.0 cm/s.

2. LITERATURE SURVEY

It is presented an overview of the reaction kinetic models and the models that have been considered to be used for kinetic analysis and simulation of heat pellet decomposition. The aim is to study the kinetics of the methods reported in the area of pyrotechnic decomposition and to evaluate the suitability and reliability of these methods.

Firstly, an introduction summarizing the thermal battery technologies and basis of reaction kinetics is presented. Then, a survey on the thermal analysis methods was done to establish the basis for experimental methods that will be used. Lastly, the tools and methods that were used to interpret the thermal analysis data were examined.

2.1. Thermal Batteries

Thermal batteries are hermetically sealed primary reserve batteries which has exceptionally high shelf life (> 15 years), mechanical stability in harsh environmental conditions (rotational force resistance, impact resistance etc.), and wide current discharge rating (50 – 1000 mA/cm^2). For its inherent advantages and high reliability, thermal batteries are mostly used in military applications such as; missile guidance kits, fuses, cruise missiles, canopy jettison systems in fighter jets etc. Apart from military applications, thermal batteries are also used in geothermal borehole applications [5, 6].

A thermal battery unit cell typically consists of anode, cathode, electrolyte and heat pellets which are in solid-state at room temperature. Thermal battery is made of stack of cells which may be connected in series or parallel. A schematic view of unit cells in a battery stack are shown in Figure 1.
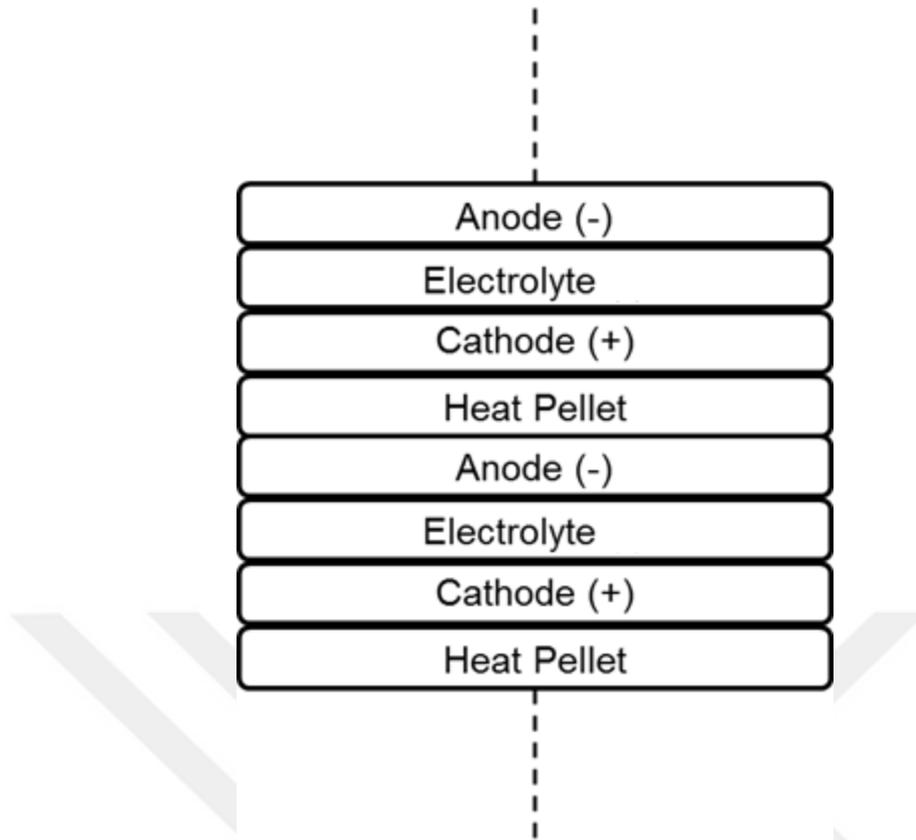
Figure 1. Schematic view of thermal battery cells in series

Thermal batteries are designed according to the requirements of the system that it is implemented in. Characteristics of a thermal battery (electrical performance, activation time, operation time etc.) are mainly defined by the species that are used in cells. Unit cell configurations (species) that are used in thermal battery and their advantages/disadvantages are given in Table 1.

Table 1. Types of unit cells used in thermal batteries

Electrochemical system: Anode/electrolyte/cathode	Operating cell voltage(V)	Characteristics and/or applications
Ca/LiCl-KCl/WO$_3$	2.4 – 2.6	Used for fuse applications where low noise levels are needed and dynamic conditions are not severe.
Ca/LiCl-KCl/CaCrO$_4$	2.2 – 2.6	Used for short-term applications (10-100 s) in severe applications.
Mg/LiCl-KCl/V$_2$O$_5$	2.2 – 2.7	Used for short-term applications (10-100 s) in

		severe applications.
LiSi/LiCl-LiBr-LiF/FeS$_2$	1.6 – 2.1	Used for short-medium applications (1 – 10 mins) with high current densities in severe conditions.
Li(Si or Al)/LiCl-KCl/FeS$_2$	1.6 – 2.1	Used for medium-long applications (10 mins – 30 mins) with medium current densities in severe conditions.
Li(Si or Al)/LiCl-LiBr-LiF/FeS$_2$	1.6 – 2.1	Used for medium-long applications (10 mins – 30 mins) with high current densities in severe conditions.
Li(Si or Al)/LiCl-KBr-LiF/CoS$_2$	1.6 – 2.1	Used for long applications (> 1 hour) with medium current densities in severe conditions.

Solid-state cell components at room temperature are the main reason for high shelf life by substantially reduced self-discharge. To activate thermal battery, certain amount of heat input is needed to melt the electrolyte and thus melted electrolyte acts as an ionic bridge between anode and cathode. Heat input is provided by the enthalpy of thermal decomposition of pyrotechnic heat pellets. Heat pellets are ignited by electro-explosive devices such as electrical squibs or mechanical igniters (ignition process is triggered by the momentum of impact or rotation for mechanical igniters). Enthalpy of heat pellets should be carefully adjusted to bring up the temperature in battery up to the point where eutectic electrolyte melts. Typical working temperature for a thermal battery is between 300 and 600 °C depending on the electrolytes used. Keeping inner temperature of thermal battery as high as possible increases the ionic conductivity of electrolyte and the rates of mass transfer and electrochemical reactions inside electroactive components. However, if too much heat is introduced to the thermal battery, electro-active materials may exothermically deteriorate and increase the inner temperature more, eventually causing thermal runaway of the battery [2-5].
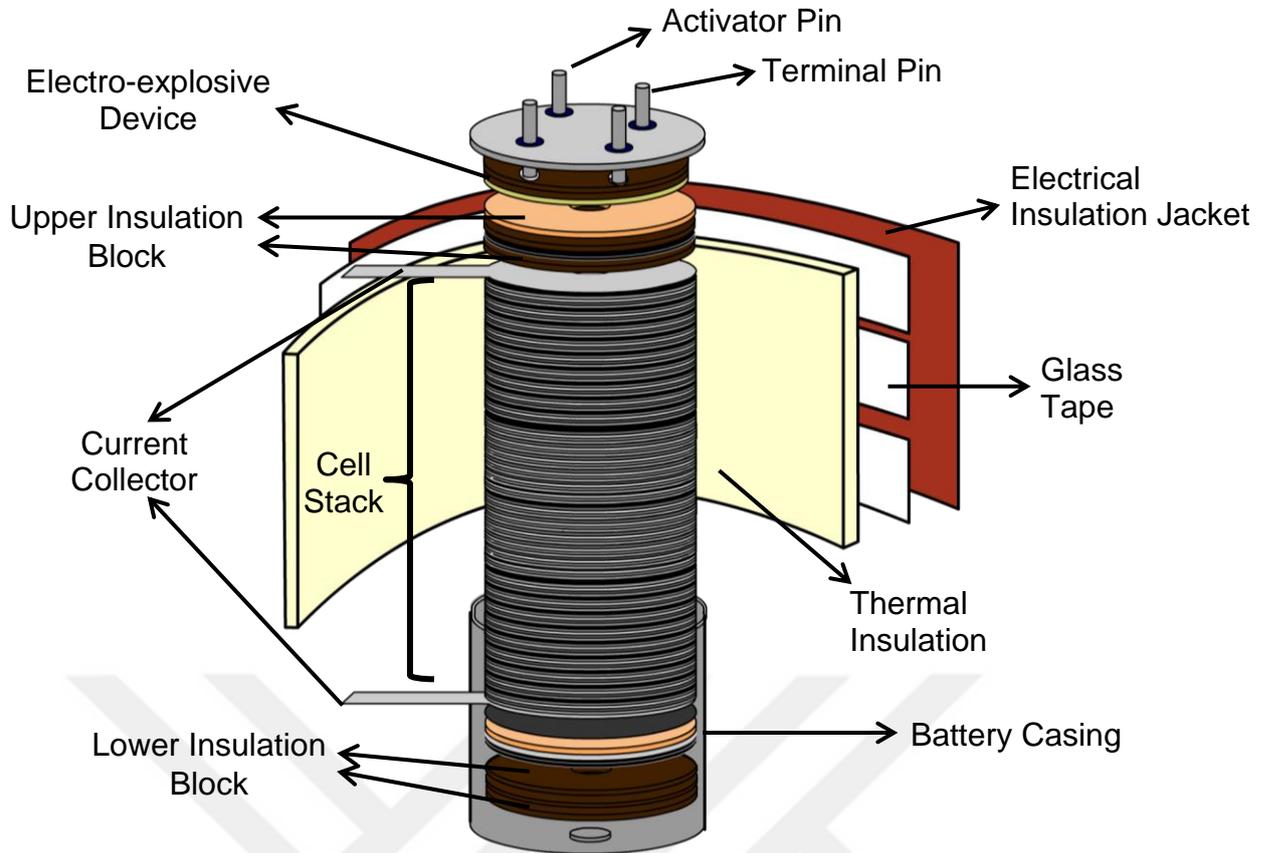
Figure 2. A schematic representation of thermal battery assembly

After igniter is fired, physical and chemical events that take place at the ignition point of heat pellets are described below and schematically shown in Figure 3:

- Heat and shock wave produced from the igniter travels through the pellet holes to the end of the thermal battery stacks.

- Heat pellets starts to ignite from the inner radius because of the energy of heat and shock wave.

- Heat produced from thermal decomposition of heat pellets raises the temperature of thermal battery up to a degree where eutectic salt (typically LiCl-KCl salt is used) in electrolyte pellet begins to melt. The process where the electrical or mechanical igniter is fired to the point where electrolyte is melted and meaningful current could be drawn from battery is termed as the activation. The time that battery takes to activate is termed as activation time.

- Immobilizing agent (typically magnesium oxide, MgO) acts as a matrix for ions in eutectic salt mixture to move freely in electrolyte pellet. If electrolyte pellet loses its mechanical integrity or lets ionic conductive eutectic salt solution to leak between cells, short circuit may arise. Short circuiting has a potential to lead thermal runaway of battery and should be avoided.

- Once ionic link between anode and cathode is established, electroactive component of anode (typically lithium, Li), oxidizes to form its positive charged ion (Li^+) and electron (e^-).

- Electrical energy released from this reaction is used for electrical work and conducted to the heat pellet. (Li^+) that is released from anode diffuses to the electrolyte matrix. To preserve ionic equilibrium, (Li^+) ion diffuses to the cathode as well.

- Cathode (typically iron sulfide commonly known as pyrite, FeS_2) undergoes reduction reaction with electron and lithium ion to end single electrochemical cycle. Once the inner temperature of the battery drops below the melting point of electrolyte or the electroactive materials are depleted because of electrochemical or side (chemical) reactions, the battery cease to provide meaningful voltage (acceptable lower voltage limit for a unit cell is 1.5 V for many applications). The process where thermal battery is activated to the point of capacity depletion is termed as operation time.
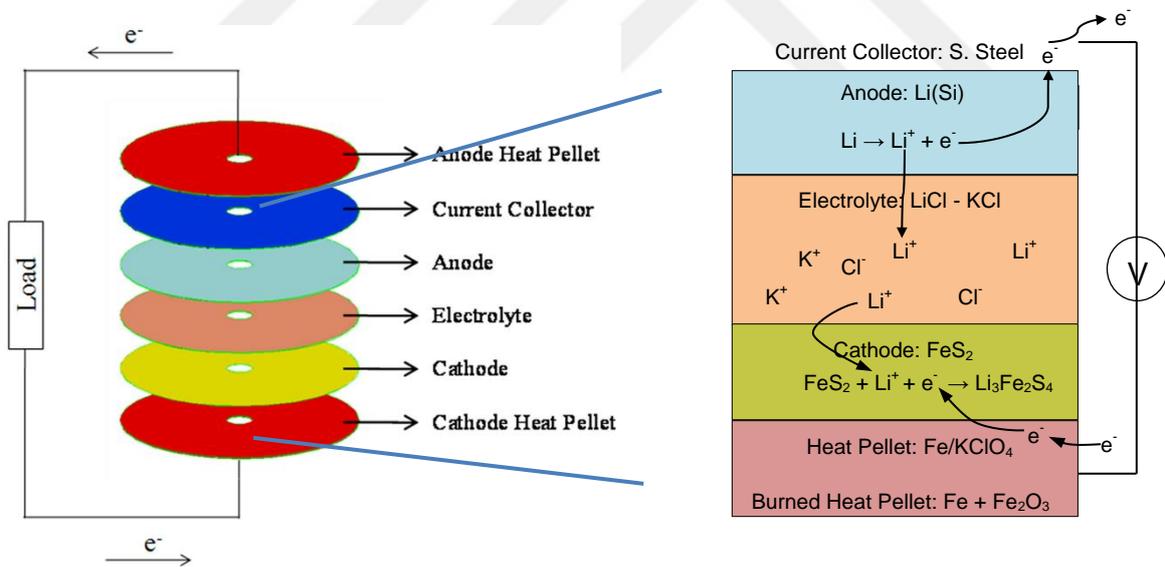
Figure 3. A schematic representation of thermal battery working principle

Overall cell discharge reaction defined from the aforementioned working mechanism of the Li(Si)/FeS_2 cell chemistry is given below.

$$3Li + 2FeS_2 \rightarrow Li_3Fe_2S_4 \ (E_{cell} = 1.6 - 2.1 \ V)$$

Internal resistance of thermal battery directly affects the voltage of unit cells. For the better electrical performance of battery, ionic conductivity of the electrolyte should be

kept as high as possible. That is accomplished by developing novel materials and cell chemistries for thermal battery or by carefully managing the heat generated inside thermal batteries. Main considerations that should be taken into account for efficient heat management are given below:

- Thermophysical properties of unit cell components,
- thermal insulation of thermal battery assembly,
- design parameters of heat pellets such as weight, calorific output (cal/g), weight composition and relative density.

Heat pellet in each cell is the main component that affects the heat management of the thermal battery. It is a paramount necessity to define the decomposition process of heat pellets for precisely designing the activation and operation phases of the battery.

2.2. Thermal Decomposition of Heat Pellets

Guidotti et al. performed a study to determine the ideal pyrotechnic mixture to be used in thermal batteries. $Fe/KClO_4$ outperformed other candidates with its electrical conductivity feature of its reaction products, high calorific output (cal/g), controllable and ideal range of linear burn rates (5 cm/s – 100 cm/s), dimensional stability, ideal ignition sensitivity and no outgassing feature [2].

Heat pellet consists of iron powder (Fe) as the fuel and crystalline potassium perchlorate ($KClO_4$) as the oxidizer. Heat pellets are produced by cold pressing of the homogenous mixture of iron and potassium perchlorate mixtures with specified particle size. The pellets have a hole in the center that it is ignited by the electro-explosive initiator. The iron content by weight is varied between 80 – 90%. The iron content is deliberately set higher than the stoichiometric ratio to preserve the electrical conductivity of heat pellet with remaining iron content. As well as electrical conductivity, excess iron moderates heat output into the battery components by reducing the thermal diffusivity [3].

For sake of better understanding of the scope of this thesis, following notations are defined:

Calorific Output:

Calorific output is the heat release of 1 g pyrotechnic mixture (Fe/KClO$_4$) during burning under inert conditions; the unit is usually defined as cal/g [7].

Adiabatic Burning Temperature:

The maximum temperature, the heat pellet would reach under thermally ideal isolation conditions.

Linear Burn Rate:

Linear burn rate can be defined as the distance the burning surface of a pyrotechnic composition advances per unit time. Heat and shock wave of the electro-explosive device ignites the heat pellet from the center hole (Figure 4).

The time when the first surface of center hole of heat pellet ignites is termed as t_0. The time when last surface of heat pellet decomposes is termed as t_f. Linear burning can be defined with the following equation [7]:

$$\text{Burn rate } (^{cm}/_s) = \frac{Outer\ radius\ of\ pellet - Inner\ radius\ of\ pellet}{t_f - t_i} \tag{1}$$
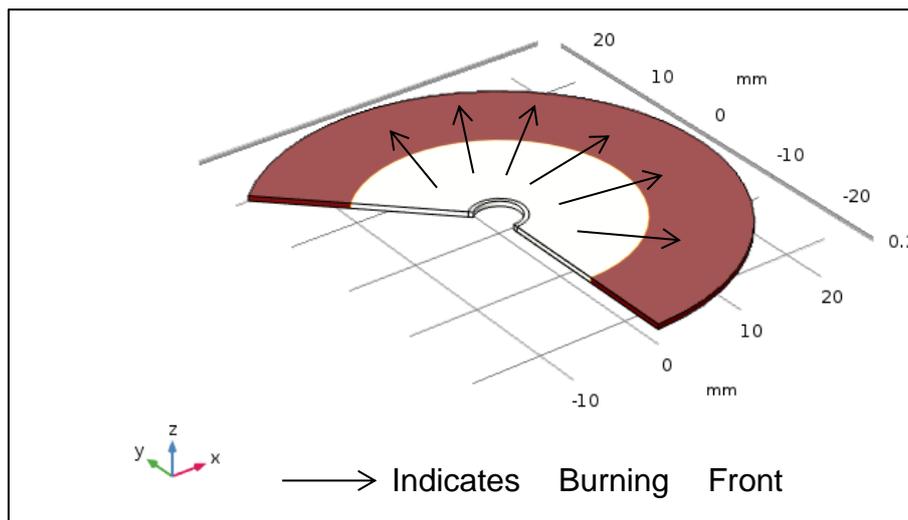
Figure 4. A Schematic view of burning process of heat pellet

<u>Percent of Theoretical Density of Heat Pellet:</u>

Also termed as degree of consolidation or green density, relative density defines the ratio of solid content in the pellet matrix. Relative density can be mathematically expressed as:

$$\text{Percent of Theoretical Density (\%)} = \frac{d_{pellet}}{d_{theo.}} \times 100\ \% \qquad \textbf{(2)}$$

where d_{pellet} is the density of prepared heat pellet (g/cm^3), $d_{theo.}$ is the theoretical density assuming that heat pellet has no inner and interparticle voids (g/cm^3).

2.3. Kinetics of Thermally Initiated Solid-State Reactions

The rate of chemical reaction and its dependency to the reactant concentration and conditions (pressure and temperature) are studied for many chemical reactions. Mechanism of the reaction dictates how these parameters affect the reaction rate [8].

2.3.1. Reaction Kinetics

The concept of reaction kinetics takes roots back into the 1800's when Wilhelmy discovered the rate depends on the amount of reactant that is in the reacting mixture. He mathematically described this dependence as follows:

$$-\frac{dC}{dt} = kC \qquad \textbf{(3)}$$

where t (s) is the time, C (mol/m^3) is the concentration, and k (m^3/s) is the rate constant.

Based on van't Hoff's works on thermodynamic model [9], Arrhenius introduced concept of activation energy that takes roots from Boltzmann statistical theory of the energy distribution of activated particles to describe the temperature dependence of the reaction rate with following equation:

$$k(T) = Ae^{\left(-E_a/RT\right)} \qquad \textbf{(4)}$$

where E_a is the activation energy (J/mol) and R is the universal gas constant (8.314 J/ mol.K).

The activation energy (E_a) can be described as the threshold value of energy needed for reactant molecules to rearrange or break its bonds in a chemical reaction. It can also be defined as the energy difference of the initial state of a reactant and the

transition state (Figure 5). The pre-exponential factor represents the frequency of collisions between reactant molecules [8].
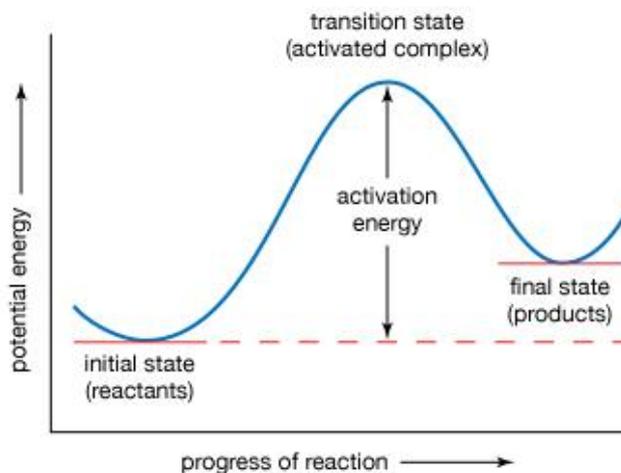
Figure 5. Change of state during the chemical reaction [10]

Heterogeneous (solid-state) thermal kinetics originates from the theory of homogenous gas or solid kinetics. Arrhenius equation is originally derived for the homogenous reactions. Therefore, several authors [11-13] criticize the use of Arrhenius equation in solid-state reactions in literature. However, Vyazovkin et al. and Galwey et al. have pointed out in his work that the reaction kinetic of solid state decomposition can be successfully described with activation energy using Arrhenius theory [14, 15].

In solid-state decomposition, reaction rate equation related to temperature and conversion can be expressed as:

$$\frac{d\alpha}{dt} = k(T)f(\alpha) \tag{5}$$

where t is the time, k(T) is the rate constant, $f(\alpha)$ is the reaction model. A reaction model is a theoretically developed mathematical expression which defines what occurs experimentally. The conversion or the extent of reaction (α) that is taken place represents the overall transformation of measured overall properties of reaction. Depending on the instrumentation used and the characteristic of studied reaction, measured properties can be the mass (i.e. thermogravimetric analysis), heat flow (i.e. differential scanning calorimetry), concentration (i.e. spectroscopic methods) etc..

11

The most typical mathematical expression for conversion is given as ratio of mass change:

$$\alpha_T = \frac{m_0 - m_T}{m_0 - m_f} \qquad \textbf{(6)}$$

For exothermic reactions, the conversion is expressed as the ratio of heat released from reaction (Figure 6):

$$\alpha_T = \frac{\int_0^T Q_{released} \times dT}{\int_0^f Q_{released} \times dT} \qquad \textbf{(7)}$$

where T is the temperature (K), $Q_{released}$ is the heat flow released from decomposition of sample per unit mass of sample (W/g), α is the conversion, m is the mass of sample (g). The subscript "0" denotes the initial state, "f" denotes the final state and T denotes the property at specified temperature.
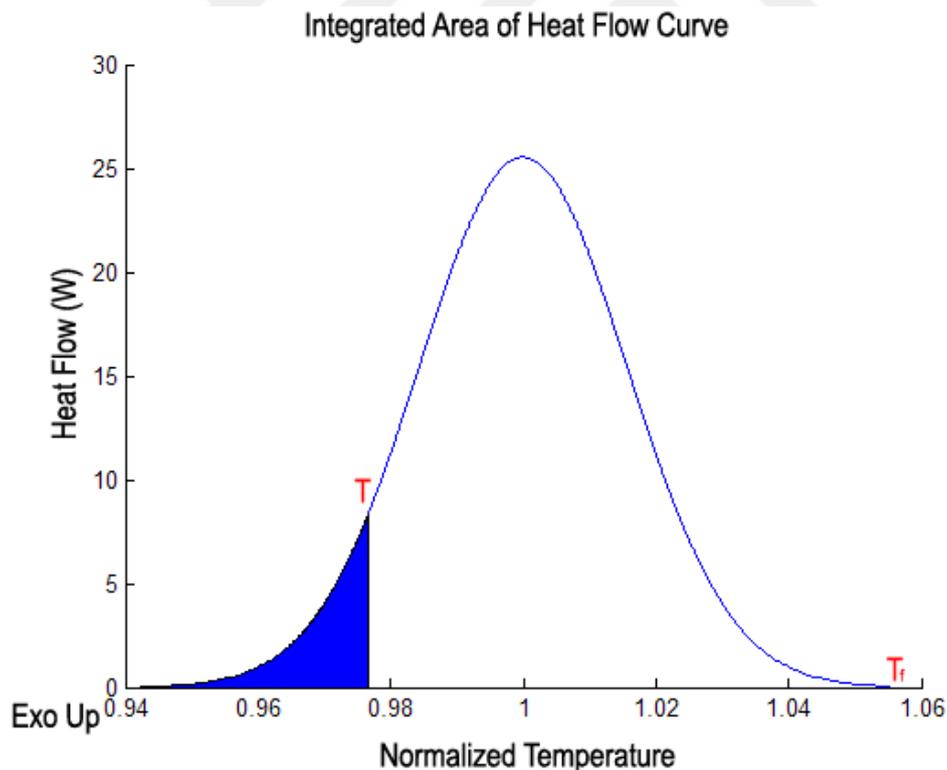
Figure 6. Heat flow released and temperature in an exothermic process

Solid-state decomposition reactions have nature of following multi-step reaction pathway [16]. The multi-step reaction pathway was studied extensively by several researchers and the concept of reaction model, f(α) which is the representation of the

reaction mechanism, was proposed [11-16]. The reaction models are reported by Flanagan et al. in Table 2 [17].

Table 2. Solid-State rate and integral expressions for reaction models [17]

Reaction Model	Differential Form $f(\alpha)$	Integral Form $g(\alpha)$
Nucleation Models		
Power law (P3)	$3\alpha^{2/3}$	$\alpha^{1/3}$
Power law (P4)	$4\alpha^{3/4}$	$\alpha^{1/4}$
Avrami-Erofeyev (A2)	$2(1-\alpha)[-\ln(1-\alpha)]^{1/2}$	$[-\ln(1-\alpha)]^{1/2}$
Avrami-Erofeyev (A3)	$3(1-\alpha)[-\ln(1-\alpha)]^{2/3}$	$[-\ln(1-\alpha)]^{1/3}$
Prout-Tompkins (B1)	$\alpha(1-\alpha)$	$\ln[\alpha/(1-\alpha)] + c^a$
Extended Prout-Tompkins (Seŝtak-Berggren) (B2)	$\alpha^m(1-\alpha)^n$	no analytical form
Geometrical Contraction Models		
Contracting Area (R2)	$2(1-\alpha)^{1/2}$	$1-(1-\alpha)^{1/2}$
Contracting Volume (R3)	$3(1-\alpha)^{2/3}$	$1-(1-\alpha)^{1/3}$
Diffusion Models		
1-D Diffusion (D1)	$1/(2\alpha)$	α^2
2-D Diffusion (D2)	$-[1/\ln(1-\alpha)]$	$[(1-\alpha)\ln(1-\alpha)] + \alpha$
3-D Diffusion - Jander (D3)	$[3(1-\alpha)^{2/3}]/[2(1-(1-\alpha)^{1/3}]$	$(1-(1-\alpha)^{1/3})^2$
Reaction Order Models		
Zero-Order (F0/F1)	1	α
First-Order (F1)	$(1-\alpha)$	$-\ln(1-\alpha)$
Second-Order (F2)	$(1-\alpha)^2$	$(1-\alpha)^{-1}$
^{a}Constant of integration.		

Vallet et al. conducted the first kinetic evaluations based on non-isothermal thermal analysis done at constant heating rate ($\beta=dT/dt$) setting on temperature program. For sake of better mathematical definition he suggested replacing the time differential of conversion in Equation (5) to the temperature differential [14]:

$$dT = \beta \times dt \qquad (8)$$

13

Based on the theories presented previously, the reaction rate for the heterogeneous solid-state reaction under isothermal conditions can be mathematically expressed as:

$$\frac{d\alpha}{dt} = A \exp^{\left(-E_a/RT\right)} f(\alpha) \tag{9}$$

Implementing Equation (8) to Equation (9), reaction rate under non-isothermal conditions can be derived:

$$\frac{d\alpha}{dT} = \frac{A}{\beta} \exp^{\left(-E_a/RT\right)} f(\alpha) \tag{10}$$

Equation (10) is the basis of the thermal decomposition reactions. A, E and f(α) parameters are the so-called kinetic triplet by the literature [14]. It can be seen from Equation (10) that decomposition rate of the pyrotechnic at a certain temperature depends on the conversion (α) at that temperature.

In the following section, literature survey on the heat pellet decomposition will be presented in conjunction with the reaction kinetics knowledge presented in this section.

2.4. Decomposition of Heat Pellet

A pyrotechnic mixture consists of solid fuel and an solid source of oxygen which are required for the self-sustaining thermal decomposition reaction. These mixtures are based on fine particles of typically metallic fuel (iron,Fe) and inorganic oxidizing agent (potassium perchlorate (PP), $KClO_4$) [7].

Typical applications for such pyrotechnic devices are given in Table 3 below.

Table 3. Applications of pyrotechnic devices [18]

Feature of Pyrotechnic	Main Use	Description
Smoke Generator	Used for obscuring, screening and signaling purposes on battlefield.	Using red phosphorus or white phosphorus gives different colors to the generated smoke.
Illuminating Flare	Produces light for signaling or visual illumination. Used as infra-red decoys in fighter jets as well.	Mixtures of only oxidizing agent and a metal fuel. Additives are used for controlling burn rate.

		Electrically initiated devices which utilize bridge-wire. Typically zirconium – potassium perchlorate mixture is used in a metal container.
Electro-explosive Devices	Used in thermal batteries as initiators.	Electrically initiated devices which utilize bridge-wire. Typically zirconium – potassium perchlorate mixture is used in a metal container.
Pyrotechnic Delays	Used in war-heads for fuze applications. Used as timers in grenades.	Larger particle size fuels and oxidizers are used to control the reaction rate.
Gas Generator	Used as an initiator in a rocket motor.	Produces large amount of hot and compressed gaseous products for ignition of rocket fuel.
Heat Source	Used as heat sources for thermal batteries, self-sustained high temperature (SHS) reactions etc..	For thermal batteries, typically in pellet form with a hole in the middle. Ignition starts from the middle with a heat pulse from an electro-explosive device.

2.4.1. Pyrotechnic Ignition and Propagation

Pyrotechnic compositions are physical and heterogeneous mixtures of fuel and oxidizer and sometimes heat mediators such as Viton®. These components may be organic or inorganic. These formulations possess the characteristic of producing large amount of heat, light and often gas. Most used fuel and oxidizer compositions and their heat of reactions are given in Table 4.

Table 4. Typical binary pyrotechnic compositions and their heat of reactions [3, 19]

Fuel	(% weight)	Oxidizer	(% weight)	ΔH_r (kJ/g)
Fe	61.8	$KClO_4$	38.2	2.974
Fe	86.0	$KClO_4$	14.0	1.088
Mg	40.0	$KClO_4$	60.0	9.372
Mg	37.0	$KClO_3$	63.0	9.581
Al	34.0	$KClO_4$	66.0	10.251
Al	40.0	$NaNO_3$	60.0	8.368
Al	25.0	FeO	75.0	4.017

Under room conditions, these compositions are stable and do not undergo any decomposition reaction. An external stimulus (laser, heat etc.) should be directed to the pyrotechnic composition to initiate the process of heat release (burning). In Figure

7, internal energy variation starting from ignition till the end of burning process is given. As it is stated, an external stimulus is needed to overcome the activation energy barrier (E_a). This is indicated as the "Energy In" part of Figure 7. After this point, pyrotechnic composition starts to release its chemical energy which is called the enthalpy of reaction (ΔH_r). This heat release is indicated as the "Energy Out" part of Figure 7. The reason why heat of reactions vary for each of the compositions given in Table 4 is the number and energy of chemical bonds that are broken and formed are different for each case.
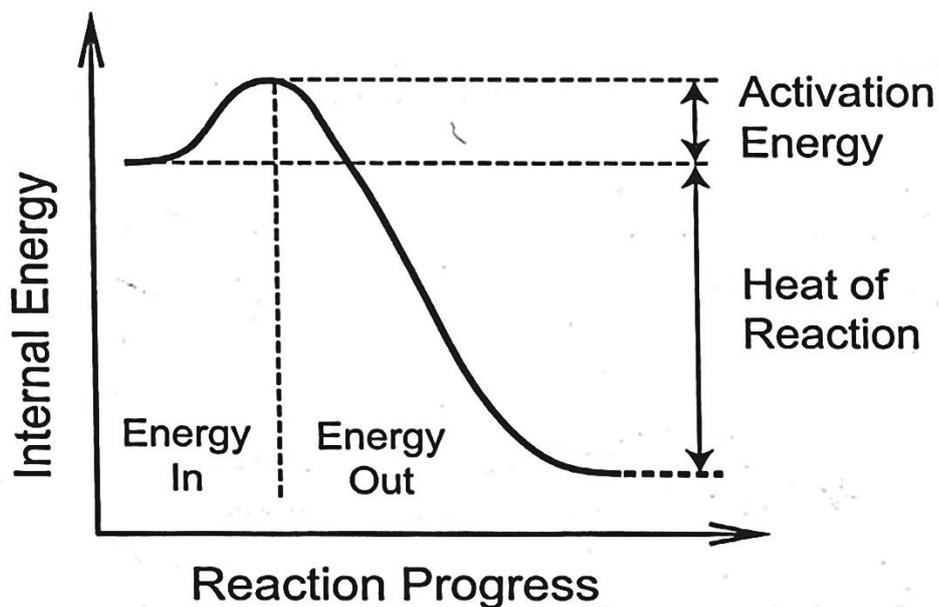
Figure 7. An illustration of internal energy variation as reaction progresses for a pyrotechnic composition [20]

The decomposition process of pyrotechnics is defined as self-sustaining. Once ignited, thermal energy produced from thermal decomposition is sufficient to overcome the activation energy barrier of the pyrotechnic mixture in vicinity ($\Delta Hr > E_a$), thus decomposition reaction proceeds until reactants are entirely consumed.

16
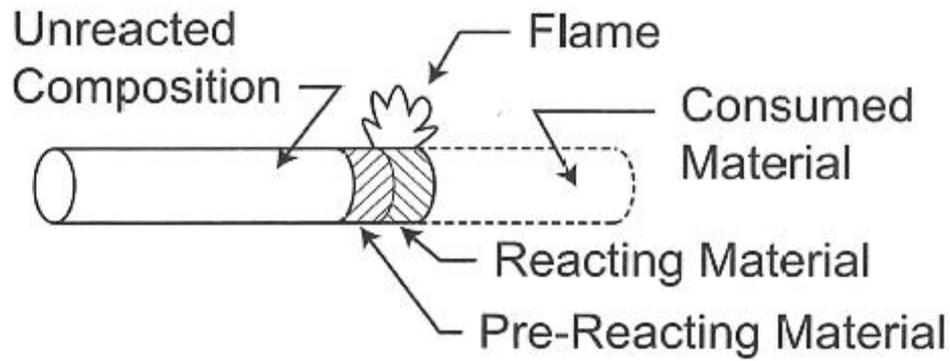
Figure 8. An Illustration of the propagation process for a rod formed pyrotechnic composition [20]

Ignition of a pyrotechnic composition with an external stimulus will only provide enough thermal energy for a small part to be started to burn. For burning front to propagate, certain conditions should be fulfilled. Most important of them is given previously: the need for higher heat of reaction than the activation energy for burning process ($\Delta H_r > E_a$). Figure 8 shows the how burning front proceeds when a rod of pyrotechnic composition is ignited. This figure not only shows how propagation occurs, it gives insight about the heat transfer mechanism in which some of the generated heat is conducted to the reacting material and some of heat is lost to the surroundings. A fraction of the heat produced by burning (ΔH_r) of pyrotechnic is lost to the surroundings. Remaining fraction of the heat of reaction reaches the burning front and brings up the temperature of pre-reacting material to the point of re-ignition. This fraction is termed as F_{fb}. Consequently, the inequality given previously ($\Delta H_r > E_a$) should be revised and rewritten as $\Delta Hr \times F_{fb} > E_a$ to fulfill the conditions needed to pyrotechnics propagation proceeds until all reactants are depleted [20]. How fast this propagation takes places is controlled by intrinsic properties of the compacted pyrotechnic composition which is covered in the next section.

2.4.2.   Burn Rate and Controlling Parameters

The rate of propagation or burn rate (cm/s) should be well adjusted to ensure safety or to solely control heat release of the pyrotechnic composition for design considerations. Therefore, understanding the factors that control burn rate should be identified and investigated. Kosanke et al. presented and discussed the main factors that affect burning process in their work as follows [7].

17

1. Choice of Fuel and Oxidizer:

The choice of fuel and oxidizer is the key element that affects the kinetic parameters which dictates the burn rate of a pyrotechnic composition. Some oxidizers may be decomposing exothermically which have a boosting effect on burn rate. In the case of $KClO_4$ decomposition, decomposition energy is 37.656 J/g which is exothermic [21]. The kinetic parameters of selected pyrotechnic compositions (in stoichiometric ratios) are given in Table 5.

As well as kinetic parameters, choice of fuel and oxidizer also affects the thermophysical properties such as thermal conductivity and heat capacity. Thermophysical properties determine the aforementioned fraction of fed back (F_{fb}) energy to the burning front.

Table 5. Arrhenius kinetic constants for PP, ZPP, BPP, FPP

Pyrotechnic Composition (Powder Form)	Apparent Activation Energy (kJ/mol)	Frequency Factor, ln(A)	Reference
Zirconium/Potassium Perchlorate (ZPP)	212	33.19	Helmy [22]
Boron/Potassium Perchlorate (BPP)	228	37.94	Miyata [23]
Iron/Potassium Perchlorate (FPP)	554	34.40	Shamsipur [4]
Potassium Perchlorate (PP)	235	39.18	Miyata [23]

2. Weight Composition:

The weight composition that gives the fastest burn rate is termed as the optimum weight composition. Moving off the composition of pyrotechnic mixture causes the burn rate to decrease as well. This behavior is best shown in the Figure 9 below.
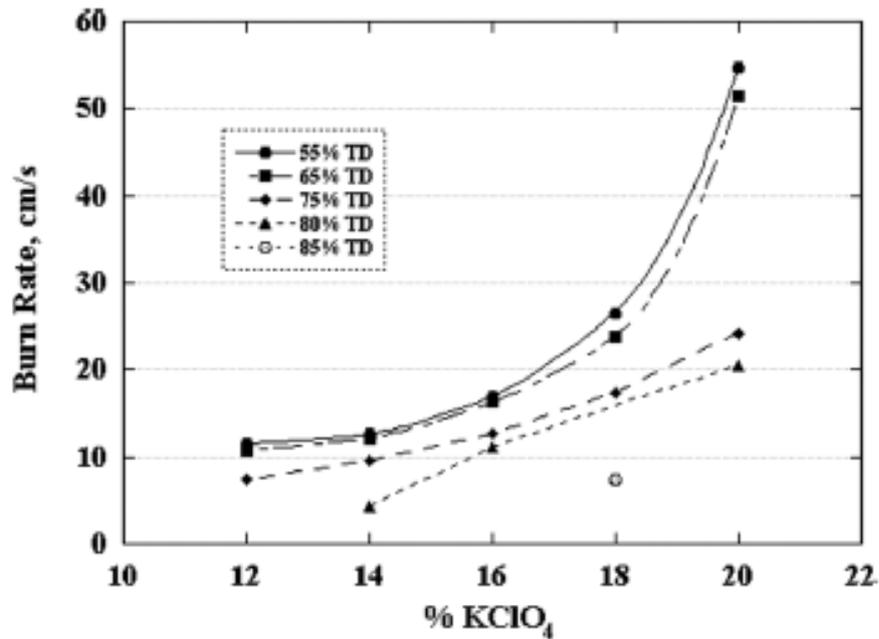
Figure 9. The effect of KClO$_4$ ratio to the burn rate for heat pellet system (TD: Theoretical Density) [2]

From this figure, one can deduce that for heat pellet system, as oxidant (KClO$_4$) composition increases burn rate increases as well in the given limits of weight percentage (%12-20). As per Guidotti et al.'s works, the use of KClO$_4$ weight ratio more than % 18 is not advisable for thermal battery applications due to shipping restrictions, safety concerns and possible negative impacts on the battery performance [2].

As well as burn rate, weight composition has influence on the calorific output as well. For heat pellets Guidotti et al. derived an equation for this relationship as follows:

$$\text{Heat Output} \left(\frac{\text{cal}}{g} \right) = 1{,}884.73 - 18.8999 \times (\% \, Fe) \tag{11}$$

where %Fe is the weight percentage of the iron in pyrotechnic composition.

The reason why the burn rate is lowered when using non-stoichiometric compositions is that the specific heat of reaction is lowered and thus temperature in reaction completion zone as well. Therefore, this condition results in slower reaction rates than in stoichiometric conditions. The effect of excess fuel reduces the heat production and its effect is doubled as the excess fuel mass absorbs

heat away from the burning front. This causes a steep decrease in reaction temperature thus burn rate [3]. It should be noted that fastest burn rates are usually achieved when using weight compositions near stoichiometric ratio [24].

3. <u>Degree of Mixing:</u>

Poor mixing may cause deviations from the specified weight composition which in return causes burn rate to fluctuate. Therefore, for precise burn rate, homogeneous mixing of the solid components must be achieved. Bauman et al. studied the mixing of solid with different mixing devices. In this work, it was concluded that V-blenders and mechanical mixing devices were defined as ideal mixing tools for powder mixing [25].

4. <u>Particle Size:</u>

In general sense, reducing the particle size of the components will cause acceleration in burning due to the increase in surface areas. Lee et al. investigated the effect of particle size on the decomposition of $KClO_4$. In his work, it was concluded that; as the particle size range was lowered from 44 - 74 µm to ≤ 44 µm, activation energy of $KClO_4$ decomposition was dropped from 113 to 106 kJ/mol under nitrogen atmosphere. This work shows that, lowering particle size of the oxidizer would have a small impact on the overall activation energy of the heat pellet. Furthermore, Kosanke et al. concludes in his work that oxidizer particle size has much small impact on the pyrotechnic characteristics compared to the particle size of the fuel used [7].

Reed et al. studied the effect of Fe particle size on the burn rate of heat pellets. It was found that rather than the particle size of Fe, the amount of surface area increase because of the particle size reduction increases the burn rate. It was recommended in this work to use iron of average particle size below 44 µm and above 10 µm for optimal burn rates [26].

5. <u>Particle Morphology:</u>

Guidotti et al. investigated the effect of iron particle morphology on the heat pellet strength, burn rate and calorific output. When the morphology of Fe is elongated

spongy structure, mechanical stability becomes the highest because of the interlocking matrix of fuel and oxidizer. As well as mechanical stability, this structure ensures high surface area interface between fuel and oxidizer; therefore ensures desirable burn rates [2].

6. <u>Pellet Theoretical Density:</u>

Guidotti et al. showed that pellet theoretical density has a dominant effect on burning characteristics. Highest burn rate was achieved when using 55 – 65 % theoretical density for all compositions. When this theoretical density is used burn rates of 7 and 55 cm/s were measured [2].

2.4.3. Mechanism of Heat Pellet Decomposition Reaction

The decomposition of heat pellets are classified as solid-state decomposition. The reason for this classification is that the chemical components and the final products are solid at the ambient temperatures. Solid state decomposition of pyrotechnics was studied by Tammann and McLain for the first time [27, 28]. They proposed that reaction of burning takes place inside the powder matrix rather than the surface of individual particles. This approach was not widely accepted by the literature. Main reason for this disapproval was that direct interaction between fuel and oxidizer would require too high activation energy for a rapid decomposition reaction like in pyrotechnics. For example in the case of zirconium/potassium perchlorate ($Zr/KClO_4$ - ZPP), activation energy for decomposition of $KClO_4$ is ≈251 kJ/mol and activation energy for zirconium atom extraction from zirconia is 608 kJ/mol. Total activation energy would be 860 kJ/mol which is too high for a fast reaction. This condition indicates that decomposition of such pyrotechnic compositions should proceed in liquid or gaseous matrix. From this perspective, Yang et al. described the pyrotechnic reaction mechanism using the relation from the combustion of solid-propellants mechanism [29]. In his work, based on the combustion of boron (B) with ammonium perchlorate (NH_4ClO_4), potassium nitrate (KNO_3) and potassium perchlorate ($KClO_4$) [23, 30], he suggested the following findings are also applicable to physically picture the decomposition of ZPP:

- As the temperature of the composition increases, oxidizer ($KClO_4$) melts. When both fuel and oxidizer are solid particles, relatively little portion of their surface are actually in physical contact. After the melting of $KClO_4$ at

21

temperatures of 350 – 500 °C, it is free to flow over the surface of the fuel. Thus, the number of fuel and oxidizer atoms in physical contact is very much greater.
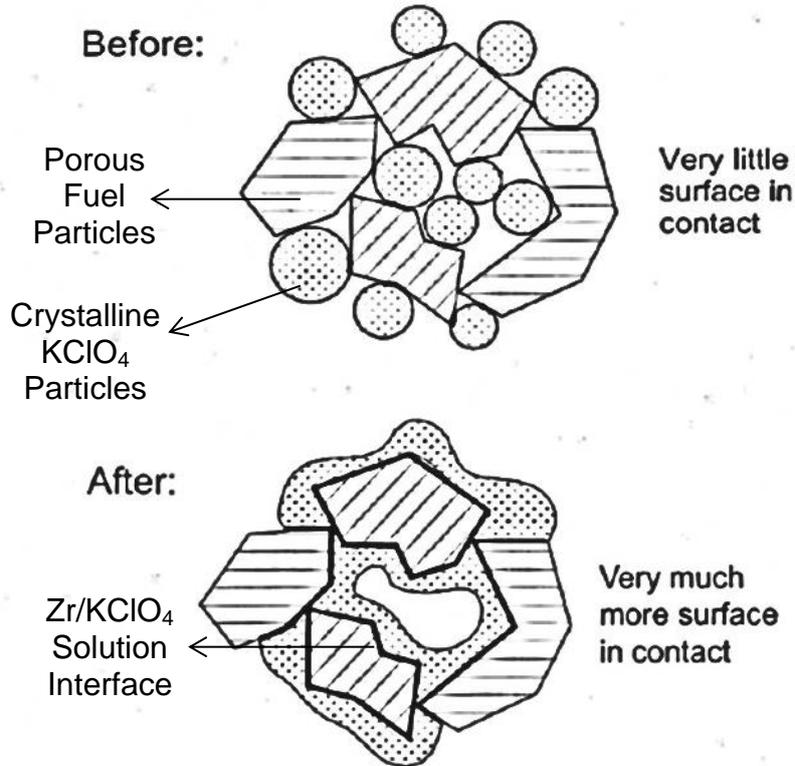
Figure 10. An illustration of melting of KClO₄ and increase in contact surface area [7]

- After melting of oxidizer, $KClO_4$ decomposes and produces free oxygen efficiently. Free oxygen atoms extracts zirconium atom from the solid state, reacts rapidly with the fuel (Zr) at the interface surface of zirconium (Figure 10). At this point, zirconium is in solid state. Through this reaction, ZrO is formed at the surface endothermically. This type of reaction has resemblance with the dissolving of salts in solvent or the etching of metals by high concentration acids. As a remark, it is presented experimentally in this study that reaction of zirconium and oxygen atom is much faster than the reaction of oxygen atoms with itself to from oxygen gas. Therefore, oxygen is retained in the system rather than being released out of the system. This is mass preserving aspect for a pyrotechnic reaction of this kind.

- At the temperatures in the reaction zone, ZrO becomes gaseous around the zirconium particles. Diffusion of free-oxygen into the ZrO which is in gaseous state occurs rapidly to from ZrO_2 which is the dominant exothermic reaction for this system.

As it is presented above, the chemical kinetics of pyrotechnic reactions is challenging to be understood due to the high reaction rates and temperatures involved and the complexity of the products of the reaction. This is the main reason thermal decomposition reactions are treated as single-step rather than multi-step reactions. The decomposition of $Fe/KClO_4$ (FPP) may be written as according to the Guidotti et al. [2]:

$$4Fe \ + \ KClO_4 \ \rightarrow \ 4FeO + KCl + \Delta H_r$$

ΔH_r for this reaction when fuel and oxidizer are used in stoichiometric ratio (61.8 % Fe / 38.2% $KClO_4$ w:w) is 3304 kJ.

During thermal decomposition process reversible and irreversible reaction steps occur. Those steps are explained below, by the insight provided by Yang et al. about the thermal decomposition of ZPP:

1. Crystal structure of potassium perchlorate ($KClO_4$) reversibly and endothermically shifts from rhombic into the regular phase at 300 °C.
2. Potassium perchlorate starts to disassociate to form oxygen atoms at 460 – 500 °C. Also just before disassociation, $KClO_4$ rapidly melts and forms a solution phase at the $Fe/KClO_4$ interface [20].
3. Released oxygen atoms immediately react with iron (Fe) molecules highly exothermically at temperatures of 490 – 510 °C.

Reaction Rate Insensitivity to Ambient and Partial Pressure

A pyrotechnic reaction does not require the oxygen from atmosphere as oxidizer. Typically an inorganic salt (KNO_3, $KClO_4$ etc.) is used as a source of oxygen atoms upon its decomposition.

Venicelli et al. conducted experiments about the dependence and generation of pressure in the decomposition reactions of lower burn rate (2 cm/s- 50 cm/s)

pyrotechnics such as $Zr/BaCrO_4$. In his experiment; decomposition reaction took place in a hermetic container which was had an pressure. He found out that there was no change in pressure after decomposition. As a result, for lower burn rate pyrotechnics such as $Fe/KClO_4$, dependence of pressure to the reaction rate can be assumed negligible. This pressure independent behavior was verified by Yang et al. and Bement et al. as well [29, 31].

On the other hand, even if $KClO_4$ decomposition is reversible and reaction rate depends on a h(P) function; since decomposition product oxygen (O) reacts with excess iron (Fe) in heat pellet as soon as oxygen gas emerges, it would be feasible to assume that decomposition of $KClO_4$ does not depend on the partial pressure of oxygen and furthermore reaction is reversible as it is also observed for the similar zirconium/potassium perchlorate system [29]. This assumption can be verified by the invariance of activation energy with respect to conversion.

2.5. Thermal Analysis Methods

For kinetic characterization of solid state reactions, thermal stimulus is the most common activation method. As well as thermal activation, magnetic field, pressure, electrochemical potential and photons are used as stimuli for solid state reaction activation. Activation method which is based on thermal stimuli is termed as thermal analysis methods. In a typical thermal analysis method, a property (e.g. mass, heat, magnetism, crystal structure etc.) of the sample is monitored as the temperature of the sample is varied linearly or modulated (sinusoidal, square etc.). For solid state reactions commonly used thermal analysis methods are Thermogravimetric Analysis (TGA), Differential Thermal Analysis (DTA) and Differential Scanning Calorimetry (DSC) [32]. TGA is a method used to measure the change of mass of the sample as a function of temperature (non-isothermal method) or time (isothermal method). DTA and DSC working principles are based on the same technique which is the measurement of the difference of the temperature of sample and reference as a function of temperature. DSC is a more sophisticated system which allows to determine calorific values such as heat of fusion, crystallization, decomposition etc.. More recently, simultaneous differential technique (SDT) is preferred for solid state reactions because SDT combines both TGA and DTA in one device [33].

2.5.1.   Differential Thermal Analysis (DTA)

DTA and DSC are most employed thermal analysis methods since all reactions that take place are endothermic or exothermic [34]. These reactions can be roughly classified as: solid state reactions, fusion, crystallization, curing and decomposition. While the temperature of the sample is varied linearly, sample goes through a reaction at certain temperature interval. This reaction causes a shift in temperature of the measured temperature due to the heat effects of reaction. Total mass of this reaction does not necessarily need to change for a change in heat to occur. These types of reactions and their output are depicted in Figure 11.
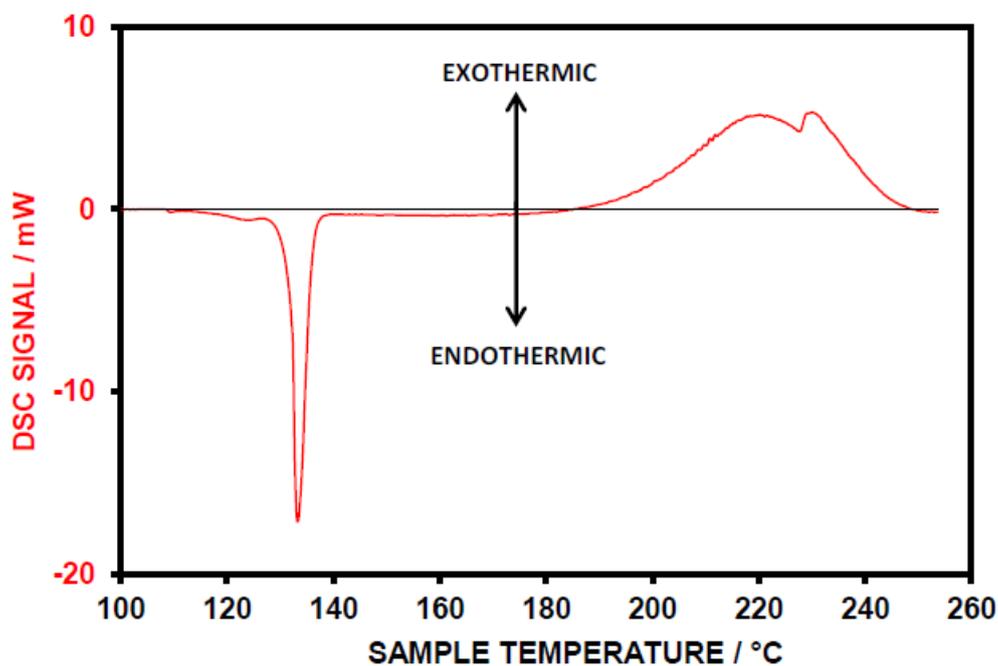
Figure 11. Typical heat flow signal for exothermic and endothermic processes

Conceptual design of DTA takes roots to the date of 1899 when W. C. Roberts-Austen produced a device that heated the sample and a reference material in same process chamber in close proximity [35]. In this device, both temperatures of the sample and reference were measured at the same time by thermocouples which were placed directly into the pan (sample holder) contents and temperature difference can then be determined. Main advantage of this design was the minimization of the temperature difference of sample and reference which in return meant whenever sample reacted, a certain amount of heat is either released or absorbed caused a difference in the temperature of sample and reference ($\Delta T = T_{sample} - T_{reference}$). When this reaction process is completed, temperature difference

reduces to the pre-reaction state. A typical endothermic sample and reference response is given in Figure 12 below.
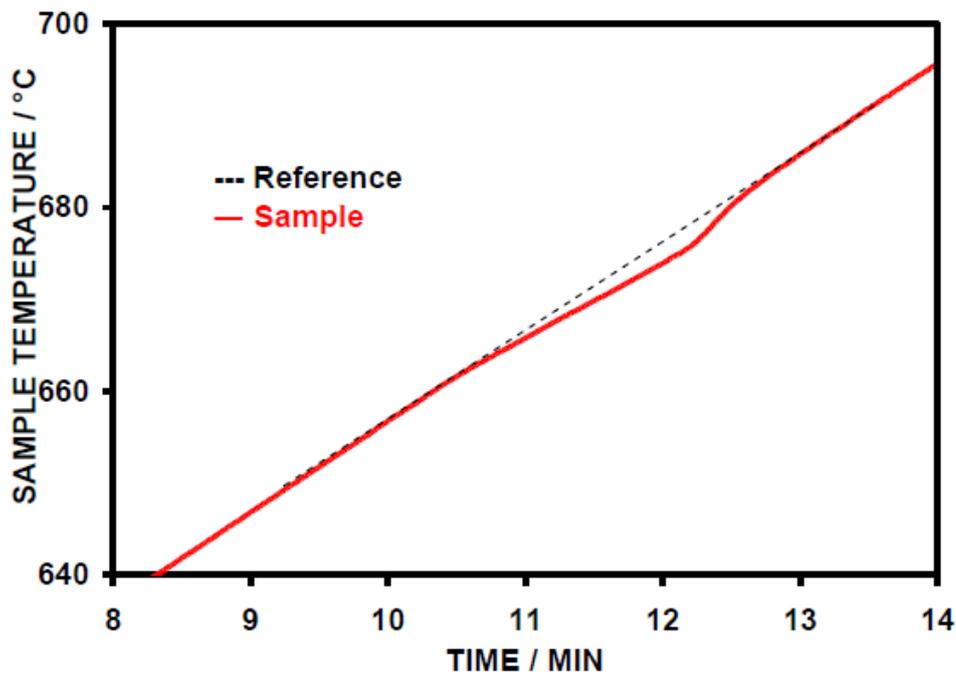
Figure 12. An endothermic temperature response signal of sample and reference in DTA setup

Thermocouple A is placed in the sample to be analyzed. Thermocouple B is placed in an inert reference material. When the temperature of sample equals the temperature of reference, the thermocouples produce identical voltage, and the voltage output, ΔT, is zero. When a physical or chemical reaction occurs in the sample, a differential signal is received and recorded. Figure 13 shows a schematic of the DTA system.
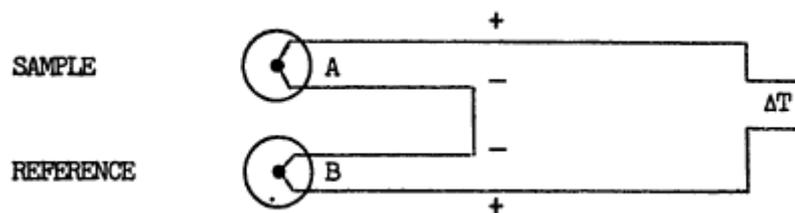
Figure 13. Schematic of DTA configuration

A typical DTA data (ΔT) generated from the temperature responses of sample and reference is given in Figure 14 below.

26
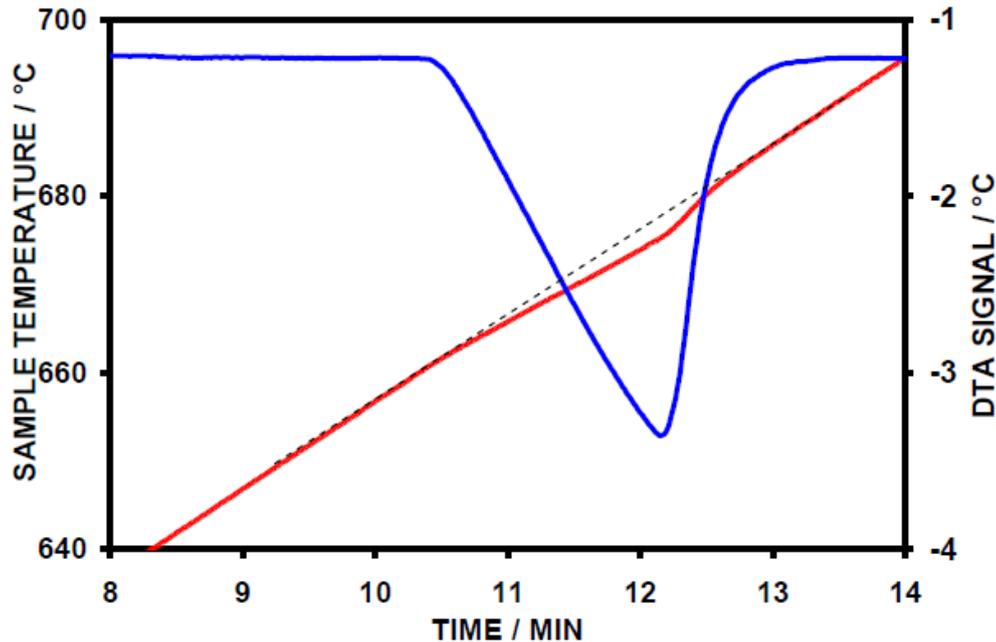
Figure 14. Typical DTA signal calculated from the response of thermocouples

In this apparatus certain aspects of the experiment should be taken into consideration:

1. The reference material should be thermally stable throughout the experiment.
2. Heat capacity of the sample and reference should be similar.
3. There should be no reaction between sample and reference.

Boersma improved Roberts-Austen's device by eliminating the considerations stated above [36]. He suggested using a conductive plate between the sample and the thermocouple to filter out the parasitic effects of the thermal properties of the sample and interactions of sample with thermocouple. This design is still used as the main configuration for both DTA and SDT devices. However, SDT device differentiates in a way that it measures weight of the sample too. The configuration that measures both DTA signal and weight of the sample is called the thermobalance.

2.5.2.   Isothermal and Non-Isothermal Processes

Earliest kinetic analysis was employed using isothermal thermal analysis experiments. In isothermal thermal analysis approach, experiment is programmed to reach to a final temperature as soon as possible and stay at that temperature until the reaction process is finished. This approach requires three or more isothermal experiments to generate kinetic parameters [14]. Main disadvantage of isothermal thermal analysis is the non-zero conversion at the start of isothermal period. Main

cause of this problem is the aging in the heat-up time period. This aging problem becomes more severe when working at more elevated temperatures and it is impossible to avoid [37]. For heat pellets, reaction initiation temperature is about 465 °C [2]. Therefore, using isothermal thermal analysis for heat pellet decomposition may result in missing out the kinetic data at the early stages of decomposition reaction.

Flynn et al. pioneered the way to the non-isothermal experiments in his study [38]. In thermal analysis at non-isothermal condition, aging problem (non-zero conversion) of sample prior to the reaction process has been overcome by implementing a scan of predefined temperature range while observing heat flow signals. In brief, decomposition reactions take place during the heating/cooling process of the system.

2.5.3.   Effects of Experimental Parameters

In order to obtain accurate kinetic parameters, thermal analysis data should low noise and high resolution. To ensure proper data, calibrations of thermal analysis equipment should be performed carefully. As defined previously, DTA is a device that heats the sample and the reference in the same proportions to scan a predefined temperature range. In this setup, sample and reference can't practically have the same specific heat capacity. Therefore, certain amount of temperature difference is inevitable between sample and reference along the temperature range of experiment. Due to nature of specific heat capacity dependence to temperature ($C_p = f(T)$), this temperature difference may become higher or lesser. Therefore, the calibration measurements should be performed under the conditions that are very close to the conditions of actual kinetic measurements. For typical non-isothermal experiment the conditions that requires calibration are; heating rate (°C/min), sample holder type (platinum/alumina), inert gas and inert gas flow rate (mL/min), sample mass [39, 40, 41]. Addition to the heat capacity effect, Vyazovkin et al. stated in his work that the temperature difference will increase when conducting experiments at faster heating rates. This deviation can cause and error of 10 – 20% in frequency factor (A) and apparent activation energy (E_a) [37].

In order to acquire the accurate thermal analysis data (moderate reaction rates and removal of evolved gas from reaction), one needs to optimize experimental

conditions of the process. The conditions that are controlled during a non-isothermal run are:

- Heating rate (°C/min)
- Pan material
- Sample mass
- Sample size and form
- Reaction chamber atmosphere
- Flow rate of purge gas (mL/min)

By investigating the impact of these experimental conditions theoretically, basis for experimental conditions will be established that is going to be used in experimental part.

Heating rate:

ICTAC Kinetics Committee recommends using heating rates as low as 2 °C/min at first. Maximum heating rate should not exceed 10 °C/min to avoid accelerating the reaction rate to the point of self-heating of the sample [41]. Self-heating can be explained as the heat accumulation inside the sample and the increase of temperature in the sample causing unwanted acceleration of reaction rate. Main causes for this phenomenon to occur are the high heat release rate or the inefficient heat transfer from sample to environment due to thermal contact resistance between sample and sample holder.

It has been reported that as heating rate is increased heat powder decomposition rate peak temperature shifts to higher values [4]. This shift of the temperature where reaction rate is maximum is based on the reaction kinetics. Lowering heating rate causes moderation of reaction, therefore heat production/absorption from reaction becomes slower.

Pan (sample holder) material:

The pan materials should be selected in a way that it does not react with sample nor catalyze the reaction. Platinum, silver, aluminum, alumina ceramic, silica glass etc. are used as typical pan materials. As well as non-reactivity with sample, pan should not go through a transition in the temperature range of thermal experiment and

should have high thermal conductivity [41]. In order to select best pan material to be used for thermal analysis of heat pellets, literature of reactivity between reactants and pan material and thermal conductivity of pan material were investigated.

The material with highest thermal conductivity is platinum with 71.6 W/m.K conductivity at room temperature. Glasner et al. found out in their research that platinum can be used as a $KClO_4$ reduction catalyst [42]. With this knowledge, platinum pan is regarded as unsuitable. As well as platinum, metal materials are known to be prone to cause catalytic parasites in $KClO_4$ reduction. Therefore, ceramic pans are investigated: Furuichi et al. stated in this study that potassium perchlorate ($KClO_4$) decomposition in the presence of alumina (α-Al_2O_3) does not affect the process of decomposition at all. Additionally, alumina has thermal conductivity of 20 W/m.K. To sum up, alumina pan will be considered as the strongest candidate for the experimental method.

Sample mass:

Ideally, sample mass should be kept small but not so small that the change in mass or heat when reaction undergoes could be easily detected. ICTAC Kinetics Committee stated in their work that, for the first run 3 mg is good choice. According to the results obtained mass of sample may be incrementally increased [41].

Sample size and form:

Large variability in the particle size of pellets may result non-uniform temperature distribution in sample; therefore it should be avoided whenever possible. As well as particle size difference, when dealing with solid samples, sample form should be as thin as possible to avoid heat accumulation inside the sample [41].

Reaction chamber atmosphere:

In the thermal analysis, nitrogen or argon as an inert gas is usually used to purge the reactor. It was pointed out in Vyazovkin et al.'s study that purging the reaction chamber for 20-30 minutes prior to thermal analysis gives best results [41, 37].

Flow rate of purge gas:

As it is pointed out in the recommendations of ICTAC Kinetic Research Committee, inert gas flow should be close to 100 mL/min for first run [41].

2.6. Survey on Kinetic Parameter Determination Procedures

The main characteristic of the SDT experiments that were developed were based on non-isothermal experiments. Because of this fact, kinetic methods that are only applicable for non-isothermal experiments will be studied in this section.

Kinetic parameters to be determined using these procedures are;

- Apparent activation energy (E_a, kJ/mol),
- Frequency factor (A, s^{-1}),
- Reaction model (f(α)).

In the next section, the review of methods that are commonly employed for determining activation energy is identified and reviewed. Visual categorization of these methods is given in Figure 15.
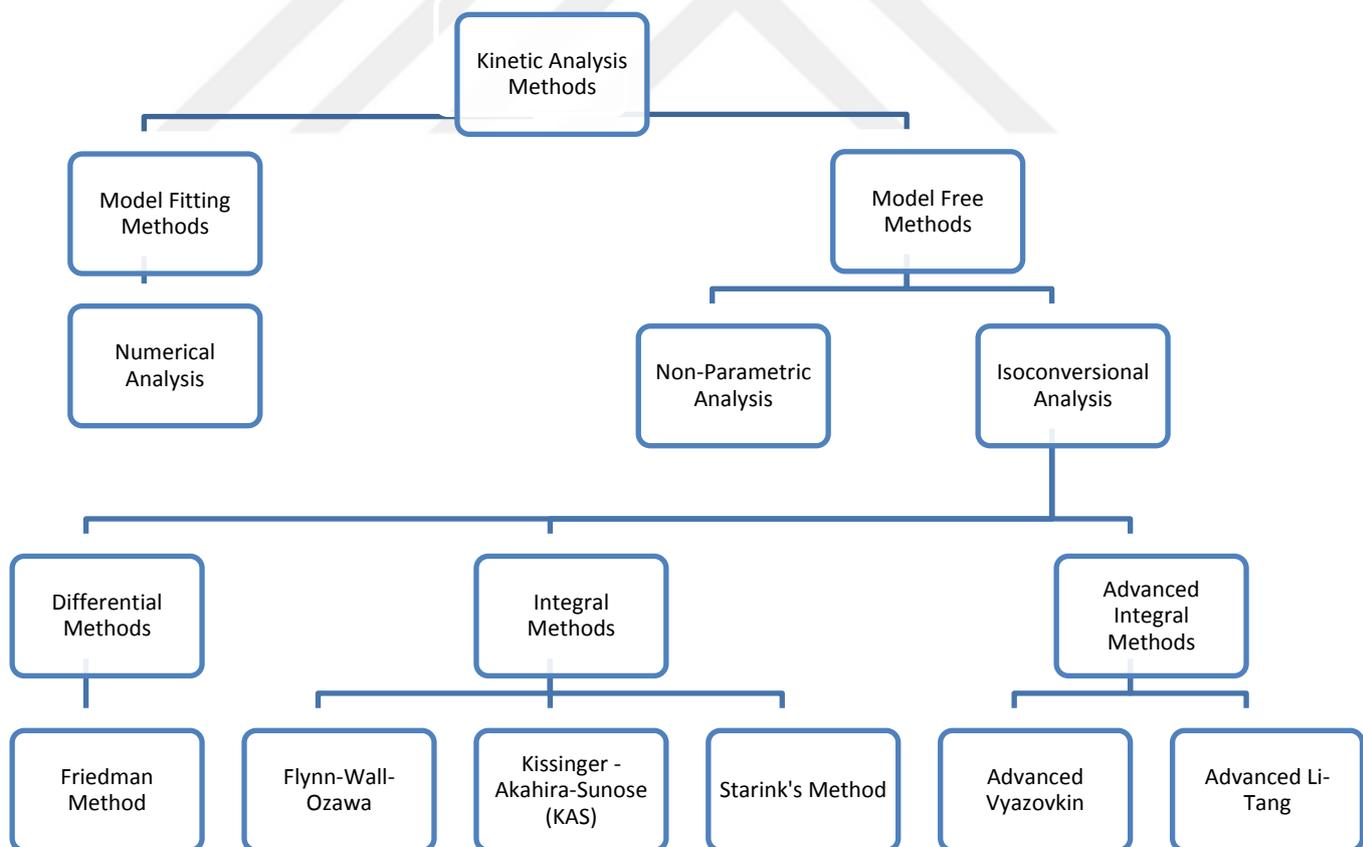
Figure 15. Methods for determination of activation energy [37]

2.6.1. Methods for Determination of Apparent Activation Energy

The methods used for determination of apparent activation energy can be classified into two as:

a. model fitting methods,
b. model-free methods.

Model Fitting Methods:

Model fitting employs fitting of reaction models f(α) or g(α) into the general kinetic equation (Equation (10)). Values of kinetic parameters (E_a, A) are determined using regression analysis. By regression analysis, the difference between experimental and theoretical data is tried to be minimized by adjusting kinetic parameters through iterative analysis [37].

Linear and non-linear approaches could be employed in model fitting methods. In linear model fitting, first step would be to linearize rate equation (Equation (10)) by taking natural logarithm. Taking natural logarithm will linearize reaction rate (dα/dt) respect to reciprocal of temperature (1/T).

$$\ln\left[\beta\left(\frac{d\alpha}{dT}\right)\right] = \ln(f(\alpha)A) - \frac{E}{RT} \tag{12}$$

In order to determine the kinetic triplet one needs to fist assume an appropriate reaction model. For linear model fitting usually a reaction model in general form is assumed:

$$f(\alpha) = c\alpha^m(1-\alpha)^n \tag{13}$$

where c, m and n are constants. This type of reaction model is called the modified truncated Seŝtak-Berggren [37, 43]. By varying parameters c,n and m this reaction model fits to the various models given in Table 2. Parameters of fitted reaction models are given in Table 6.

Table 6. Modified truncated Seŝtak-Berggren parameters for selected reaction models [37]

Reaction Model	f(α)	Parameters of M. T. Seŝtak-Berggren Equation
Contracting Area	$2(1-\alpha)^{1/2}$	$2(1-\alpha)^{1/2}$
Contracting Volume	$3(1-\alpha)^{2/3}$	$3(1-\alpha)^{2/3}$
First Order	$(1-\alpha)$	$(1-\alpha)$
Avrami-Erofeyev-2	$2(1-\alpha)[-\ln(1-\alpha)]^{1/2}$	$2.079(1-\alpha)^{0.806}\alpha^{0.515}$
Avrami-Erofeyev-3	$3(1-\alpha)[-\ln(1-\alpha)]^{2/3}$	$3.192(1-\alpha)^{0.748}\alpha^{0.693}$
2-D Diffusion	$-[1/\ln(1-\alpha)]$	$0.973(1-\alpha)^{0.425}\alpha^{-1.008}$

Rearranging Equation (12) and (13) one can get the general form of the equation to be used in linear model fitting [44]:

$$\ln\left[\left(\frac{\beta}{\alpha^m(1-\alpha)^n}\right)\left(\frac{d\alpha}{dT}\right)\right] = \ln(cA) - \frac{E}{RT} \tag{14}$$

To evaluate kinetic parameters utilizing Equation (14), one needs to acquire conversion (α) or reaction rate (dα/dt) values versus temperature experimentally. These data are acquired using thermal analysis methods. Through using several non-isothermal thermal analyses with varying heating rate, β, linearized data of the left hand side of the Equation (14) vs. reciprocal of temperature (1/T) can be acquired for different sets of n and m parameters.

Non-linear model fitting is ideal for the kinetic analysis of multi-step processes. This method uses regression by minimizing the difference between the experimental and calculated data without linearizing the general kinetic equation (Equation (10)). This common method is termed as least squares method and mathematically expressed as follows [37]:

$$\text{Residual Sum of Squares (RSS)} = \sum (y_{exp} - y_{calc})^2 \tag{15}$$

This methodology consists of finding the values of kinetic parameters (E_a, A, c, n and m) that minimizes the residual sum of square for different heating program experiments. To accomplish that, good initial values should be used. After attaining initial values to parameters, iterative procedure calculates RSS for each iteration until global minimum is found [45]. This iteration routine can be constructed using software

(MATLAB, COMSOL) easily. Importance of the initial values should be emphasized because it is pointed out that results are highly dependent upon the initial values used [37].

Summing up, utilizing model-fitting methods without prior knowledge about the kinetics of the investigated process give rise to accuracy problems. According to ICTAC Kinetic Committee, preliminary work should be conducted such as applying Malek's kinetic procedure (or Master-plot method) to determine the reaction model. Without defining reaction model correctly or other kinetic parameters, solving for kinetic parameters becomes fruitless [37]. Consequently, it would be ideal to first establish the correlation between conversion, α and reaction model, f(α) (Equation (10)).

Model-free Methods:

Model-free methods or isoconversional methods are employed without assuming reaction model to determine the activation energy. Model free methods can be classified into three different categories according to the mathematical method it utilize:

a. Differential isoconversional,
b. Integral isoconversional,
c. Modulated or advanced integral methods [46].

Isoconversional Methods:

Without assuming any reaction model for the investigated kinetic process, isoconversional method lets one to acquire apparent activation energy (E_a) at a given conversion (α). Isoconversional methods are widely employed in pyrotechnic kinetic analysis [19, 47, 48, 49, 50]. Particularly Starink's method based on the Kissinger-Akahira-Sunose (KAS) method is known to be more accurate than its predecessor [37, 51].

Isoconversional principle takes root from the principle that reaction rate is only the function of temperature at a given conversion. Mathematically this assumption can be described as:

$$\frac{d\alpha}{dT} = f(T)_\alpha \tag{16}$$

This assumption is mathematically further explained using general kinetic equation (10) with the given expression taking natural logarithmic derivative:

$$\left[\frac{\partial \ln(d\alpha/dT)}{\partial T^{-1}}\right]_\alpha = \left[\frac{\partial \ln k(T)}{\partial T^{-1}}\right]_\alpha - \left[\frac{\partial \ln f(\alpha)}{\partial T^{-1}}\right]_\alpha \tag{17}$$

At a fixed conversion, since reaction model f(α) becomes constant, derivation gives zero and equation (17) becomes as follows:

$$\left[\frac{\partial \ln(d\alpha/dT)}{\partial T^{-1}}\right]_\alpha = \frac{-E_\alpha}{R} \tag{18}$$

Isoconversional methods take root from the relation presented in Equation (18).

Differential Isoconversional Methods:

Mathematical start point of differential isoconversional method is the Equation (10). This method is firstly employed by Friedman et al. [52] for kinetic analysis of the thermal degradation of phenolic resins. According to the thermal analysis method to be used (isothermal and non-isothermal) general kinetic equation of (9) or (10) is used. Since, non-isothermal methods are chosen to be the valid method for pyrotechnic kinetic analysis as per literature review, only non-isothermal expression will be considered.

Differential isoconversional expression for non-isothermal experiments can be derived by taking natural logarithms of the general kinetic equation. Through this derivation one can arrive to the equation (12) with appropriate subscription, i denoting the heating rates (β) used.

$$\ln\left[\beta_i\left(\frac{d\alpha}{dT}\right)\right] = \ln(f(\alpha)A) - \frac{E_a}{RT_i} \tag{19}$$

Recall that in isoconversional principle, at a given conversion, α reaction model, f(α) and frequency factor, A should be constant. Therefore, slope of the plot of ln[βi(dα/dT)] vs. 1/Ti for experiments with different heating rates will give the apparent activation energy (E_a). Since differential data is directly used in this approach, possible noise in the data is magnified and may lead to apparent activation output

with high deviation [37, 53]. Therefore, ICTAC Kinetics committee advises the use of integral isoconversional methods.

ICTAC Kinetics Committee also advises the use of at least three or more non-isothermal analysis data with different heating rates [37]. In order to obtain linear curve with good correlation factor ($r > 0.98$) at the plot of $\ln[\beta_i(d\alpha/dT)]$ vs. $1/T_i$, using at least three non-isothermal data is a necessity. Also, Vyazovkin et al. pointed out in his work that for accurate determination of activation energy, linear curves with correlation factor that is higher than 0.98 should be used in plot of $\ln[\beta_i(d\alpha/dT)]$ vs. $1/T_i$ [54].

Integral Isoconversional Methods:

This approach is based on the separation of variables and integrating Equation (10). Obtained integral form of reaction conversion for utilization of integral conversion methods:

$$g(\alpha) = \int_0^\alpha \frac{d\alpha}{f(\alpha)} = \frac{A}{\beta} \int_0^T e^{\left(-E_a/RT\right)} dT \cong \frac{AE}{\beta R} p \left[\left(E/RT \right)_\alpha \right] \qquad \textbf{(20)}$$

where $g(\alpha)$ is termed as the integral form of reaction model, $f(\alpha)$. Temperature integral is analytically unsolvable. Therefore, $p(E/RT)$ approximation is used. The equation to be used to solve the temperature integral approximation, $p(E/RT)$ at the right side of the equation makes the difference between various methods such as Kissinger, Kissinger-Akahira-Sunose (KAS), Flynn-Wall-Ozawa (FWO) and Starink method. Like the differential isoconversional methods, integral isoconversional methods also require analysis of plot which is $\ln(\beta/T^x)$ vs. $1/T$. "x" uppercase varies with the method to be used. "x" value is dictated by temperature integral approximation that is used in the integral isoconversional method. The accuracy of the mentioned integral isoconversional methods are discussed below:

1. *The FWO Method:*

    The FWO method uses the Doyle appromixation to calculate temperature integral in the right hand side of the Equation (20) [55]. By implementing approximation of

36

Doyle, p(E/RT) to the Equation (20), FWO method's equation can be derived as follows:

$$\ln\beta_i = -1.0.516\frac{E}{RT_i} + ln\frac{0.0048AE}{Rg(\alpha)} \tag{21}$$

where g(α) is the integral form of the reaction models given in Table 2. g(α) function has a constant value for a given conversion. Therefore, activation energy value is obtained by calculating the slope of the linear $\ln\beta_i$ vs. $1/RT_i$ plot for fixed conversion values.

Some studies reported that FWO method gives inaccurate results for estimation of activation energy due to errors of the Doyle approximation [56, 57, 54].

2. *The KAS Method:*

The KAS method uses Coats-Redfern approximation to calculate temperature integral in Equation (20) [58]. This method is the most known and employed isoconversional method. By using Coats-Redfern approximation, derived equation is as follows:

$$\ln\left(\frac{\beta}{T_i^2}\right) = -\frac{E}{RT_i} + ln\frac{AR}{Eg(\alpha)} \tag{22}$$

The slope of plotting $\ln(\beta/T^2)$ vs. $1/T$ gives the value of E/R for given conversion.

3. *Starink Method:*

Starink pointed out in his work that using his approximation for the temperature integral leads to a highly accurate method for estimating activation energy as it is acknowledged by the ICTAC Kinetic Committee as well [37, 51]. The following equation derived for this approximation is given below.

$$\ln\left(\frac{\beta}{T_i^{1.92}}\right) = -1.0008\frac{E}{RT_i} + ln\frac{AR}{Eg(\alpha)} \tag{23}$$

Similar to the KAS method, the slope of plot $\ln(\beta/T^{1.92})$ vs. $1/T$ gives E/R at a specified conversion.

Example of the Starink plot for the evaluation of apparent activation energy, Ea for the Mg/NaNO3 pyrotechnic ignition process for conversions between 0.1 - 0.9 is given below [48].
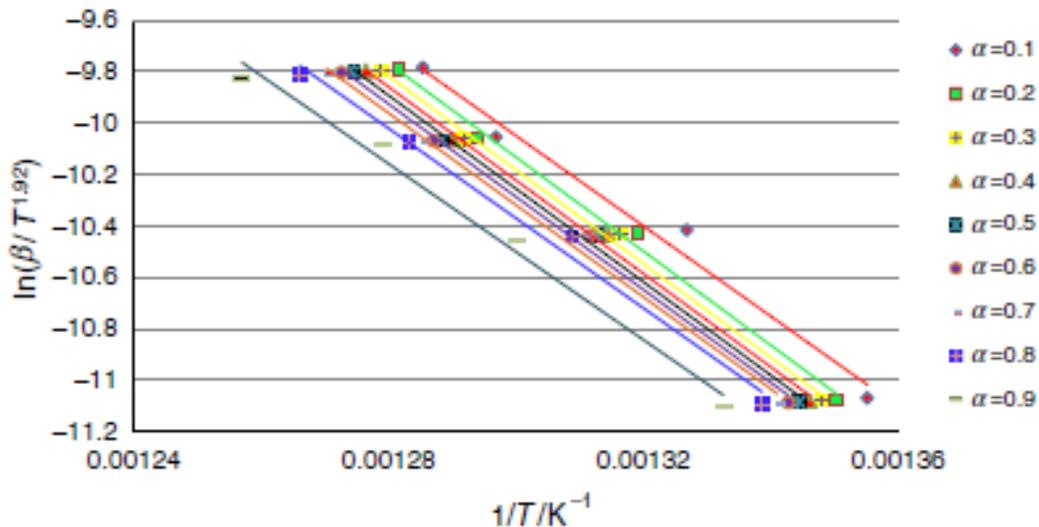
Figure 16. Starink plots for conversions starting from 0.1 to 0.9 with four (4) different heating rates

Modulated Isoconversional Methods:

In this method, temperature program is not set to constant heating rate. It is modulated for the process at hand. Typical modulation used is the frequency dependent, $T = \sin(2\pi\omega t)$ type [37].

2.6.2.   Methods for Determination of Reaction Model

A reaction model is a theoretical, mathematical description of what occurs experimentally. In solid state reactions, a model describes a particular reaction mechanism. By applying the reaction model, one can determine the reaction rate dictated by that particular mechanism.

Two simple techniques are employed in literature to determine the reaction model (f(α)) as well as the frequency factor (A) of the kinetic process at hand. These methods are:

a. Invariant Kinetic Parameters Method
b. Malek's Kinetic Method

Invariant Kinetic Parameters Method:

This method arises from the relation called the "compensation effect" that can be mathematically expressed as follows [59, 60]:

$$\ln(A) = a + bE \qquad \textbf{(24)}$$

where $a=1/RT_{max}$ and $b=\beta E/RT^2_{max}$. Max subscript denotes the temperature value when the reaction rate is maximum. Using this relation, Lesnikovich et al. proposed that for several heating rate experiments, linear regression lines of Equation (24) intersect at a point for unique set of kinetic parameters. Using this relation, one can obtain the frequency factor(A). Using the frequency factor and activation energy, model fitting methods can be directly employed.

Malek's Kinetic Method:

Malek's kinetic procedure principle depends on graphically analyzing $y(\alpha)$ and $z(\alpha)$ "master plots" calculated from the experimental data. Utilizing this method in conjunction with the aforementioned isoconversional methods, one would be able to determine all the kinetic parameters (E_a, A, $f(\alpha)$) for a kinetic process.

To use this method, first check would be to be sure that investigated kinetic process obeys the Arrhenius kinetic relation. This check can be done by obtaining activation energy (E_a) with varying conversion using isoconversional methods. If the variation of the obtained activation is limited to $\pm$ 10-15 %, then it can be assumed that reaction proceeds in one step fashion, thus obeys the Arrhenius relation. Average value of the obtained activation energy (E_{avg}) is implemented to the equation below to obtain one of the master plots, $y(\alpha)$:

$$y(\alpha) = \left(\frac{d\alpha}{dt}\right)_\alpha exp\left(\frac{E_{avg}}{RT_\alpha}\right) = Af(\alpha) \qquad \textbf{(25)}$$

Equation (25) is derived from the equation (10), by inserting the experimentally obtained data $(d\alpha/dt)_\alpha$ and the average value of activation energy (E_{avg}) obtained by using isoconversional methods, $y(\alpha)$ can be calculated. For the investigated kinetic process, $y(\alpha)$ vs. α plot is obtained and then compared with the theoretical $y(\alpha)$ curves obtained for the reaction models given in Table 2.

Since frequency factor (A) is constant, $y(\alpha)$ plot is determined by the reaction model. Therefore, it is considered to be a valid tool to use for determination of reaction model [37, 59]. Theoretical $y(\alpha)$ plots for selected reaction models from Table 2 is given in Figure 17 below.
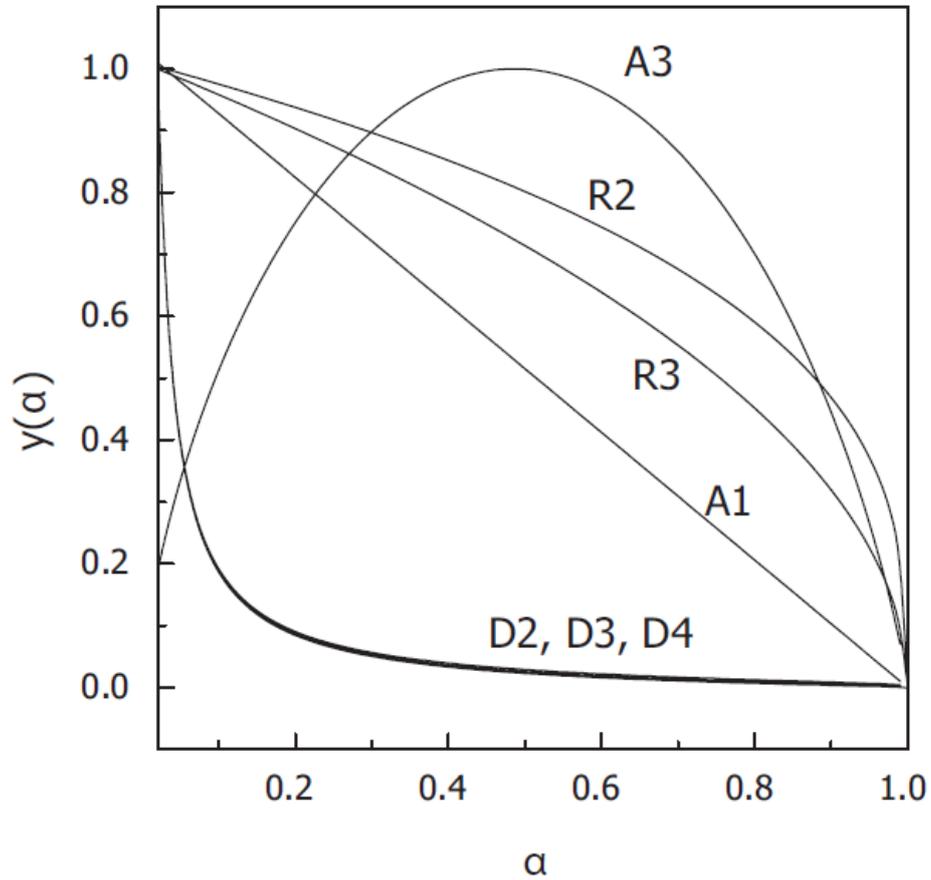
Figure 17. Theoretical y(α) plots [37]

For each reaction model, there is a certain conversion value (α_y) when the $y(\alpha)$ function has its maximum value. Likewise, conversion where $z(\alpha)$ has maximum is termed as α_z. These conversion values for kinetic models are given below.

Table 7. α_y and α_z values for the y(α) and z(α) functions [54]$\alpha\alpha$

Reaction Model, f(α)	The conversion where y(α) is maximum, α_y	The conversion where z(α) is maximum, α_z
Contracting Area (R2)	0	0.750
Contracting Volume (R3)	0	0.704
First-Order (F1)	0	0.632
Avrami-Erofeyev (A2)	0.393	0.632
Avrami-Erofeyev (A3)	0.283	0.632
Extended Prout-Tompkins (B2)	m/(n+m)	–
2-D Diffusion (D2)	0	0.834

Additionally, z(α) master plot is used as well. z(α) plot is mathematically expressed as the multiplication of the differential (f(α)) and the integral (g(α)) reaction model vs. conversion. Recalling integral form of the reaction model (Equation (20)):

$$g(\alpha) = \int_0^\alpha \frac{d\alpha}{f(\alpha)} = \frac{A}{\beta}\int_0^T e^{\left(-E_a/RT\right)}dT \cong \frac{AE}{\beta R}p\left[\left(E/RT\right)_\alpha\right]$$

z(α) is expressed as follows combining equations (10) and (20):

$$z(\alpha) = f(\alpha)g(\alpha) = \left(\frac{d\alpha}{dt}\right)_\alpha T_\alpha^2 \left(\frac{p[(E/RT)_\alpha]}{\beta T_\alpha}\right) \qquad \textbf{(26)}$$

where p(E/RT)$_\alpha$ is the temperature approximation at a given conversion. Using equation (26), z(α) vs. α plot can be obtained for theoretical reaction models as follows in Figure 18.
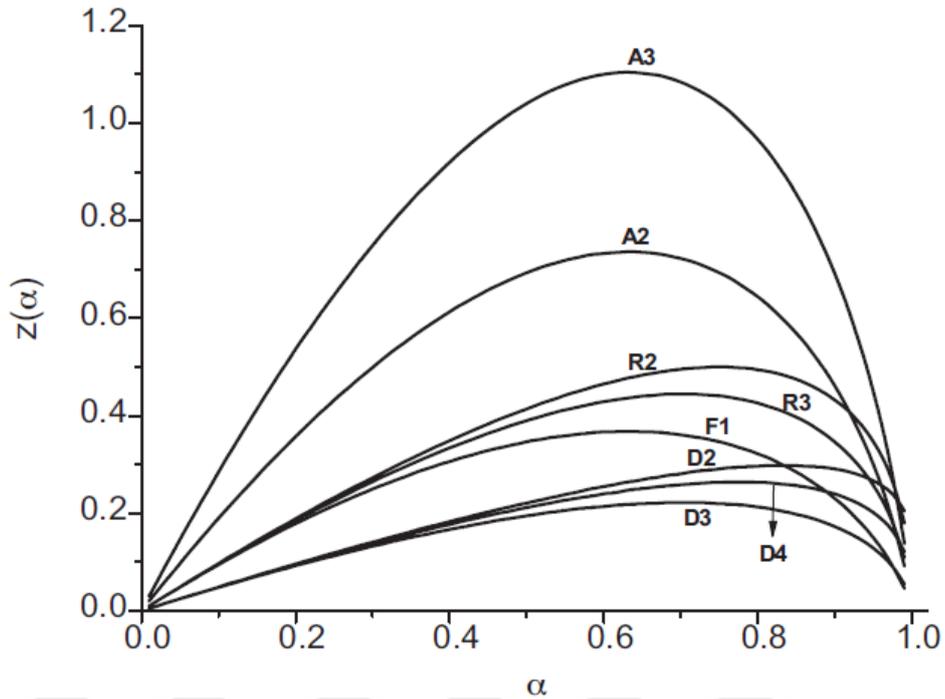
Figure 18. Theoretical z(α) plots [37]

2.7. Modelling of Burning Process

Starting from 2010, thermal battery research efforts are directed to a multi-physics simulation tool for efficient and faster development of thermal battery technologies [61, 62]. First step for the activation of thermal battery is the burning process of the heat pellet. In order to construct an accurate simulation for the operation period of thermal battery, heat pellet burning process should be well identified and studied. Significance of the heat pellet burning process is pointed out in the literature as well [63].

Several studies investigated the theory of the propagation of burning front in thermite reactions and gun propellants [64, 65, 66]. In the recent study of the Eisenreich et al. similar to the work of previously discussed Yang et. al.'s work, they proposed that for a composition of fuel and oxidizer, one or both components are in molten state before decomposition process. Moreover, Eisenreich et. al. stated that for a burning process of a pyrotechnic composition to be simulated, both mass and heat transfer equations needs to be solved simultaneously (multi-physics). The governing partial differential equations for burning process in 3-D are given below [24]:

$$\rho c_p \frac{\partial \text{T}}{\partial t} - \lambda \cdot \Delta \text{T} = \Delta \text{H}_{rxn} \frac{\partial c}{\partial t} \qquad \textbf{(27)}$$

$$\frac{\partial c}{\partial t} - D \cdot \Delta c = -\text{k(T)} C_0 f(\alpha) \qquad \textbf{(28)}$$

where ρ is the density (kg/m^3), c_p is the specific heat capacity (J/mol.K), λ the thermal conductivity (W/m.K), D is the diffusion coefficient (m^2/s), c the concentration (mol/m^3), ΔH the enthalpy of decomposition (J/mol), C_0 the initial concentration of the reactant. Equation (27) is the heat transfer equation and the equation (28) is the mass transfer equation. Eisenreich et. al. indicated that to solve these equations numerical calculation should be implemented.

In this Master's Thesis, burn rates of different weight composition $Fe/KClO_4$ heat pellets are calculated using COMSOL Multiphysics with kinetic boundary conditions which were obtained using kinetic analysis methods. Obtained theoretical burn rate values were compared with the literature values.

2.8.   Concluding Remarks on Literature Survey

The literature survey presented above showed that:

1. Since heat pellets provides necessary heat to increase the temperature in thermal battery to a certain point, accurate kinetic parameters (E_a,A,f(α)) are needed to efficiently simulate and validate new thermal battery designs.

2. Heat pellet decomposition reaction mechanism is well identified using several sources of the literature. First step of the mechanism is the melting of the one or both components of the fuel and the oxidizer of pyrotechnic heat source. Second step is the thermal decomposition of oxidizer to form oxygen atoms. Third and final step is the oxidation of the fuel in highly exothermic fashion. Additionally, it was found that reaction rate is not dependent to the ambient pressure or partial pressure.

3. Factors controlling the burn rate were discussed and the optimal physical characteristics of a heat pellet are determined. It was found that to vary the

heat output and burn rate of the heat pellet, main variable that is controlled is the weight composition of the pellet. Furthermore, for safety and performance considerations weight composition of oxidant should be varied between 12 – 18 %.

4. Most appropriate thermal analysis method for mass-preserved reaction was determined to be DSC/DTA non-isothermal experiments. To ensure accurate kinetic data results by verifying Arrhenius behavior, it was also pointed in literature that at least three runs must be conducted.

5. Kinetic parameter determination methods were evaluated. It was found out that for model fitting methods or iterative procedures, procedure should be started from some initial "guessed" values of kinetic parameters. Good starting points are obtained by using Starink's isoconversional method. Furthermore, for reaction model determination Malek's kinetic procedure was found to be an appropriate method for pyrotechnic decomposition.

6. In order to simulate burning process accurately, both energy and mass transfer equations should be calculated coupled for each mesh element. Additionally, it can be assumed that heat transfer in heat pellet media is only achieved by conduction.

3. EXPERIMENTAL METHODS

This chapter consists of the information about the materials and apparatus used in the experiments and the methodology that was pursued to determine, test and validate the kinetic parameters of heat pellets. Experimental method starts with the preparation of heat pellets by cold compaction. Before pelletizing, raw materials were obtained and characterized. Subsequently raw materials were subjected to conditioning phase which were grinding, sieving, drying and mechanically mixing. The heat pellets were prepared with varying weight compositions starting from 82/18 to 88/12 Fe/KClO$_4$ (w:w). Theoretical density percentage of pellets ($d_{pellet}/d_{theo.particle}$) was kept constant (57.5 ± 0.5%) for all heat pellets prepared. Since raw materials are susceptible to the effects of moisture, all sample preparation stages were done in dry room conditions (< 1 % RH). Kinetic analysis data were obtained using TGA/DTA. For kinetic data analysis, EXCEL® (2010) and MATLAB® (R2014A) were used as tools for data processing. COMSOL Multiphysics software (COMSOL 5.3) was used as a tool for both model fitting and the simulation of the burning process. The flowchart for the followed experimental procedure is given in Figure 19.
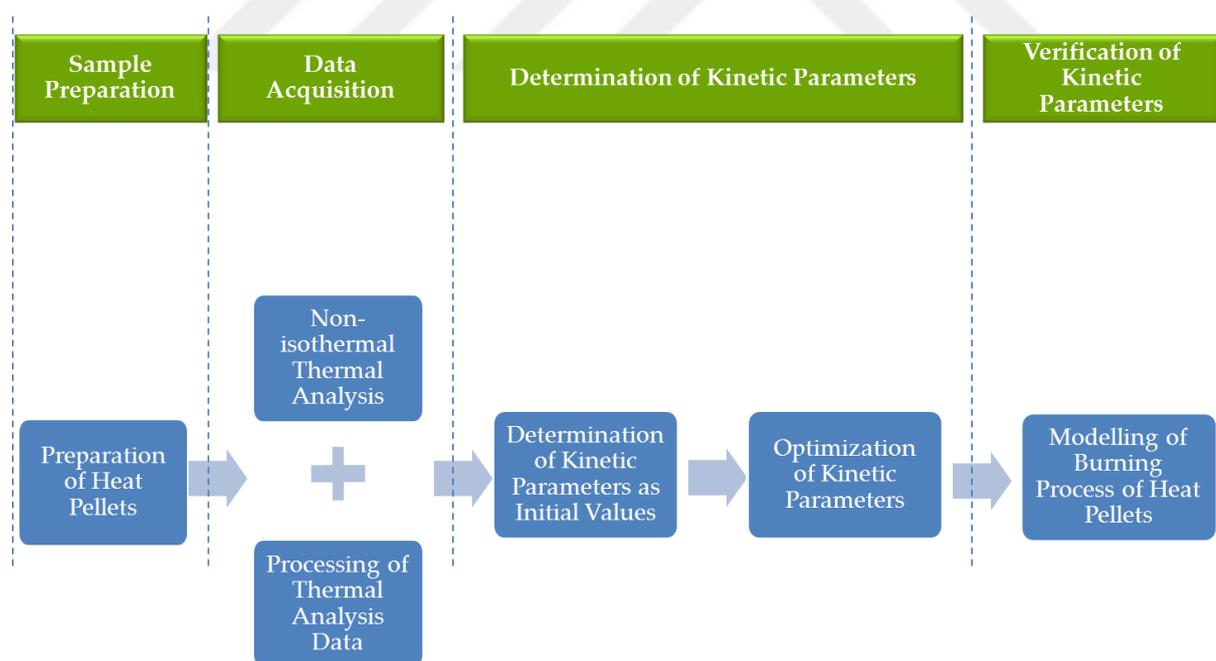
Figure 19. Flowchart of the experimental procedure

3.1. Materials

Components of heat pellet are the sponge type iron powder and the potassium perchlorate powder. Classification of sponge type is the indication of the spongy morphology of particles of iron. This morphology was verified by the micrographs obtained from a scanning electron microscope (SEM).

Iron,Fe with sponge type morphology was obtained. Average particle size of the iron powder was 46 µm and the purity was above 99.9 %. It had a theoretical particle density of 7.8 g/cm^3, which was determined by a gas displacement pycnometer system.

Crystalline potassium perchlorate, $KClO_4$, was obtained. It is a white powder classified as 5.1 A oxidizer powder according to the manufacturer's safety datasheet. Its purity was above 99.5 %.

3.1.1. Chemical and Physical Structure of Raw Materials

Characterization of the raw materials was conducted using SEM micrograph, theoretical particle density, particle size and XRD analysis. The experiments were conducted in the laboratory of Defense Industries Research and Development Institute of The Scientific and Technological Research Council of Turkey at Power and Battery Unit.

3.1.1.1. Determination of Particle Size

Particle size analysis of grinded $KClO_4$ and supplied Fe powders were carried out. For particle size analysis Malvern MasterSizer 2000 was used. It had a tolerance of ±1% for measuring average particle size. For particle analysis of both samples ($KClO_4$ and Fe), sample weights of 0.2 – 0.3 grams were used. For Fe particle size analysis, pure water (Type 3) was used as the dispersant medium and for $KClO_4$ particle size analysis isopropyl alcohol (≥98% purity) was used.

3.1.1.2. Determination of Particle Morphology

Particle morphology of supplied sponge type iron was determined using a scanning electron microscopy (SEM). The SEM was based in the Middle East Technical University, Metallurgical Engineering Department with brand and model of Jeol JSM

6400. 20 kV accelerating voltage was used to acquire micrographs with magnifications of 500X, 1000X, 4000X and 5000X.

3.1.1.3. *Determination of Theoretical Density of Particles*

Theoretical density of grinded $KClO_4$ and supplied sponge type iron were determined by helium (He) pycnometer with brand and model of Accupyc II 1340. He gas was used as the penetrating agent. Care was taken to only calculate the displaced He which penetrated into the particles not voids between particles.

3.1.1.4. *Determination of Powder Purity*

X-Ray Diffraction on sponge type iron was performed to make sure that supplied iron didn't have any crystal impurities. Rigaku Miniflex II 600 was used equipped with Cu-anode as the X-Ray source. XRD analysis was performed within the 2 °theta range of 3 – 90 2 °theta with scanning rate of 1 °/mins.

3.2. Sample Preparation

The procedure that was followed to produce the heat pellets with the raw materials that were prepared was described in this section.

3.2.1. Pre-treatment of Raw Materials

Before using iron powder for the production of heat pellets, it was vacuum-dried using a vacuum furnace at 90 °C for 48 hours under dynamic vacuum. To avoid agglomerate formation, powder was sieved through No. 120 mesh (125 μm) after the drying process.

The obtained potassium perchlorate was wet due to safety considerations. Therefore, it was vacuum-dried using a vacuum furnace at 90 °C for 48 hours under dynamic vacuum. Then it was grinded using an impact mill to average particle size of 9 ± 2 μm. Average particle size was determined per the screening results for the optimal heat pellet from the study of Guidotti el al. [2]. Theoretical particle density of the grinded $KClO_4$ was determined as 2.52 g/cm^3. Before using $KClO_4$ for heat pellet preparation, agglomerates in the powder were eliminated by sieving the powder through No. 120 mesh (125 μm).

Before compaction process, powders were homogenously mixed for 120±5 minutes (90 rpm) with appropriate amounts of iron and potassium perchlorate powders using mechanical shaker and mixer. The antistatic container used for this process was the 3M Velostat with 1L volume due to its electro-discharge characteristics to avoid unwanted ignition in the pyrotechnic mixture while mixing the powders. After blending, pyrotechnic mixture was again sieved using No. 120 mesh (125 μm).

3.2.2.   Preparation of Heat Pellets

Heat pellets with four different weight compositions were prepared. The compositions used for this study are given in Table 8. Most used optimal range of weight compositions was determined from the literature analysis. Each heat pellet had a different theoretical particle density. To calculate theoretical particle densities of the pellets used, following equation was used.

$$d_{theo.,particle} = \frac{100}{Mass\,\%_{KClO4}\Big/d_{theo.,KClO4} + Mass\,\%_{Fe}\Big/d_{theo.,Fe}} \qquad \textbf{(29)}$$

where $d_{theo.,particle}$ is the theoretical particle density (g/cm^3), mass % is the mass ratio of Fe or $KClO_4$ in the pyrotechnic mixture.

Table 8. Weight composition and theoretical particle density of heat pellets

Sample No.	Iron Powder Composition (weight %)	Potassium Perchlorate Powder Composition (weight %)	Theoretical Particle Density (g/cm^3)
1	82	18	5.699
2	84	16	5.880
3	86	14	6.072
4	88	12	6.387

The instrumentation used for the pelletizing of powder mixture of iron (Fe) and potassium perchlorate ($KClO_4$) is given in Figure 20.
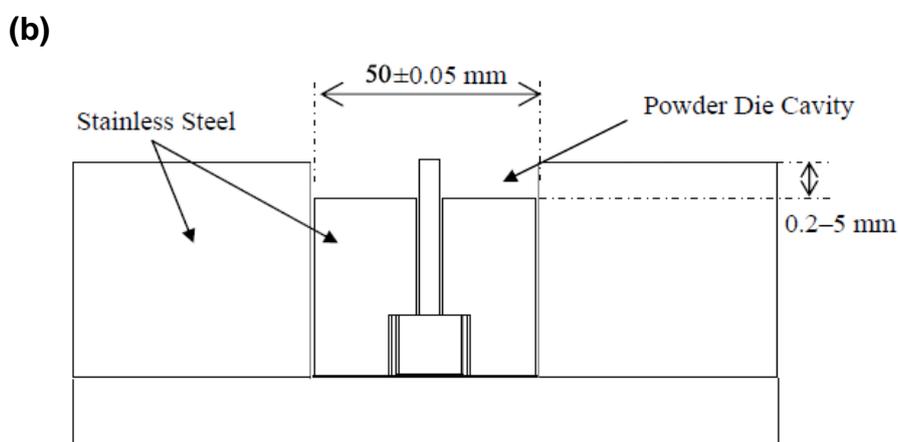
Figure 20. (a) Manual hydraulic press for heat pellet compaction, (b) representation of the die used for pellet preparation

The compaction of different weight ratio of heat pellets was done using a manual press with capability of producing load of 0 – 100 tons (Figure 20 – (a)). The press had an error margin of ±2% for load. For preparing heat pellets with outer diameter of 50 mm and hole diameter of 5 mm, appropriate tooling was used (Figure 20 – (b)). First, pyrotechnic mixture was weighed using an analytical balance with ±0.01 g

accuracy. Weight of the pyrotechnic pellets were kept constant at 3.92 ± 0.05 g. Prepared pyrotechnic mixture was dispersed using a rod into the powder die cavity of the tooling used. To maintain theoretical density percentage of pellets at 57.5 ± 0.5%, thickness of the pellets were varied by applying different compression loads between 10 – 40 tons. Calculations for the thickness value for different weight ratio heat pellets were performed using the equations below:

$$\frac{d_{pellet}}{d_{theo.,particle}} \times 100\% = 57.5\% \tag{30}$$

$$d_{pellet} = \frac{m_{pellet}}{(\pi R_o^2 - \pi R_i^2)h_{pellet}} \tag{31}$$

where d_{pellet} is the density of the heat pellet (g/cm^3), m_{pellet} is the mass of heat pellet (g), R_0 is the outer radius of pellet (cm), R_i is the inner radius (cm) and h_{pellet} is the thickness of the pellet (cm).

Calculated thickness values for preparing heat pellets with theoretical percent density of 57.5% are given in Table 9 below.

Table 9. Thickness values of heat pellets used

Sample No.	Thickness (mm)
1	0.61
2	0.59
3	0.57
4	0.55

Thickness values of the prepared heat pellets were measured using a digital caliper with an accuracy of 0.01 mm. For each weight composition, 20 pellets were produced. If the pellets were not used immediately for testing, they were stored in inert atmosphere of argon (0.1 atm) in sealed packages.

The heat pellet formed by pelletizing pyrotechnic mixture is given in Figure 21.
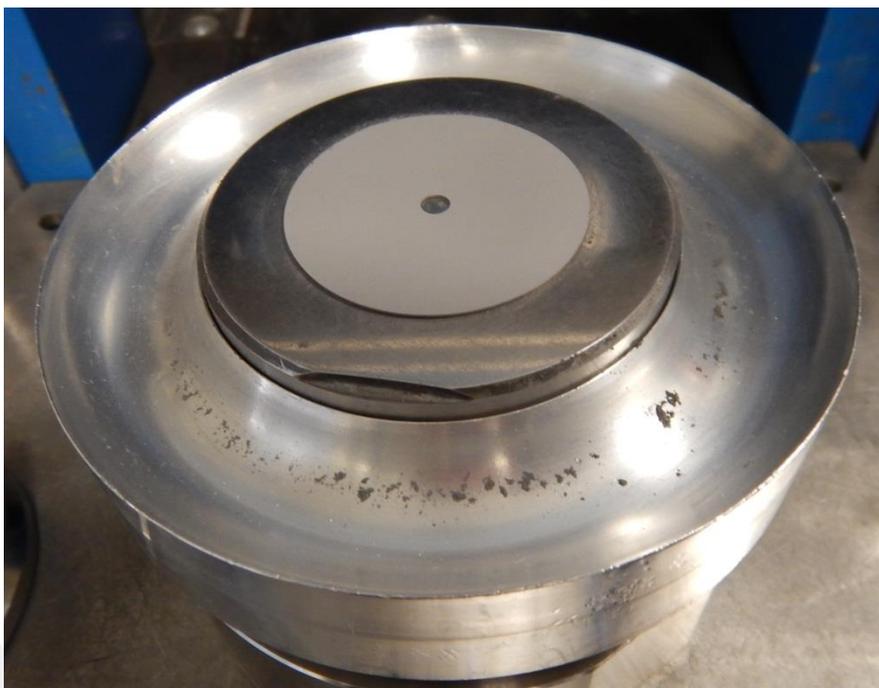
Figure 21. Compacted pyrotechnic mixture (heat pellet)

For thermal analysis tests, samples were prepared by clipping 4.5 ± 0.5 mg of heat pellet with tweezers from the edge of pyrotechnic pellet. Care was taken not to deform the clipped sample while clipping. Clipped pellets were immediately analyzed by SDT (Simultaneous Differential Technique) device with different heating rates.

3.3. Experimental Setup and Procedure

Prepared heat pellets with varying weight compositions were subjected to thermal analysis with objective of acquiring kinetic parameters. Acquired kinetic parameters were validated using burning model of the heat pellets.

Experimental procedure contained the following procedures:

1. Obtaining thermal analysis data with SDT,
2. Processing the obtained thermal analysis data,
3. Conducting kinetic analysis to obtain kinetic parameters of decomposition,
4. Fine tuning of the obtained kinetic parameters,
5. Simulation of burning process with obtained kinetic parameters.

3.3.1. Thermal Analysis Apparatus: SDT

Non-isothermal heat flow data for thermal decomposition process of heat pellets with different weight compositions were collected by TA Instruments SDT Q600 model unit with horizontal thermo-balance (Figure 22).

Figure 22. TA Instrument SDT Q-600 for thermal decomposition analysis

Experimental conditions for DTA analysis were provided to instrument using the software called Q Series Advantage Software that was provided by the manufacturer. This software also enables the constant communication between computer and instrument thus recording the heat flow data at specified time intervals. Time interval for data collection for all experiments was set to *0.5 s/data point*. Obtained data was accessed using the TA Universal Analysis software. Detailed instrumentation information for a SDT was provided in the previous section (see Chapter 2.5).

3.3.1.1. Settings for Thermal Analysis

According to the suggestions from ICTAC kinetics committee on data collection [41], prior to non-isothermal thermal analysis, furnace chamber was purged with N_2 gas for 20 minutes to remove any remaining air inside the chamber to avoid oxidation of Fe particles in pellet. Additionally, heat flow calibrations were performed for elimination

of thermal background effects, every time an analysis condition (heating rate, alumina crucible) was changed.

In order to optimize thermal analysis conditions for most accurate heat flow results, several experiments were carried out with varying heating rate, flow rate of purge gas and sample mass. Sample masses were decreased from 10 mg until no evidence of self-heating was observed. Flow rate of purge gas was varied within 50 – 200 mL/mins.

Heating program was established after optimizing the experimental conditions. Optimization study is briefly discussed in the next chapter. Heating program that was applied for all experiments are given below:

- Sample holder: Alumina
- Flow rate of N_2 gas: 100 mL/min.
- Heating rate: 2, 3 and 5 °C/min.
- Heating program: To observe thermal decomposition process without parasitic reactions certain heating program was applied for all experiments. Since the thermal decomposition of $KClO_4$ starts in the range of 450-465 °C. Rapid heating up to 400 °C was selected to avoid limit oxidation of Fe in the pyrotechnic mixture. Heating program was composed of following steps:
    1. Temperature equilibration of sample pans at 50 °C.
    2. Isothermal part for 20 minutes for purging of the remaining air inside reaction chamber.
    3. Temperature equilibration of sample pans at 400 °C. The starting temperature for the experiment.
    4. Ramping the temperature with a specified heating rate (2,3 and 5 °C/min) to final temperature of 600 °C.

To observe the statistical variation of the thermal analysis data, experiments were conducted three times for different weight compositions of heat pellets.

3.3.2.   Data Processing

Objective of data processing was to transform the experimental temperature vs. heat flow per sample mass (W/g) to temperature (°C) vs. conversion (α) to perform kinetic analysis.

The data obtained for the 84/16 (w:w) heat pellet and the sample data processing is represented in the figures below. The experimental data (heat flow, W/mg) is accessed using TA Universal Analysis software. It is first imported to the MATLAB® (R2014A) software. A script was executed using the input of thermal analysis data (code for this script is given in Appendix C). This script lets user to select interpolation data points on the heat flow curve (Figure 24). This interpolation curve is calculated with "cubic spline interpolation". Heat flow that was acquired three times for each dataset was averaged before they were converted to conversion vs. temperature data.
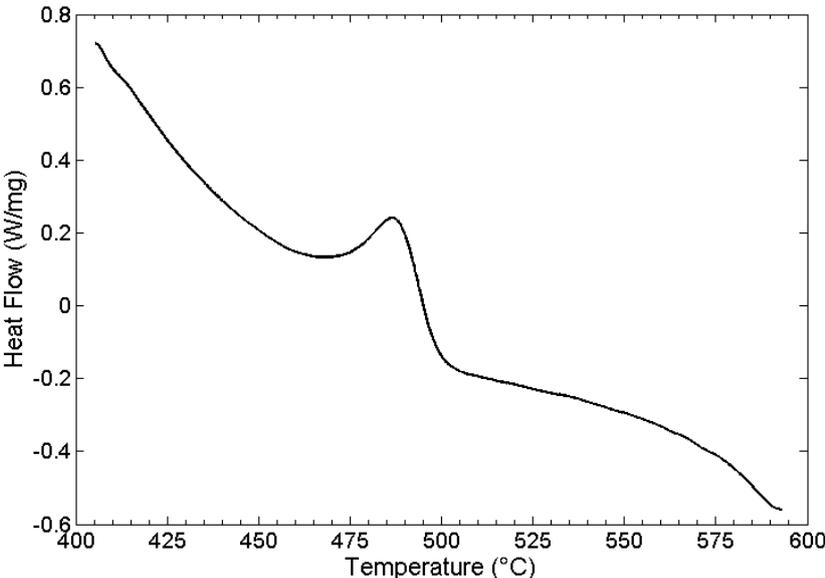
Figure 23. Raw data of 84/16 (w:w) heat pellet with heating rate of 3 °C/min
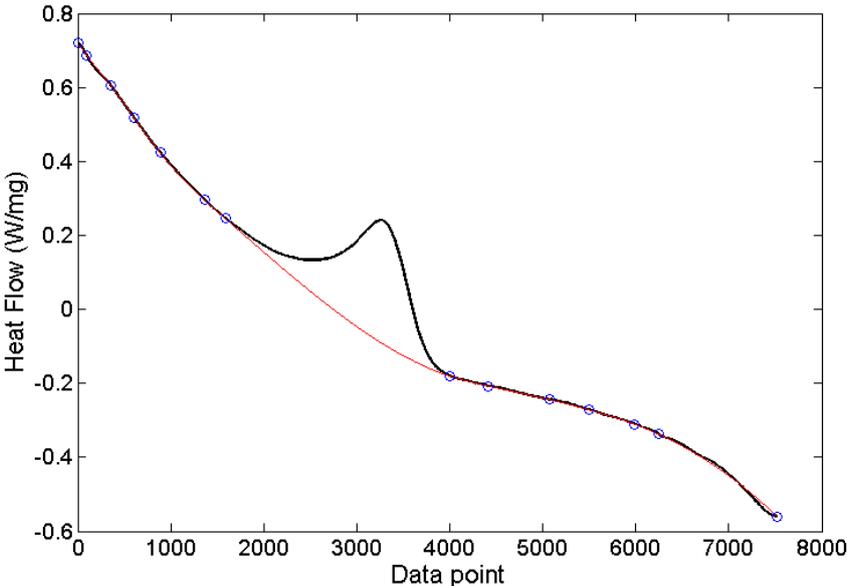
Figure 24. Cubic spline interpolated baseline of raw data given in Figure 23

54

After the determination of baseline curve, subtraction of baseline curve and heat flow curve gives the heat flow normalized to the integral heat flow or baselined heat flow (Figure 25). The necessity to obtain baselined heat flow curve comes from the need to better interpret heat flow to calculate conversion values.
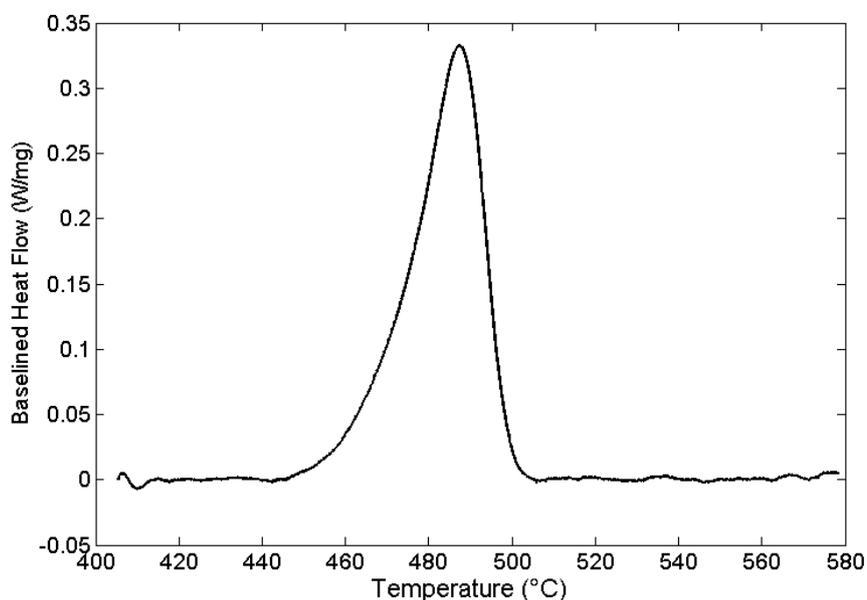
Figure 25. Subtracted baseline from raw data given in Figure 23

Equation (7) was implemented to the MATLAB® script to calculate the conversion value from baselined heat flow data for every data point starting from the thermal decomposition process till the end. Representation of the calculated total area for conversion calculation is given in Figure 26.
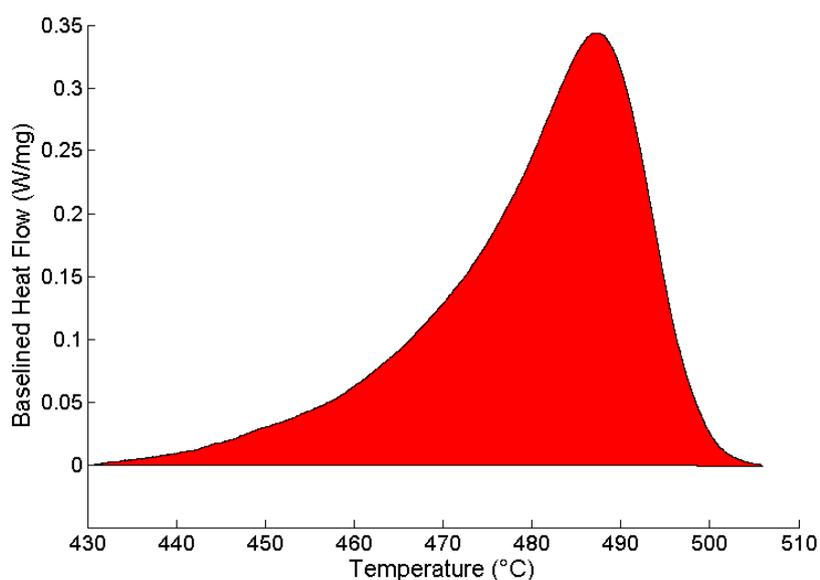
Figure 26. Calculated area of heat flow between temperatures of thermal decomposition process

55
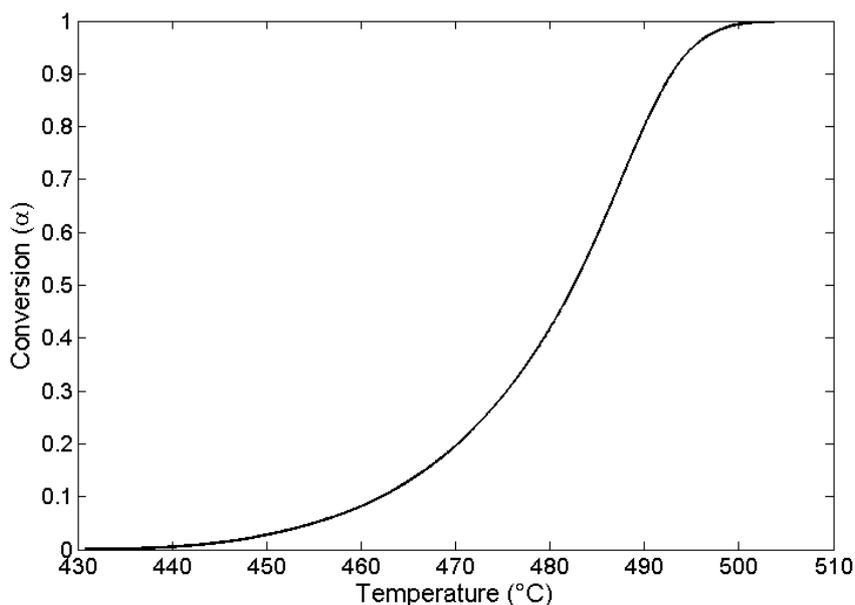
Figure 27. Transformed data of temperature (°C) vs. conversion (α) from raw data

For calculations of kinetic parameters EXCEL® (2010) was utilized as well.

3.3.3. Kinetic Parameter Determination Procedure

From the evaluation conducted in the literature survey, following kinetic parameter determination procedure steps were devised:

1. Adequate method for the determination of apparent activation energy was determined to be isoconversional method which is the Starink's modification of KAS.
2. For the determination of reaction model, using the mean activation energy as the input, master plots y(α) and z(α) were plotted and *Malek's procedure* was followed.
3. Mean activation energy and reaction model parameters were calculated analytically.

3.3.3.1. Determination of apparent activation energy

The calculated temperature vs. conversion data was transferred to EXCEL® software. Utilizing the Equation (23) which is the isoconversional expression of Starink, slope of the (1/T) vs. ($\beta/T^{1.92}$) plot gives the apparent activation energy at a specified conversion.

$$\ln\left(\frac{\beta}{T_i^{1.92}}\right) = -1.0008\frac{E}{RT_i} + ln\frac{AR}{Eg(\alpha)}$$

Starink plot of 84/16 heat pellet at conversion of 0.1 is given in the figure below.
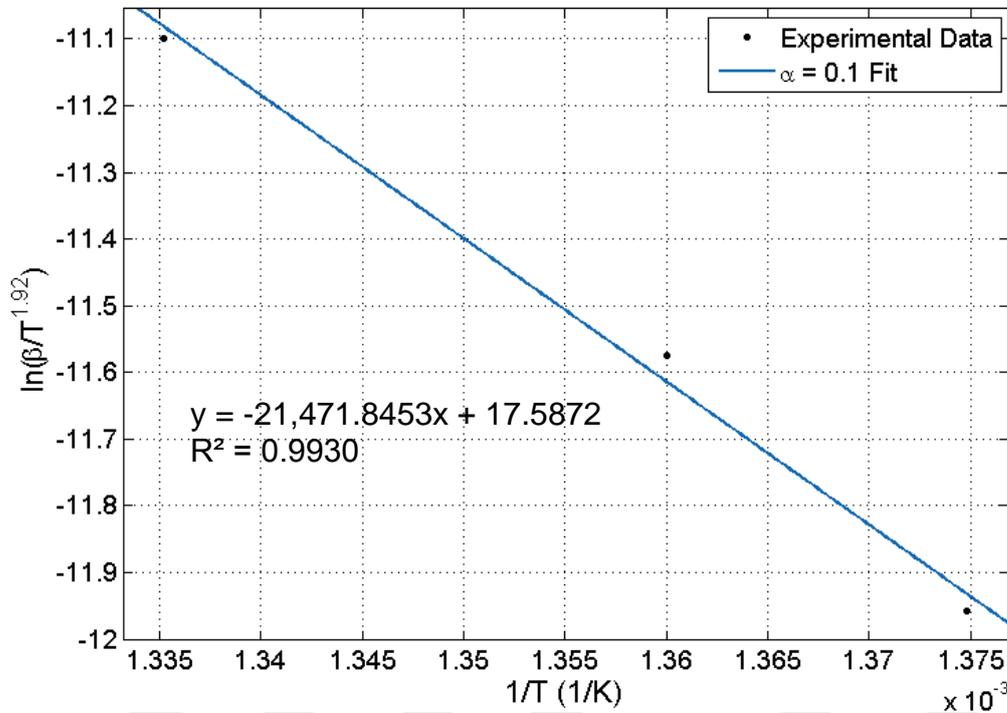
Figure 28. Sample Starink plot for 84/16 (w:w) heat pellet when conversion is 0.1

Apparent activation energy values for each conversion at the interval of $\Delta\alpha = 0.1$ were determined for heat pellets with different weight compositions. Variation of the apparent activation energy was related to the correlation factor (r) value at specified conversion value. Activation energy between conversion of 0.1 and 0.9 were calculated using the same routine.

3.3.3.2. *Determination of reaction model*

According to ICTAC Kinetics Committee, mechanistical clues about the reaction could be drawn from the thermal analysis data at the extremum heating rate [41]. In this study fastest heating rate was 5 °C/min. Beyond this value of heating rate, there were indications of self-heating (presented in results and discussion) that introduced parasitic effects to the heat flow. The slowest heating rate (2 °C/min) contains more noise resulted by the introduction of parasitic effects to the heat flow than the data

with fastest heating rate. Noise in thermal analysis data is prone to affect results dramatically [67].

As it is stated before, three experiments for each weight composition at a specified heating rate were carried out. The dataset (which contained 2,3 and 5 °C/min heating rate data) with least noise were selected for the determination of reaction model for each weight composition. Master plots, $y(\alpha)$ and $z(\alpha)$ normalized between (0,1) were plotted for thermal analysis data with 5 °C/min heating rate.

Following the procedure given in the literature survey (see Chapter 2.6.2), reaction model of the thermal decomposition of each heat pellet with different weight composition was determined.

3.3.3.3. *Determination of the pre-exponential factor*

Pre-exponential factor, A is calculated using the equation given below [37]:

$$A = -\frac{\beta E_0}{RT_{max}^2 f'(\alpha_{max})} exp\left(\frac{E_0}{RT_{max}}\right) \tag{32}$$

where max subscript denotes the temperature or conversion value where thermal analysis data reaches its maximum at the specified heating rate, β (°C/min) and E_0 (J/mol) is the average apparent activation energy calculated from isoconversional method. For the determination of pre-exponential factor, same data used for the reaction model was used. Determination of pre-exponential is the last step for kinetic parameter calculation analytically. To this point, E_a (apparent activation energy) as a function of conversion, f(α) (reaction model) and A (pre-exponential factor) were calculated. Using these parameters, reaction rate for thermal decomposition dependent upon temperature and conversion can be calculated. However, validity of the kinetic parameters is not proven yet. For validation non-linear regression utilizing optimization routine was used.

3.3.4.   Optimization of Kinetic Parameters by Model-Fitting

Non-linear regression was implemented using the optimization tool of the COMSOL Multiphysics Software 5.3. The SNOPT (Sparse Nonlinear Optimizer) optimization solver was used in this optimization tool as the algorithm for solving nonlinear least squares problem. Kinetic parameters that were obtained using analytical methods

were used as the initial values. All three heating rate experiment data were used concurrently to compare with the computed conversion data with regards to temperature.

SNOPT is a gradient-based optimization solver and is used by defining upper/lower limits for control variables. In this case, control variables are the kinetic parameters (E_a, reaction model parameters and pre-exponential factor). Initial values for the optimization model are given below.

- initial temperature (°C) of the experiment for each heating rate,
- initial concentration (mol/m^3) of the limiting reactant (C_{KClO4}),
- kinetic parameters that were obtained using analytical methods (E_a (J/mol), A (s^{-1}), $f(\alpha)$).

Initial values for the optimization model are given in Table 10 below.

Table 10. Initial values of thermal decomposition model

Weight Composition of Heat Pellet (w:w)	82/18			84/16			86/14			88/12		
Heating Rate (°C/min)	2	3	5	2	3	5	2	3	5	2	3	5
Temperature (°C)	423	433	444	419	432	445	421	429	454	423	447	460
C_{KClO4} (mol/m^3)	4257			3903			3528			3181		
C_{Fe}	48117			50838			53767			57871		
Analytically obtained kinetic parameters are given as initial values.												

Reaction engineering interface was used for the modelling of the thermal decomposition process. Interface for the COMSOL Multiphysics software for reaction engineering is shown in Figure 29. Equation (28) was used to calculate the

concentration of $KClO_4$ (limiting reactant) as a function of both temperature and conversion.

Assumptions for the optimization model are given below:

1. Thermal decomposition reaction takes place in the liquidus interface of Fe and $KClO_4$. Therefore; concentration terms are valid to be used in reaction rate expression.

2. Volume of heat pellet does not change during heat pellet decomposition.

3. Since $KClO_4$ is used below the stoichiometric ratio of 61.8/38.2 (w:w), limiting reactant is the $KClO_4$. Therefore, concentration of $KClO_4$ was used as the objective variable (objective variable is the function defined as "y" in Equation (15)).

4. Optimality tolerance was left default at 0.01.
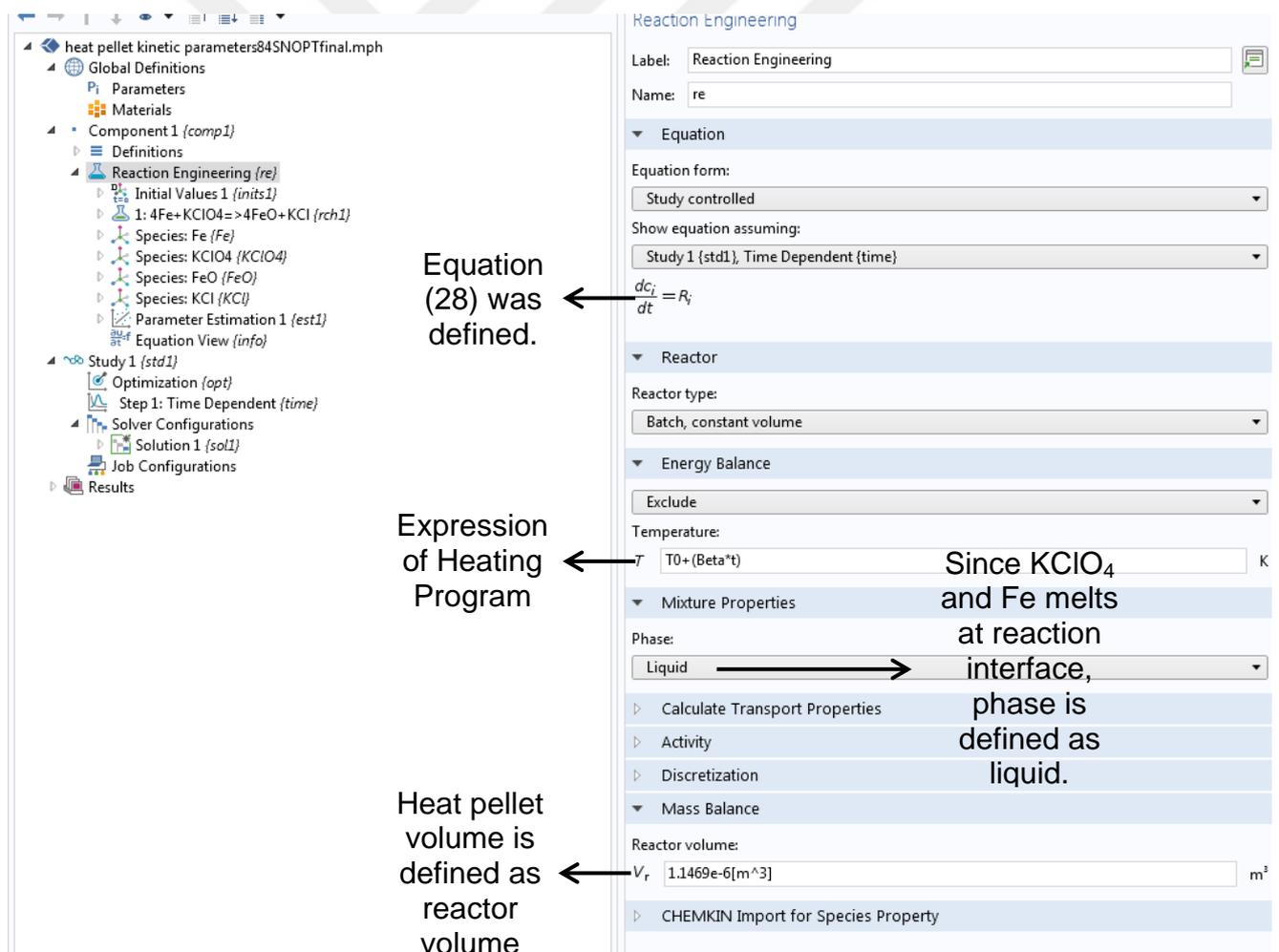
Figure 29. Interface of COMSOL Multiphysics reaction engineering module

Software is constructed to iteratively compute until the objective (the difference between model and experimental data) value is minimized within the given optimality tolerance. Using this technique, correlation coefficient between experimental and model data and optimized kinetic parameters are obtained to be used in modelling of the burning process.

3.3.5. Model Description of Burning Process

Burn models were constructed using COMSOL Multiphysics Software 5.3. Many science and engineering simulations require partial differential equations (PDE) to be solved coupled and simultaneously. This simultaneous approach is the main reason for the term "Multiphysics". In this study, physics of heat transfer of solids (which use heat transfer equation) and chemistry/transport of diluted species (which use mass transfer equation) interfaces are used to solve PDE's of heat and mass transfer simultaneously using COMSOL Multiphysics. Coupled variable for this analysis was the <u>temperature</u>.

COMSOL Multiphysics software utilizes "Finite Element Method" (FEM) as the algorithm to approximate the solution of PDE's of the physical phenomena that it deals with. FEM is basically a numerical method that is widely used by simulation software which solves PDE's using weak formulation.

Ignition and burning reactions occur quite rapidly in heat pellets and is quantified as 10 – 20 cm/s depending upon the characteristics of heat pellet (pelletizing pressure, pellet composition etc.). Accurate simulations for these types of rapid reactions largely depend on the accountability of the kinetic parameters provided. Kinetic parameters obtained from the aforementioned methods are validated utilizing the model described in this section.

Geometry of the heat pellet was identical to the prepared ones. Geometry of 84/16 heat pellet is given in Figure 30.
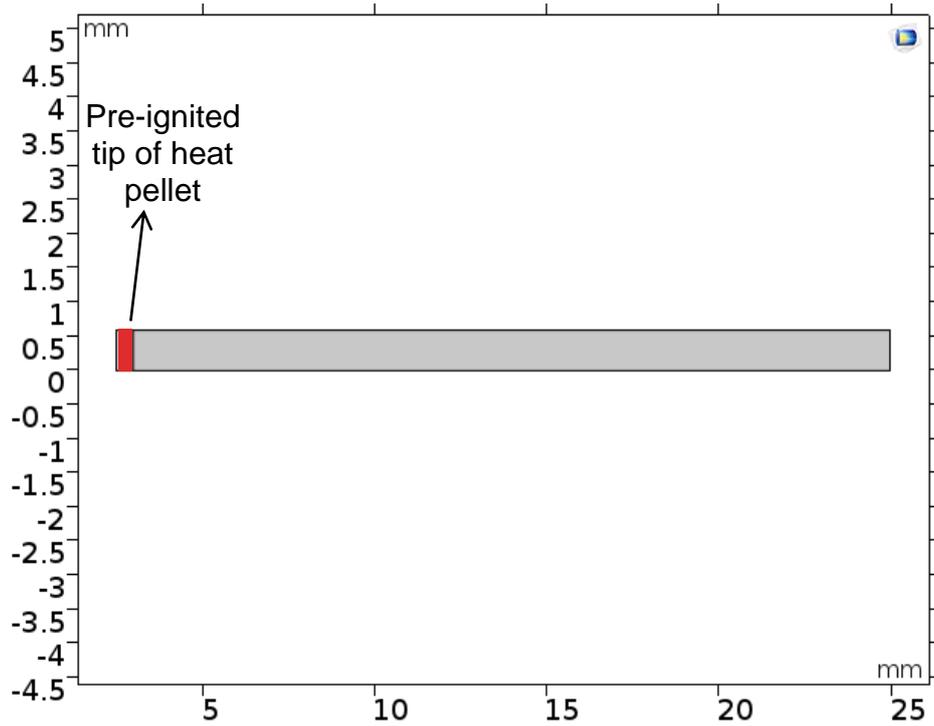
Figure 30. Geometry (domain) of heat pellet for burning process modelling

2D dimensional axisymmetric heat and mass transfer analysis were conducted based on Equations (30) and (31).

$$\rho c_p \frac{\partial \text{T}}{\partial \text{t}} - \lambda \cdot \Delta \text{T} = \Delta \text{H}_{rxn} \frac{\partial c}{\partial t} \tag{30}$$

$$\frac{\partial c}{\partial t} - D \cdot \Delta c = -\text{k(T)} C_0 f(\alpha) \tag{31}$$

For the sake of feasible convergence times in the error range of 10^{-12} and 10^{-13} following simplifications and assumptions were made:

1. It was assumed that heat transfer in the heat pellet is dominated by conduction.
2. Uniform distribution of particles throughout the heat pellet was assumed due to ideal mixing of Fe and $KClO_4$ powders prior to pelletizing.
3. Negligible mass diffusion occurs in solid state heat pellet.
4. All oxygen gas emerged from the decomposition of $KClO_4$, oxidizes Fe powder in the heat pellet due to the porous Fe particles and the interlocked structure of the binary mixture in pellet state.
5. Decomposition reaction occurs irreversibly.

6. For the typical thermal battery design, in order to ignite heat pellets in a stack with electro-explosive device, small portion of the heat pellet is positioned in the center hole. Described small portion is assumed to be heated to 1450 °C (which is the adiabatic peak temperature for the 84/16 heat pellet) at the beginning of the model, t=0.

7. Activation energy (E_a), pre-exponential factor (A), reaction model parameters are not a function of conversion nor temperature and remains constant throughout the burning process.

8. At the boundary of heat pellet, it was assumed to be no heat flow: thermal insulation.

3.3.5.1.   Settings for Modelling of Burning Process

COMSOL Multiphysics software uses different physics interfaces to simulate mathematical models. For the thermal decomposition of heat pellets following physic interfaces were used:

- Heat Transfer in Solids: used for calculating $T=f(t,r,z,Q_{reac})$.
- Chemistry: used for calculating –rA, reaction rate.
- Transport of Diluted Species, used for calculating Conversion=$f(T,r,z,t)$ and heat of reaction (Q_{reac}).

COMSOL "Model Builder" interface is shown in Figure 31 below.
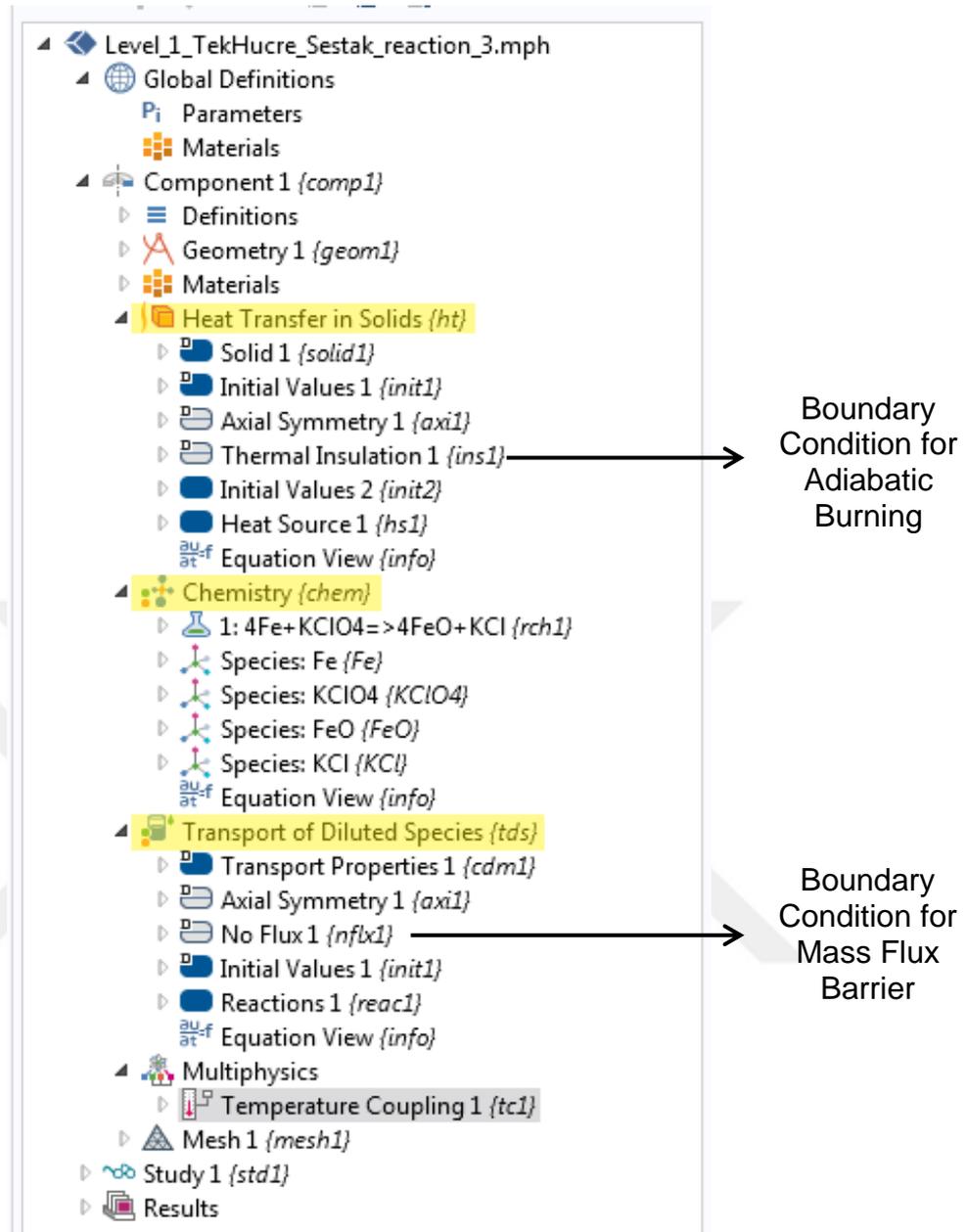
Figure 31. Physic interfaces used in model

Domain Settings:

- In heat transfer in solids interface, initial temperature values for igniting tip and rest of heat pellet is defined in Initial Values 1 {init1} and Initial Values 2 {init2}.

- In heat transfer in solids interface, heat source from reaction is defined in Heat Source 1 {hs1}.

- In transport of diluted species, initial values of concentrations of Fe and $KClO_4$ were defined in Initial Values 1 {init1}.

- In transport of diluted species, rate expressions for consumption/generation are defined for individual species under the Reactions 1 {reac1}.

64

3.3.5.2. Boundary Conditions

At the boundaries of the simulation domain, certain conditions are specified according to the assumptions. For different physic interfaces different settings were used (Figure 31):

1. For heat transfer, since it was assumed that heat pellet burns adiabatically, "thermal insulation" was defined as the boundary condition.

2. For mass transfer, since it was assumed that no diffusion occurs in and out of heat pellet domain, "no flux" was defined as the boundary condition.

3. For both physic interfaces, since it axisymmetric geometry was used "axial symmetry" was defined automatically by COMSOL.

3.3.5.3. Initial Conditions

Thermophysical and thermodynamic initial values for burning process are given in table below.

Initial concentration values were same with the optimization model (Table 10). "Value of property before burning" in Table 11 represents the unreacted part of heat pellet and "value of property after burning" represents the reacted part of heat pellet. Heat capacity and thermal conductivity of heat pellet changes depending on the state of heat pellet. Other properties (enthalpy of reaction, pellet density) that are given in Table 11 do not depend on the burned/unburned state of heat pellet. Optimized kinetic parameters were used as the initial value to calculate reaction rate.

Table 11. Thermophysical and thermodynamic initial values for heat pellet

Material Property	Value of Property before Burning	Value of Property after Burning
Enthalpy of Reaction (kJ/mol Fe)	-413.23	
Heat Capacity of Heat Pellet (J/kg.K)	430	1010
Thermal Conductivity of Heat Pellet (W/m.K)	9.32	20.40

Pellet Density of Heat Pellet (kg/m^3)	82/18	84/16	86/14	88/12
	3277	3380	3491	3673
Initial Temperature (°C)	Tip of Heat Pellet (Figure 30)		Rest of Heat Pellet (Figure 30)	
	1450		24	

For validation of kinetic parameters, kinetic parameters (E_a, A, f(α)) that were unique for that weight composition were varied for each pellet used.

3.3.5.4. Simulation Procedure

To accomplish heat pellet propagation, the used mesh should have the similar shape of propagation. Additionally, mesh density should be optimized in a way that simulation gives solution with least error in feasible times. Following this logic, meshing of the domain was done using "Mapped" mesh. Settings that accomplished least error with feasible times (30 minutes/simulation) are when maximum element size of the mesh is limited to 0.075 mm. The mesh generated using the defined settings are given in Figure 32 below.
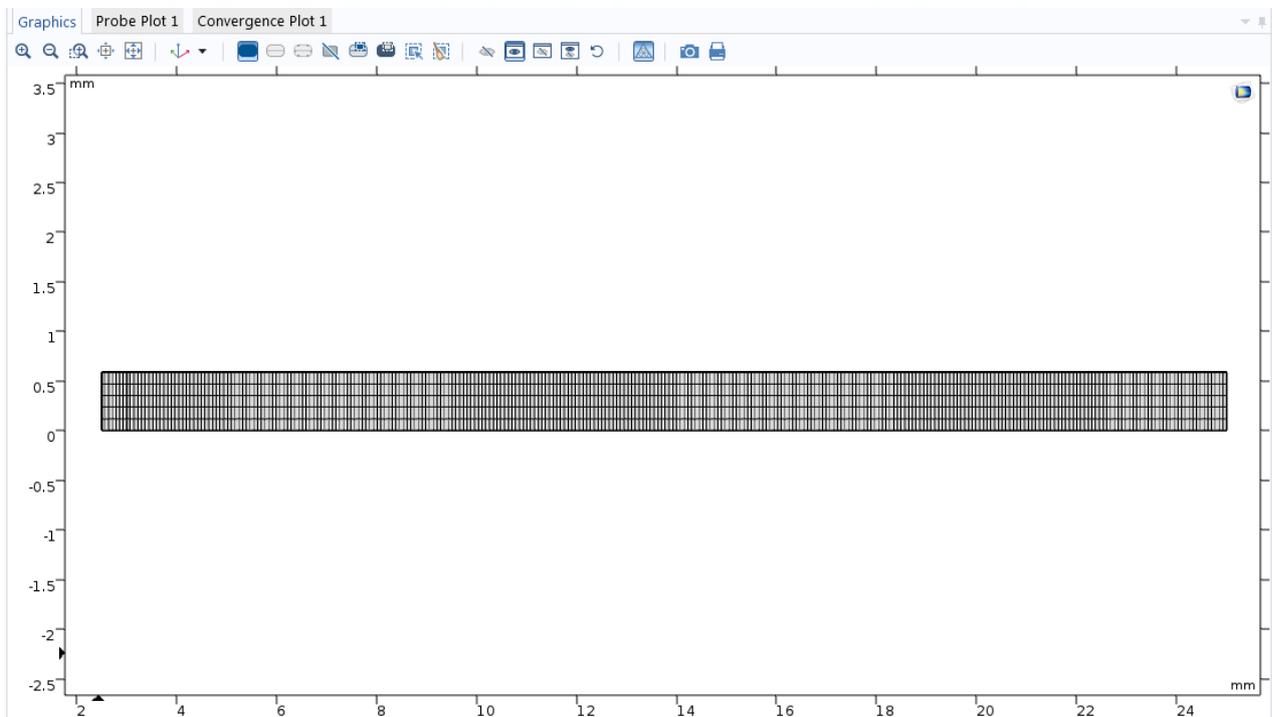
Figure 32. Mesh used for heat pellet domain

Study type for this simulation was "Time-dependent". Simulation final time was set to 1000 ms. Time interval for the simulation was automatically adjusted by COMSOL with its algorithm that keeps relative error under 1 %.

4. RESULTS AND DISCUSSION

The results of the experiments and kinetic analysis were presented in the following section. Firstly, characterization results of the used raw materials and the determined weight ratios of the heat pellets for the same theoretical percent density (57.5 %) were shown with images and tables. In the second step, the outputs from thermal analysis of heat pellets were reported as the released heat versus temperature. The kinetic parameters for the selected model were obtained by utilizing the method of analytical isoconversional and master plots. The kinetic parameters obtained from experiments were compared with the model and the correlation of the experimental results with the model was represented. Finally, burn rate results of the simulation of burning process were compared with literature values to verify that the determined kinetic parameters are accurate.

4.1. Chemical and Physical Structure of Pyrotechnic Powder and Pellet

Morphology of the iron particles affects the adequate compaction of heat pellets. Guidotti et al. stated in his study that due to interlocking structure, iron with sponge type morphology outperformed other candidates [2]. Therefore, the morphology of the iron particles was investigated using SEM analysis. It is seen from the Figure 33 that, supplied Fe particles had sponge type morphology and was suitable for heat pellet preparation.
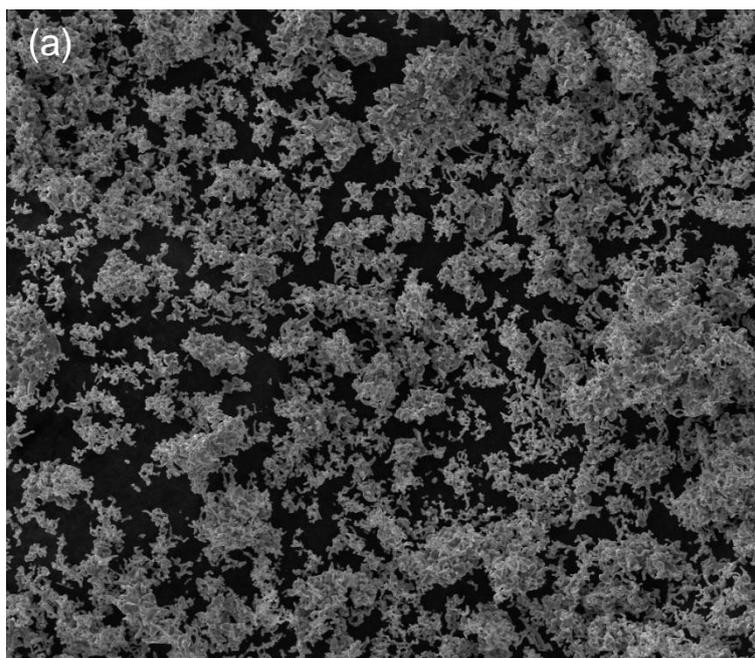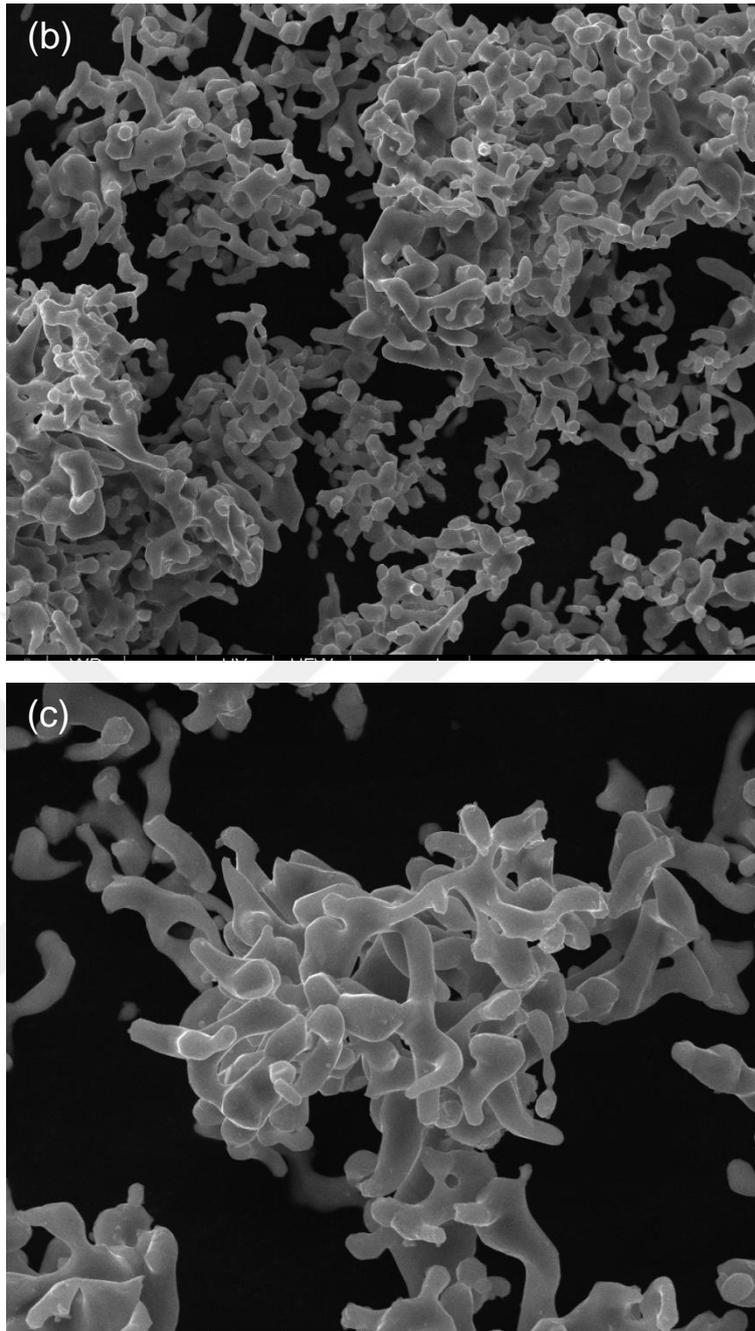
Figure 33. SEM Images of Fe Powder (a) X1000, (b) X5000, (c) 10000

The average particle size of Fe powder was found 46 µm and the theoretical particle density was determined to be 7.85 g/cm^3. From the exact matching of the XRD diffractrogram of Fe with the database (Appendix A), it was seen that supplied Fe did not have any impurities. Impurity is an important factor that affects burning [7].

Average particle size of the impact milled $KClO_4$ was found to be 10 µm and the theoretical particle density was 2.54 g/cm^3. CoA (certificate of analysis) of the $KClO_4$ revealed that it had Cl^- and SO_4^{2-} ionic impurities (Appendix A). Detailed results of

average particle size, theoretical particle density and XRD for Fe and KClO$_4$ powders are presented in Appendix A.

Fe and KClO$_4$ powders were homogenously mixed in different weight ratios and by uniaxial compression heat pellets were formed. In order to keep theoretical density percentage constant (57.5 %), thicknesses of the prepared heat pellets were controlled by varying compression loads. Properties of heat pellets with different weight compositions are summarized in Table 12. Calculation method used to calculate these properties (theoretical particle density, desired thickness of heat pellet) are presented in Appendix B.

Table 12. Properties of prepared heat pellets with varying weight compositions

Property	Calculated and Experimental Values			
Weight Composition of Heat Pellet (w:w)	**82/18**	**84/16**	**86/14**	**88/12**
Mass of Heat Pellet (g)	3.90 ± 0.01			
Outer / Inner Diameter (mm)	50 / 5			
Load of Compression (tons)	17	20	25	36
Thickness of Heat Pellet (mm)	0.61	0.59	0.57	0.55
Volume of Heat Pellet (cm^3)	1.20	1.16	1.12	1.07
Pellet Density (g/cm^3)	3.28 ± 0.01	3.38 ± 0.01	3.49 ± 0.01	3.67 ± 0.01
Theoretical Pellet Density (g/cm^3) (assuming no void inside pellet)	5.70	5.88	6.07	6.39
Pellet Density/Theoretical Pellet Density (Theoretical Density Percentage)	0.575 ± 0.010			

4.2. Determination of Setting Parameters of Thermal Analysis

The certain parameters are to be considered in thermal analysis implemented to heat pellets. Heat pellet decomposition reaction releases high amount of energy. The input of energy more than necessary to the analysis equipment causes distortion in thermal analysis data or may even damage the equipment used [41, 47]. Therefore,

settings for thermal analysis are needed to be adjusted carefully. The settings of thermal analysis that were studied were:

- heating rate, β (°C/min),
- sample mass, m (mg),
- flow rate of purge gas, ϑ (mL/min).

4.2.1. Effect of Heating Rate

The range of heating rate was tried between 2 and 10 °C/min. Heating rates lower than 2 °C/min were avoided because Fe in the sample is susceptible to oxidation caused by the impurities that may exist in the furnace chamber. Additionally, the ability of non-isothermal experiments is practicality to give rapid results. Using too low heating rates would render the practicality of non-isothermal experiments useless.

To investigate the effect of heating rate to thermal analysis data, heat pellet with weight composition of 84/16 (w:w) was used. The mass of the sample was adjusted to 4.5 mg ± 0.5 mg. Purge flow was set to 100 mL/min.

The results of varying heating rates are given in Figure 34.
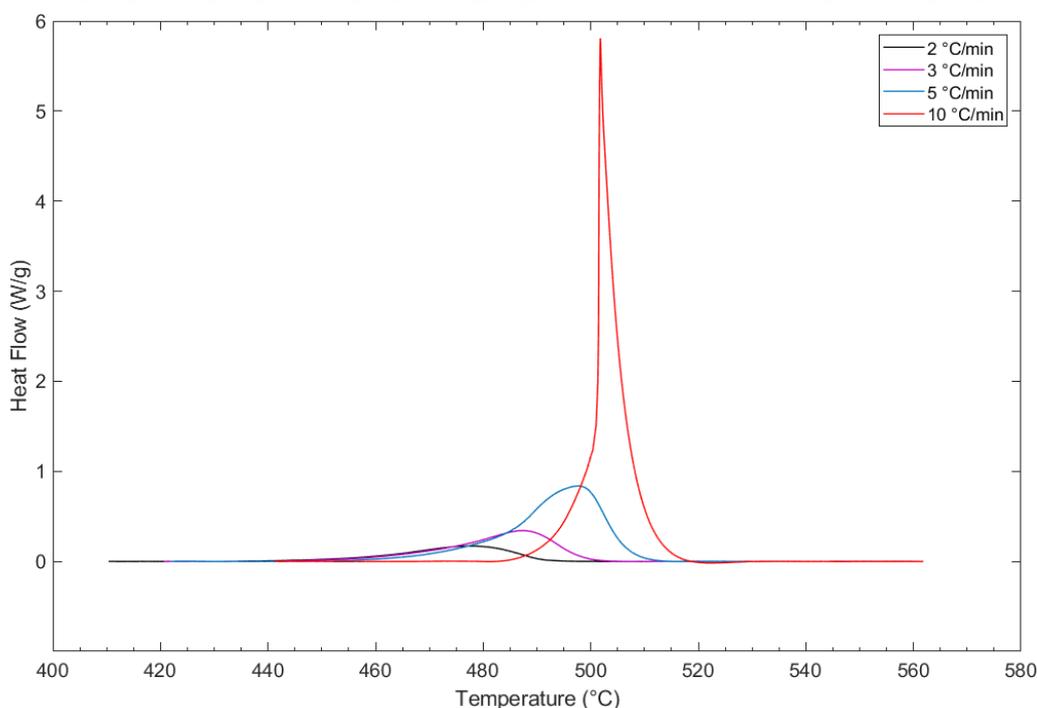
Figure 34. Effect of heating rate to the heat flow. Temperature range: 400 °C < T < 580 °C, sample mass: 4.5 mg, flow rate of purge gas: 100 mL/min.

This result indicates that, when the heating rate is increased to 10 °C/min, the increase of reaction rate is much higher than anticipated compared to 2, 3 and 5 °C/min heating rates. Therefore, the increase of heating rate causes an increase in inner temperature of sample resulted from more rapid decomposition (self-heating). Consequently, it results with a sharp increase in heat flow as it can be seen from the Figure 34. The sharp increase in heat flow results with a peak shaped curve. This type of heat flow is not suitable for kinetic analysis. For kinetic analysis, Gaussian type curve should be observed like the heat flow obtained with 2, 3 and 5 °C/min.

4.2.2. Effect of Sample Mass

The sample mass affects the thermal analysis in the same way as heating rate. As the sample mass increases, the amount of heat generation increases as well. Excess sample mass may cause self-heating of the sample, causing distortion in thermal analysis data. On the other hand, sample mass should not be too small that the heat flow the reaction generates goes beyond the limit of detection.

To investigate the effect of sample mass, heating rate was kept constant at 5 °C/min and the purge flow was adjusted to 100 mL/min. The results of varying sample masses are given in Figure 35.

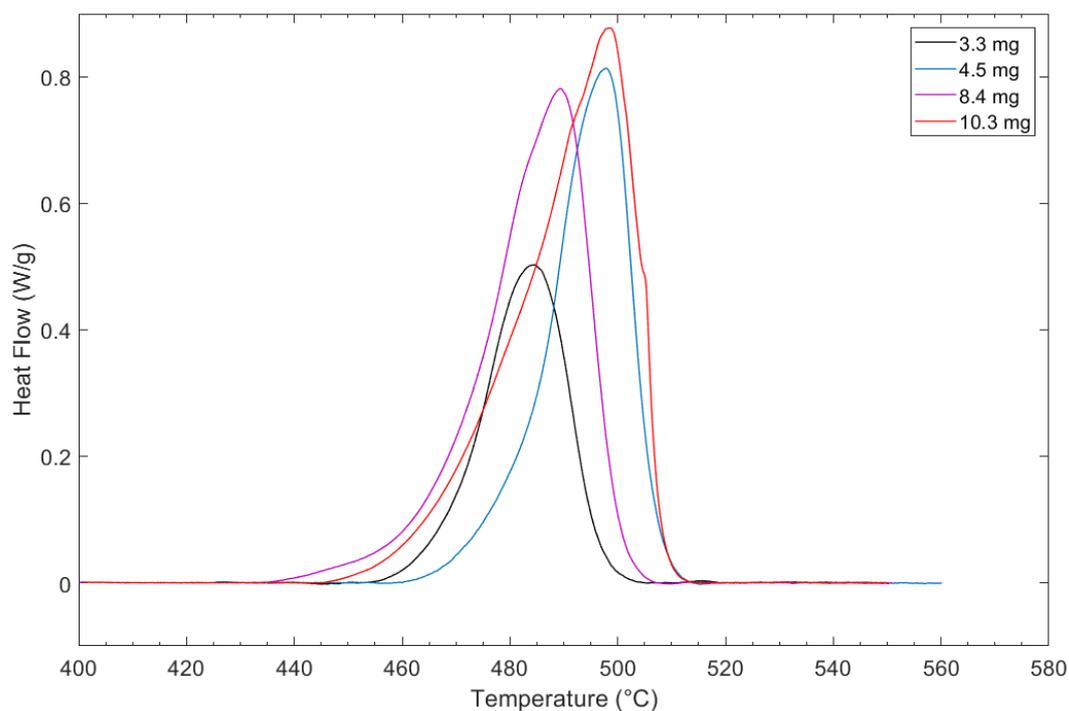**Figure 35. Effect of sample mass to heat flow. Temperature range: 400 °C < T < 580 °C, heating rate: 5 °C/min, flow rate of purge gas: 100 mL/min.**

In this figure, it was observed that, for the highest sample mass (10.3 mg), self-heating of the sample was evident because of the steep temperature increase and distortion in heat flow. The thermal analysis with the lowest sample mass (3.3 mg) had the lowest heat flow among all. That is caused by the low heat generation from reaction. Low heat generation may not be enough to give information about the thermal decomposition mechanism of heat pellets. This may cause issues when using heat pellets with lower calorific output (i.e. heat pellets with weight composition of 86/14 and 88/12 (w:w)). Therefore, sample of 4.5 mg was used from the choice of 4.5 mg and 8.4 mg because the 8.4 mg sample mass is more prone to self-heating when the heat pellet with more calorific output is used (i.e. heat pellet with weight composition of 82/18 (w:w)).

The results showed that heating rate and sample mass have the effect of increasing on heat flow. Based on the observed results, the heating rate range and sample mass was selected as 2 – 5 °C/min and 4.5 ± 0.5 mg, respectively

4.2.3.   Effect of Flow Rate of Purge Gas

Nitrogen purge gas was used in the chamber that the heat pellet sample to be blanket from the oxidizing atmosphere. Flow rate of purge gas should be adjusted in a way that, it can efficiently cover the sample but also should not affect thermal analysis data with buoyancy force effect. The buoyancy force effect resulted by the heating up of the accumulated purge gas in furnace chamber, is caused by the certain decrease in the density of purge gas. As the density drops, fluid starts to move vertically in the furnace chamber which affects the sample/reference pans and causes the misreading of the weight of the sample [68].

Experiments for the effect of flow rate of purge gas were carried out using the heating rate, β=5 °C/min and sample mass, m=4.5 ± 0.5 mg. The recorded heat flow from the thermal analysis for different flow rate of purge gas is shown in Figure 36.
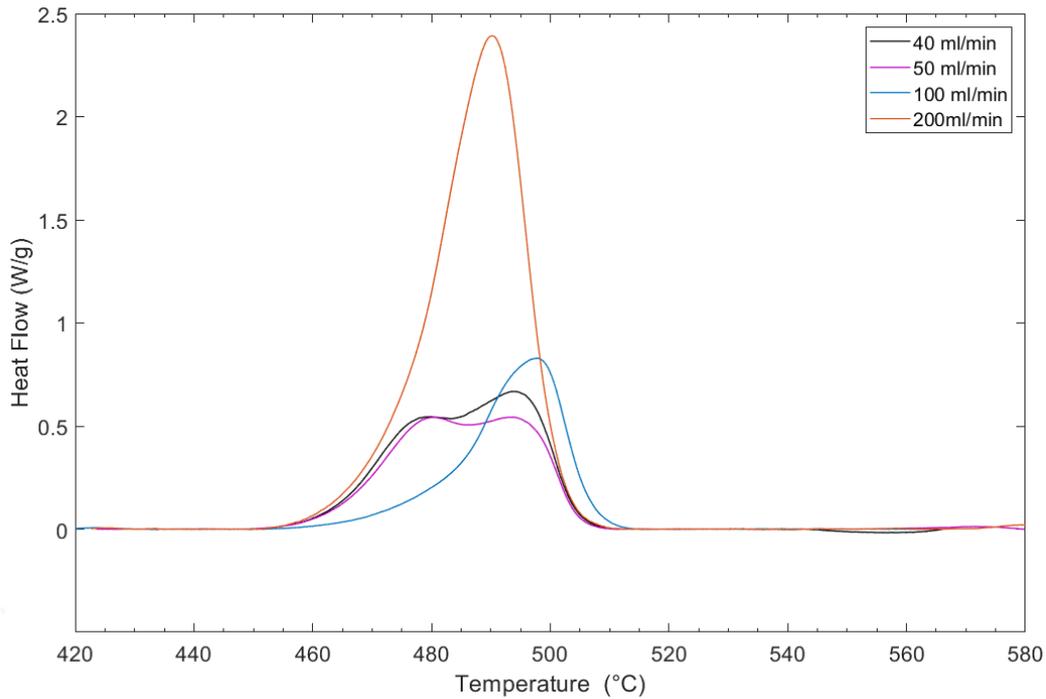
Figure 36. Effect of flow rate of purge gas to heat flow. Temperature range: 420 °C < T < 580 °C, heating rate: 5 °C/min, sample mass: 4.5 ± 0.5 mg.

Thermal analysis in the conditions of the lowest two flow rates (40 and 50 mL/min) showed two distinct reactions took place. This is the result of oxidation of Fe particle in the sample. When the flow rate of purge gas is too low, effective removal of air from furnace chamber could not be accomplished.

When Fe particles are used above stoichiometric ratio in heat pellet, if there is oxygen present from outer source in furnace chamber, it results in parasitic oxidation reactions. According to the principle of conservation of mass, oxidation of Fe with oxygen from outer source causes sudden increases in the mass of sample. In the Figure 37, the occurred parasitic oxidation reactions were seen as steps of weight gains of sample for the flow rate of 40 mL/min.
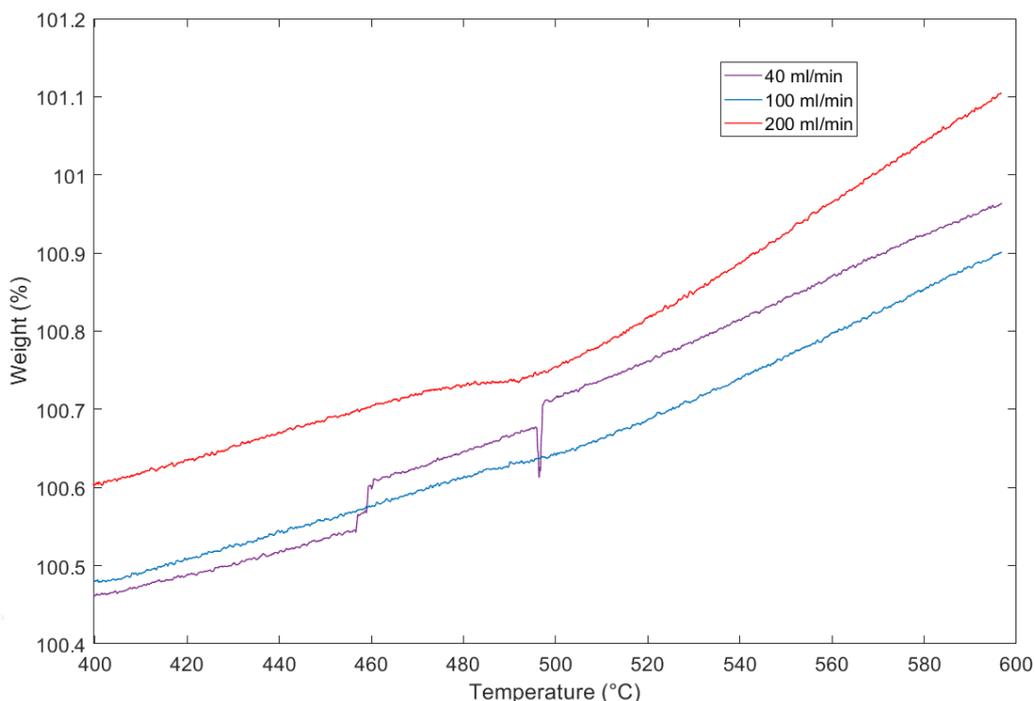
Figure 37. Comparison of weight change when ϑ = 40 mL/min, 100 mL/min and 200 mL/min.

As seen in Figure 37, high flow rate (200 mL/min) causes the accumulation of N_2 gas inside the furnace chamber and it affects the sample pans, that are caused the error in the weight reading resulted from buoyancy force effect. Therefore, 100 mL/min was selected to be the optimal flow rate that save the sample from the effect of oxidizing environment and do not let N_2 gas to accumulate inside the furnace chamber. The experimental parameters determined to the previous evaluations were given in Table 13.

Table 13. Parameters of experimental conditions to be used

Experimental Condition	Parameter		
Heating Rate (°C/min)	2	3	5
Sample Mass (mg)	4.5 ± 0.5 mg		
Flow Rate of Purge Gas (mL/min)	100		

4.3. Thermal Decomposition of Heat Pellet

In order to conduct kinetic analysis, heat flow of thermal decomposition of heat pellet with heating rates of 2, 3 and 5 °C/min were obtained. To ensure, heat flow is not affected by the slight changes of the sample geometry or the apparatus [53], thermal analysis at each heating rate were conducted three times. In the figure below, all three experiments for the heat pellet with weight composition of 82/18 (w:w) with varying heating rates are shown in terms of temperature versus heat flow.
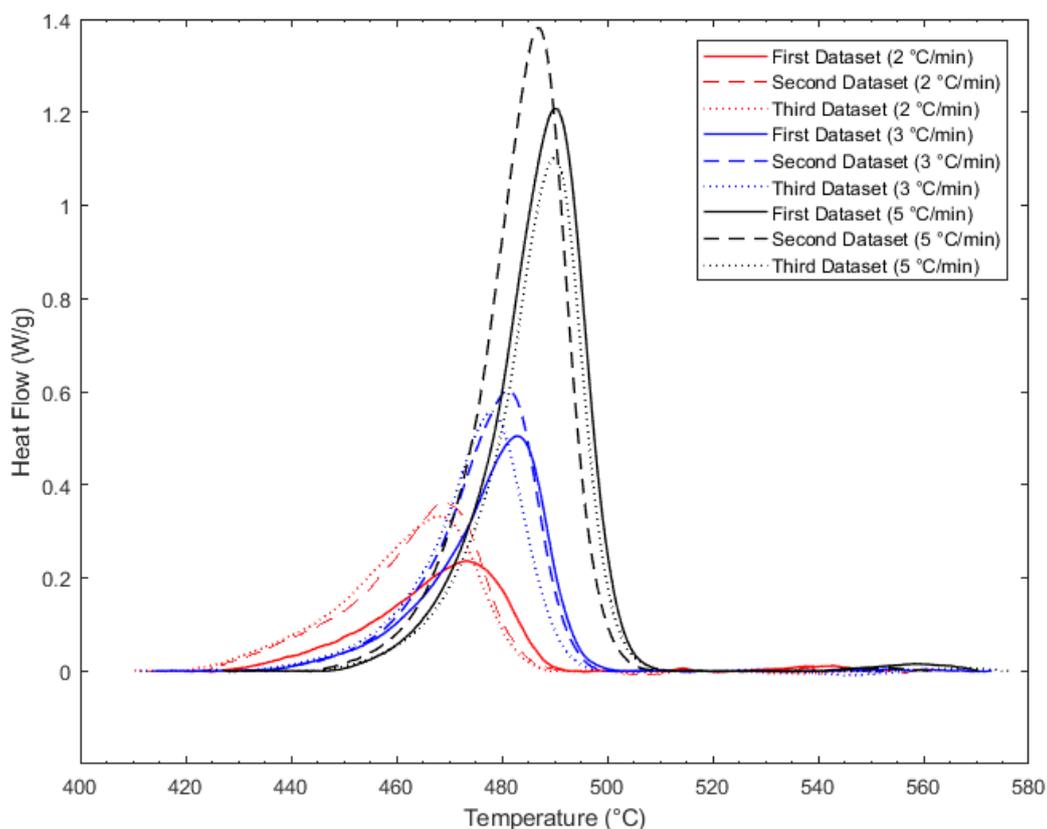
Figure 38. Heat flow from the thermal decomposition of heat pellets for different heating rates, heat pellet: 82/18 (w:w)

Figure 38 shows the variation in heat flow data for three different experiments. Starting, peak and final temperatures of the heat flow profiles are nearly the same which is main parameter that defines the apparent activation energy (E_a). Apart from that, shapes of the profiles are relatively the same which defines the reaction model, $f(\alpha)$. Same repeatability analysis was conducted for other heat pellets with different weight compositions as well. Similar results were reported in Appendix D. Heat flow data were averaged before converting heat flow to conversion to be used for kinetic analysis. Average heat flows for heat pellets with different weight composition are given in Figure 39 below.

76
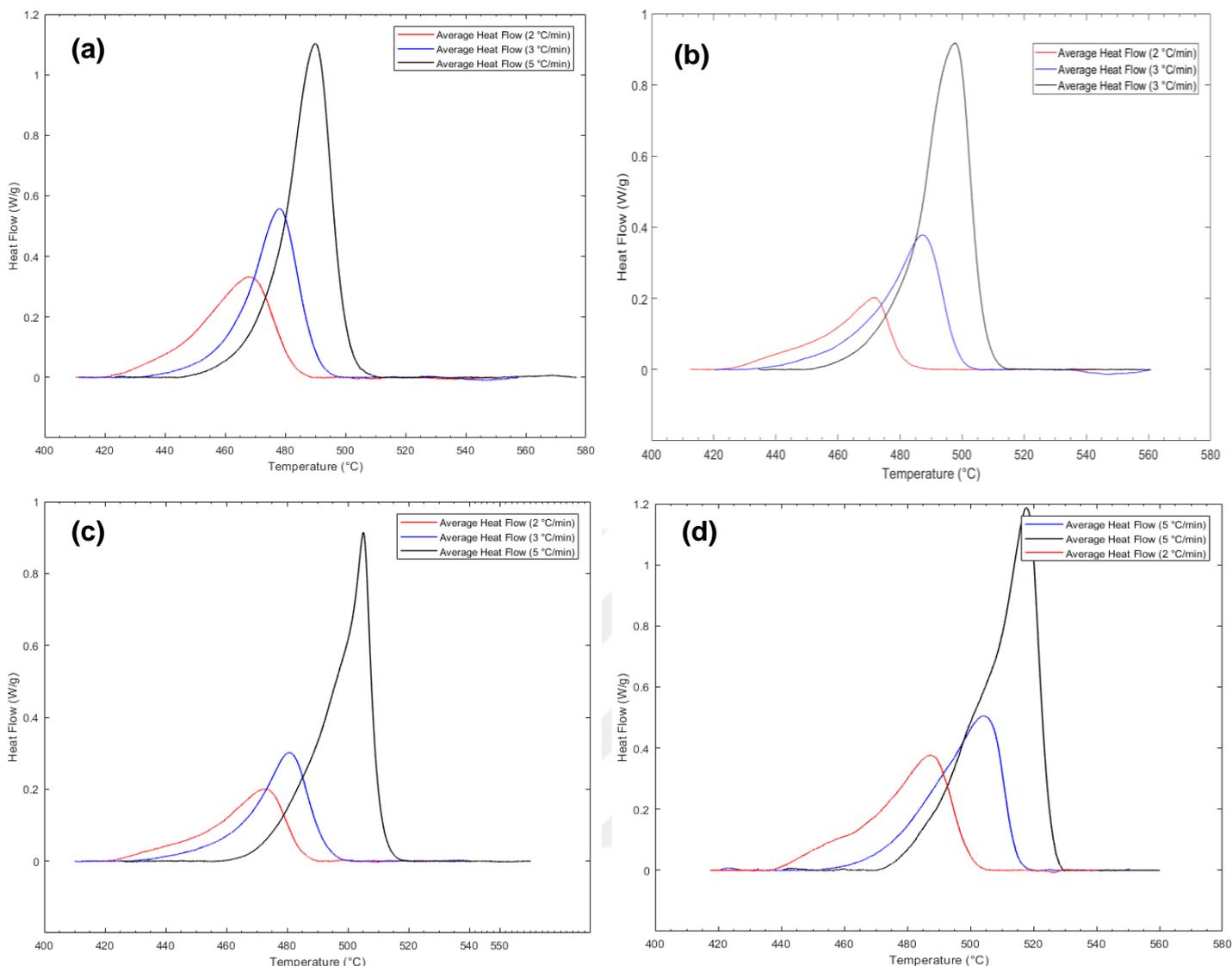
Figure 39. Average heat flow from the thermal decomposition of heat pellets for different heating rates, (a) heat pellet: 82/18 (w:w), (b) heat pellet: 84/16 (w:w), (c) heat pellet: 86/14 (w:w), (d) heat pellet: 88/12 (w:w)

The heat flow for all heating rates shifted to higher temperatures with decreasing % content of $KClO_4$. Main reason for this shift is thought to be the decreasing surface of area of interaction between molecules of Fe and $KClO_4$. The cause of this shift will be further investigated with the obtained kinetic parameters.

In further studies, the averaged values of the thermal analysis data were used. Averaged heat flow was converted to temperature vs. conversion using the script (see Appendix C) that was written for this purpose on MATLAB® (2014A). The mathematical expression that was used to convert heat flow to conversion is given below (Equation (7)).

$$\alpha_T = \frac{\int_0^T Q_{released} \times dT}{\int_0^f Q_{released} \times dT}$$

Results of the conversion vs. temperature data for all heat pellets studied with heating rate of 2 °C/min, 3 °C/min and 5 °C/min are given in Figure 40, Figure 41 and Figure 42, respectively.

Figure 40. Conversion of decomposition reaction of heat pellets as a function of temperature with heating rate of 2°C/min

Figure 40 shows that, there was a asymmetric behavior (slight tilt of curve to the higher temperatures) of the thermal decomposition carried on to the conversion vs. temperature data as well. This is a representation of the reaction model. It shows that reaction rate reaches its maximum rate between conversion values of 0.5 – 0.8. This observation is in agreement with Yang et al.'s work in which he indicated decomposition of $KClO_4$ and oxidation of Fe are consecutive exothermic reactions that takes place quite rapidly and furthermore oxidation step is the fastest [3, 29]:

$$KClO_4 \longrightarrow KCl + 2O_{2} + \Delta H_{r,1}$$

78

$$2Fe + O_2 \longrightarrow 2FeO + \Delta H_{r,2}$$

When using non-isothermal experiments, both $k(T)$ and $f(\alpha)$ changes simultaneously. This is the reason for the sigmoidal shaped curve of temperature vs. conversion.
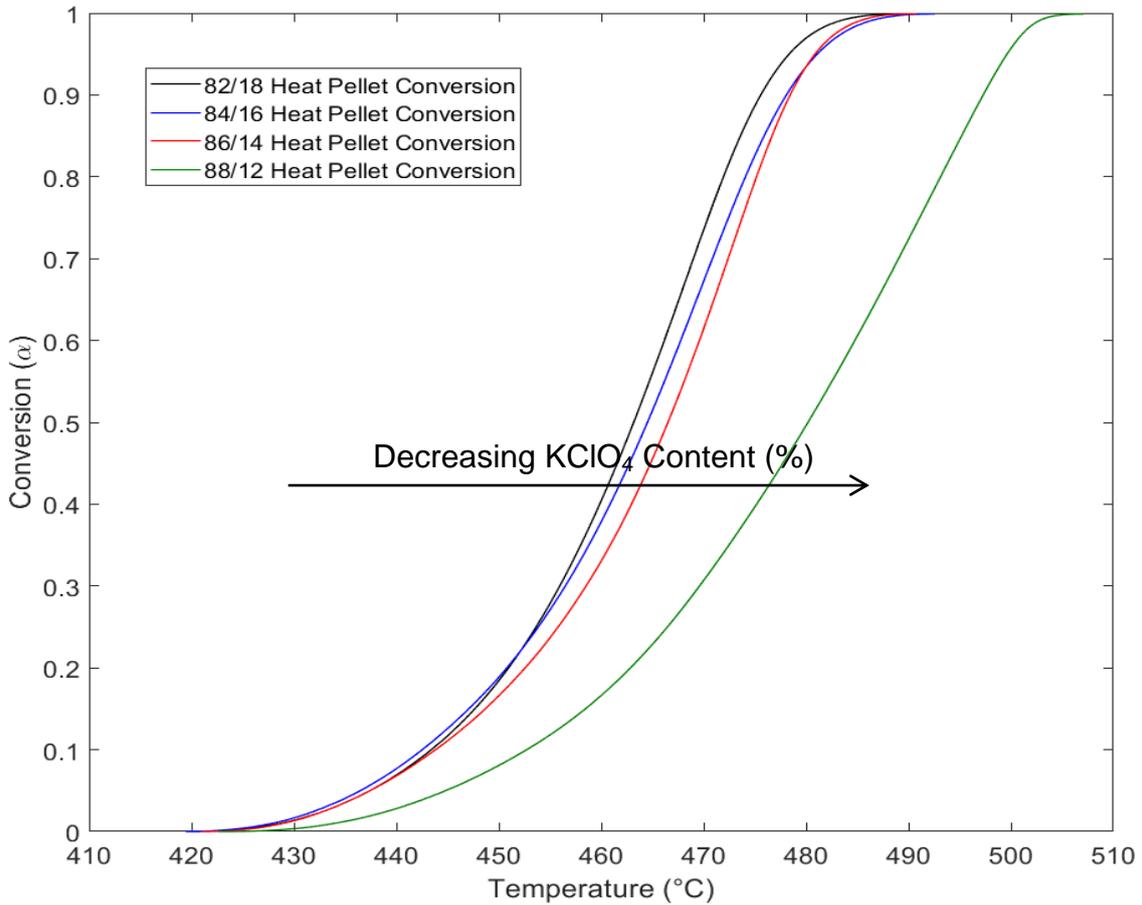

Figure 41. Conversion of decomposition reaction of heat pellets as a function of temperature with heating rate of 3°C/min

Figure 41 shows that the inflection point became apparent on 88/12 heat pellet (w:w) data. It is thought that inflection point is caused by the thermal lag in the reaction zone. According to Equation (11), heat pellet with 88/12 (w:w) weight composition gives the least amount of energy per gram of heat pellet. This causes the temperature of reaction zone to increase gradually compared to other heat pellets. However, when the temperature of reaction zone reaches the point of auto-ignition, reaction rate dramatically increases. This causes an inflection point. By further increasing the heating rate, this thermal behavior occurs at a lower conversion value (Figure 42). Since the increase in reaction rate for 3 °C/min heating rate, auto-ignition temperature is reached earlier when heating rate is 5 °C/min.
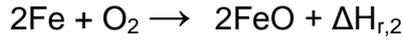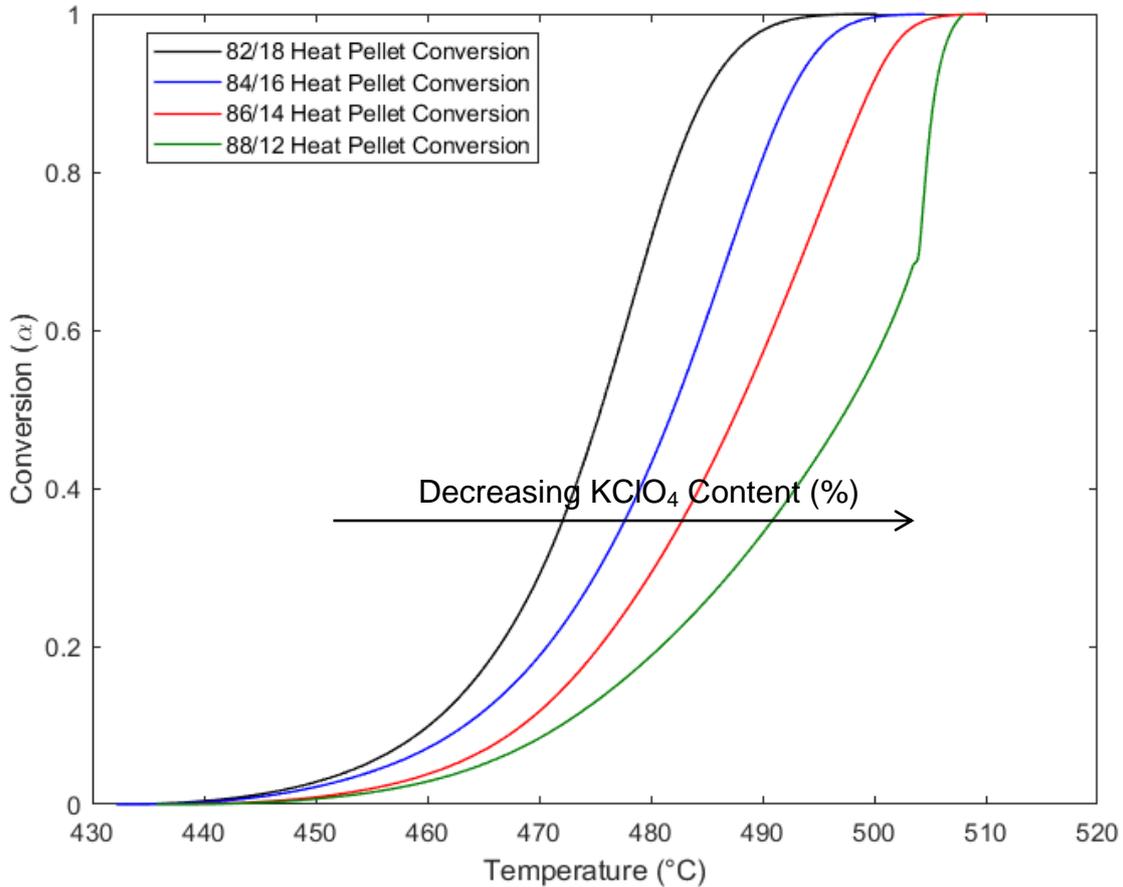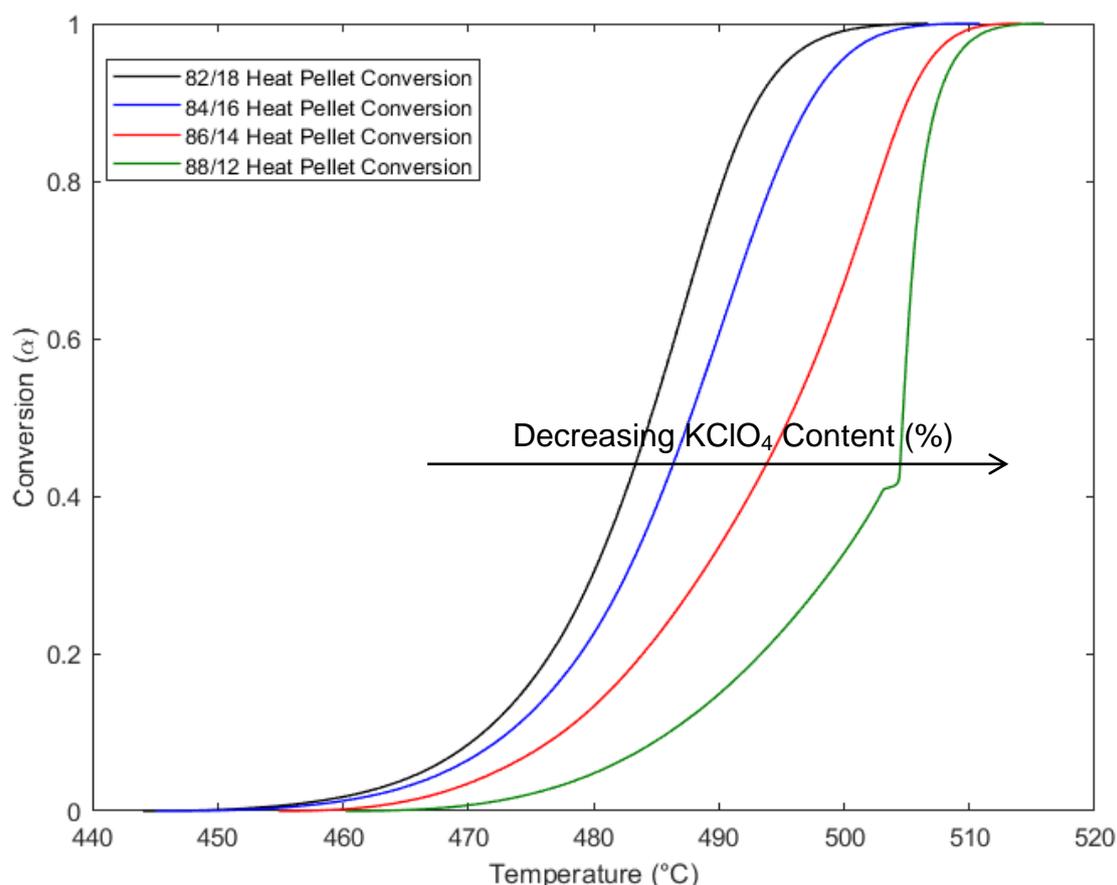
Figure 42. Conversion of decomposition reaction of heat pellets as a function of temperature with heating rate of 5°C/min

Results of thermal analysis show that multi step decomposition of $Fe/KClO_4$ occurs too rapidly to be detected. Only two of the data belonged to 88/12 with heating rates of 3 and 5 °C/min gave inflection points. These inflection points were interpreted as the thermal lagging of the decomposition process. Therefore, assumption of one-step mechanism to identify the kinetic parameters of heat pellets appears favorable. Variation of activation energy with respect to conversion was analyzed using the conversion vs. temperature dataset.

4.4. Determination of Kinetic Parameters

In this section, the kinetic parameters obtained from the thermal analysis of the samples of heat pellet are presented. For determination of apparent activation energy, Starink's isoconversional method was used due to its proven high accuracy [37, 51]. With acquired average activation energy values (E_a), reaction model, f(α) was investigated with Malek's procedure. Malek's procedure was preferred because it gives the knowledge of the reaction model from a simple graphical method. Finally, pre-exponential value was calculated with obtained E_a and f(α) values.

4.4.1.　Apparent Activation Energy

Starink's integral isoconversional method was selected to determine apparent activation energy for the thermal decomposition process of heat pellets because of its high accuracy. Starink's integral isoconversional method is model-free which can be used without assuming any reaction model. The mathematical expression for this method is derived from non-isothermal kinetic equation (Equation (10)) by integrating and taking natural logarithm for linearization (Equation (23)).

$$\ln\left(\frac{\beta}{T_i^{1.92}}\right) = -1.0008\frac{E}{RT_i} + ln\frac{AR}{Eg(\alpha)}$$

Slope of 1/T (K^{-1}) vs. ln($\beta/T^{1.92}$) curve (Starink plot) gives the apparent activation energy for the specified conversion. The Starink plot for a composition 82/18 (w:w) of heat pellet for varied conversion are given in Figure 43.
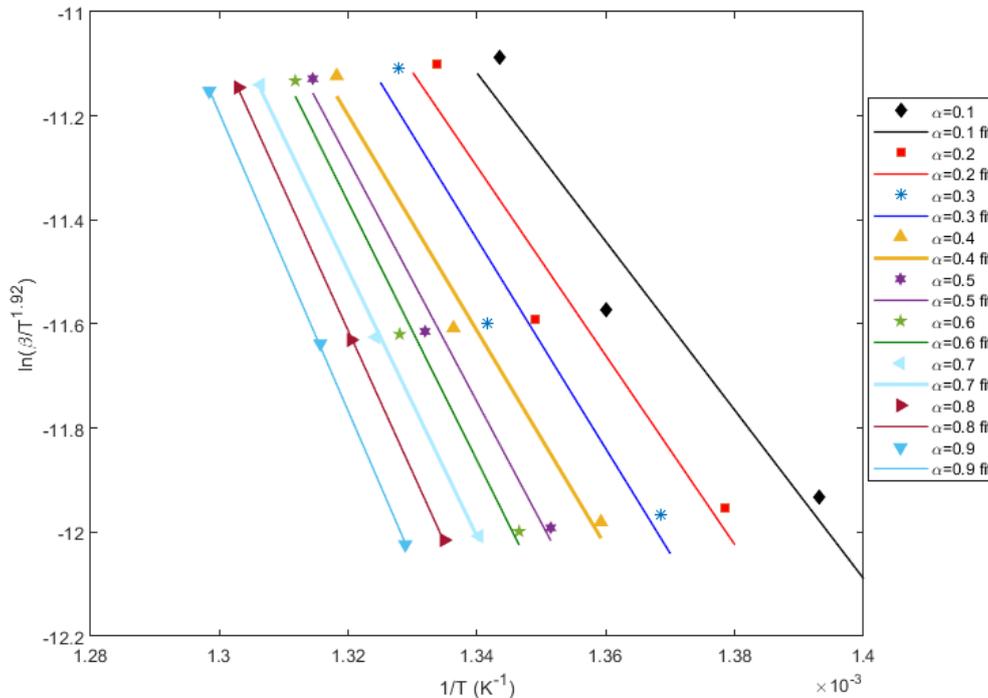
Figure 43. Starink plot for thermal decomposition process of 82/18 heat pellet at three heating rates and various conversions (α : 0.1 – 0.9)

As it can be seen from the figure, fits of first order polynomials in the form of (ax+b) are not good in the conversion range of 0.1 – 0.3. Main reason for this is the simultaneous reactions of $KClO_4$ decomposition and Fe oxidation. After conversion is 0.4, goodness of the fits increases because the $KClO_4$ decomposition reaction ceases. To define goodness of the fits, correlation factor (r) was calculated.

Activation energy values for 82/18 (w:w) heat pellet with increasing conversion ($\Delta\alpha$=0.1) are given in Table 14.

Table 14. The apparent activation energy (E_a) its correlation factors for the decomposition reaction of 82/18 (w:w) heat pellet

α	E_a (kJ/mol)	r (Correlation Coefficient)
0.1	134.4	0.93
0.2	150.7	0.93
0.3	167.1	0.93
0.4	171.9	0.99
0.5	193.4	0.99
0.6	206.1	0.99
0.7	212.3	0.99
0.8	226.1	0.99
0.9	237.7	0.99
Average	**208.0 ± 33.0**	**0.99**

According to ICTAC Kinetics Committee, activation energy value with correlation coefficient lower than 0.98 should be disregarded and not be included in the calculation of average apparent activation energy for a solid-state reaction [54]. For that reason, activation energy values with correlation coefficient values lower than 0.98 were disregarded. Average activation energy for heat pellet with weight composition of 82/18 (w:w) was calculated as **208.0 ± 33.0 kJ/mol**. Variation of average activation energy was **± 16 %**.

The Starink plot for a composition 84/16 (w:w) of heat pellet for varied conversion are given in Figure 44 below.

Figure 44. Starink plot for thermal decomposition process of 84/16 heat pellet at three heating rates and various conversions (α : 0.1 – 0.9)

Similar to the 82/18 (w:w) heat pellet, fitting in the conversion range of 0.1 - 0.3 was not adequate. In the following table, values of apparent activation energy and correlation coefficients are given.

Table 15. The apparent activation energy (E_a) and its correlation factors for the decomposition reaction of 84/16 (w:w) heat pellet

α	E_a (kJ/mol)	r (Correlation Coefficient)
0.1	170.4	0.96
0.2	173.1	0.95
0.3	191.2	0.97
0.4	194.4	0.99
0.5	202.0	0.99
0.6	205.0	0.99
0.7	209.6	0.99
0.8	220.2	0.99
0.9	229.7	0.99
Average	**210.2 ± 17.6**	**0.99**

Excluding the data with correlation coefficient below 0.98, average activation energy was calculated as **210.2 ± 17.6 kJ/mol.** Variation of average activation energy was **± 8.4 %**.

The Starink plot for a composition 86/14 (w:w) of heat pellet for varied conversion are given in Figure 45 below.

Figure 45. Starink plot for thermal decomposition process of 86/14 heat pellet at three heating rates and various conversions (α : 0.1 – 0.9)

Same behavior with 82/18 and 84/16 heat pellets were observed for the 86/14 heat pellet as well. In the table below apparent activation energy with respect to conversions and their correlation coefficients are given.

Table 16. The apparent activation energy (E_a) and its correlation factors for the decomposition reaction of 86/14 (w:w) heat pellet

α	E_a (kJ/mol)	r (Correlation Coefficient)
0.1	164.8	0.95
0.2	175.6	0.97
0.3	187.4	0.97
0.4	201.0	0.98
0.5	205.1	0.99
0.6	212.6	0.99
0.7	223.1	0.99
0.8	229.5	0.99
0.9	236.5	0.99
Average	**218.0 ± 17.7**	**0.99**

Excluding the data with correlation coefficient below 0.98, average activation energy was calculated as **218.0 ± 17.7 kJ/mol.** Variation of average activation energy was **± 8.1 %**.

The Starink plot for a composition 88/12 (w:w) of heat pellet for varied conversion are given in Figure 46 below.
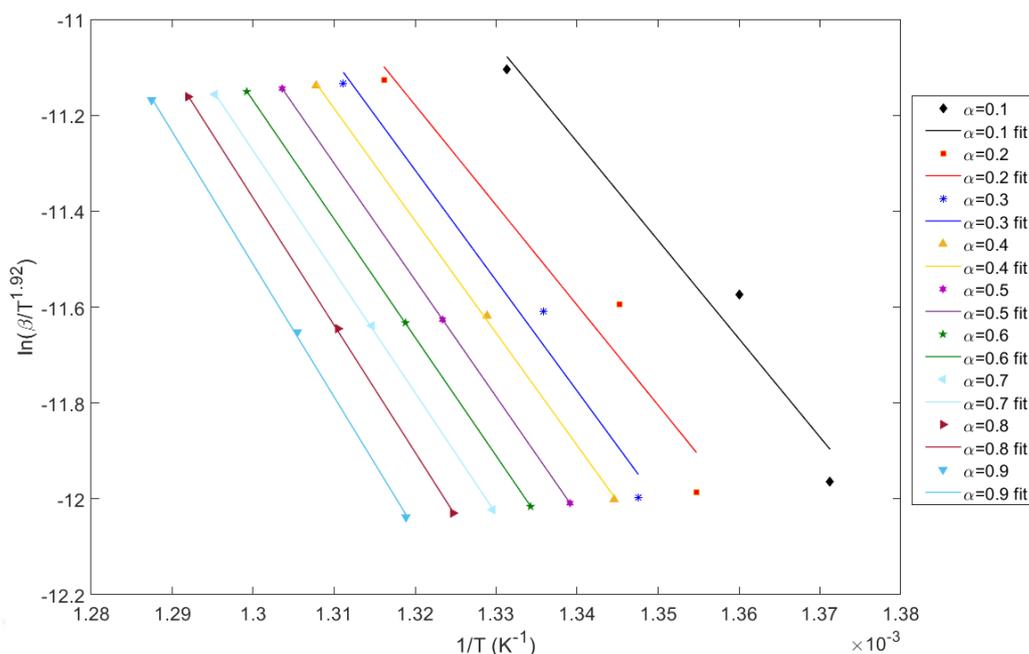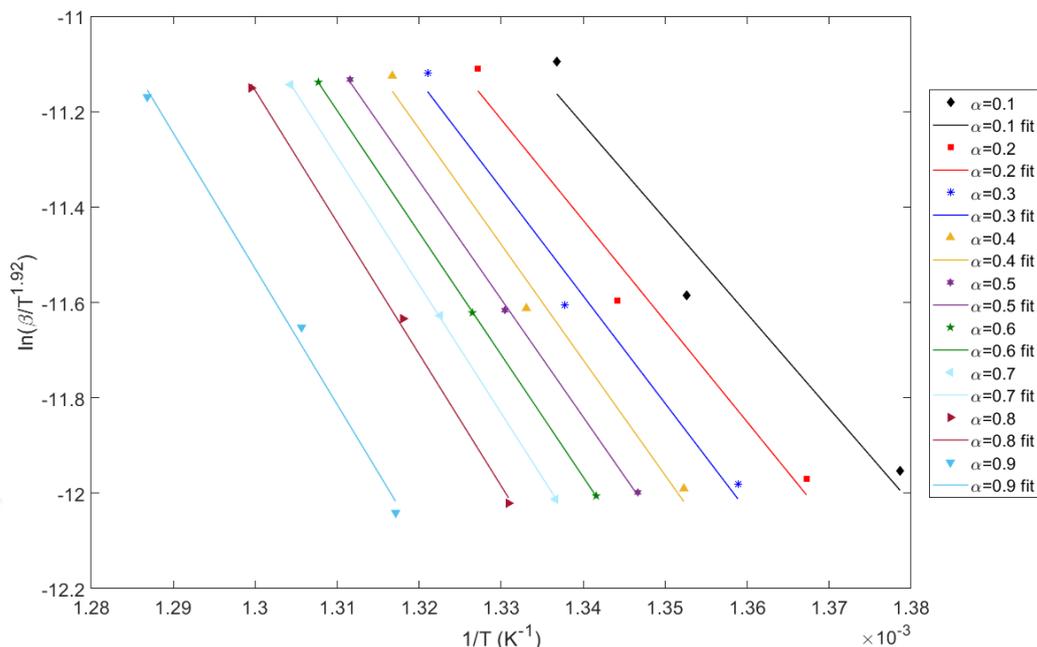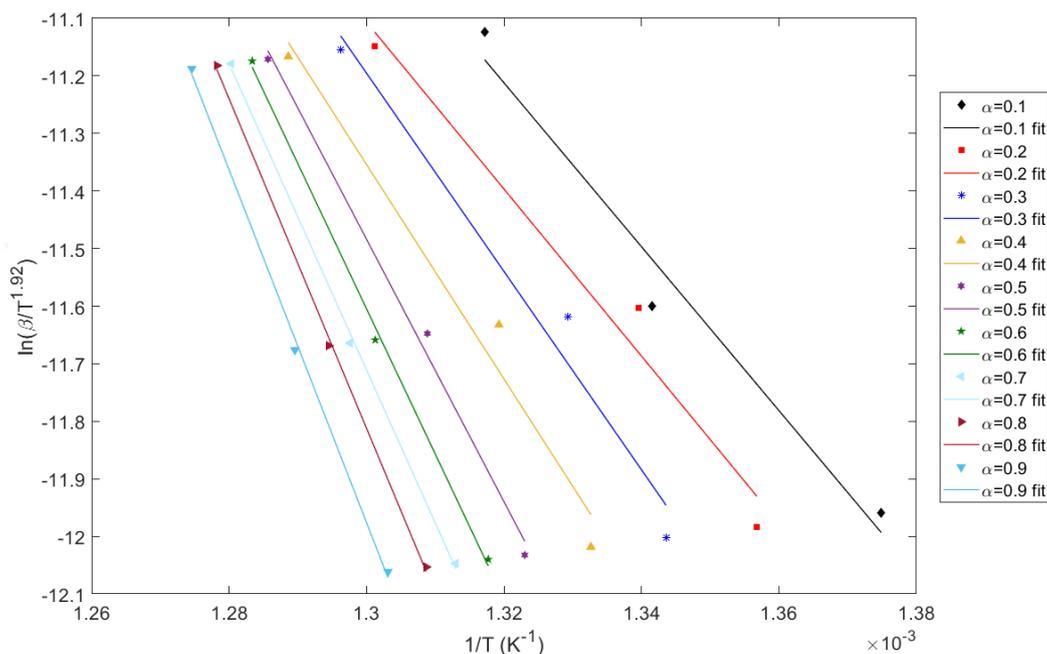

Figure 46. Starink plot for thermal decomposition process of 88/12 heat pellet at three heating rates and various conversions (α : 0.1 – 0.9)

Starink plot of 88/12 (w:w) heat pellet revealed that good fits was not achieved until the conversion is 0.5. This is an indication of still ongoing $KClO_4$ decomposition reaction together with Fe oxidation until conversion of 0.5 is reached. In the following table calculated values of apparent activation energy and correlation coefficient are given.

Table 17. The apparent activation energy (E_a) and its correlation factors for the decomposition reaction of 88/12 (w:w) heat pellet

α	E_a (kJ/mol)	r (Correlation Coefficient)
0.1	118.2	0.97
0.2	120.4	0.97
0.3	143.0	0.97
0.4	154.7	0.97
0.5	189.3	0.99

0.6	209.5	0.99
0.7	220.9	0.99
0.8	237.7	0.99
0.9	254.5	0.99
Average	**222.4 ± 32.6**	**0.99**

Excluding the data with correlation coefficient below 0.98, average activation energy was calculated as **222.4 ± 32.6 kJ/mol.** Variation of average activation energy was **± 14.6 %**. The variation in the activation energy with respect to conversion is due to the two-step decomposition of $Fe/KClO_4$ pyrotechnic. Variation in activation energy for heat pellets with different weight compositions is in the range of 10 – 15 %, therefore assumption of single step reaction with single averaged activation energy was made. The results of activation energies obtained for all samples that were examined are given in Figure 47.
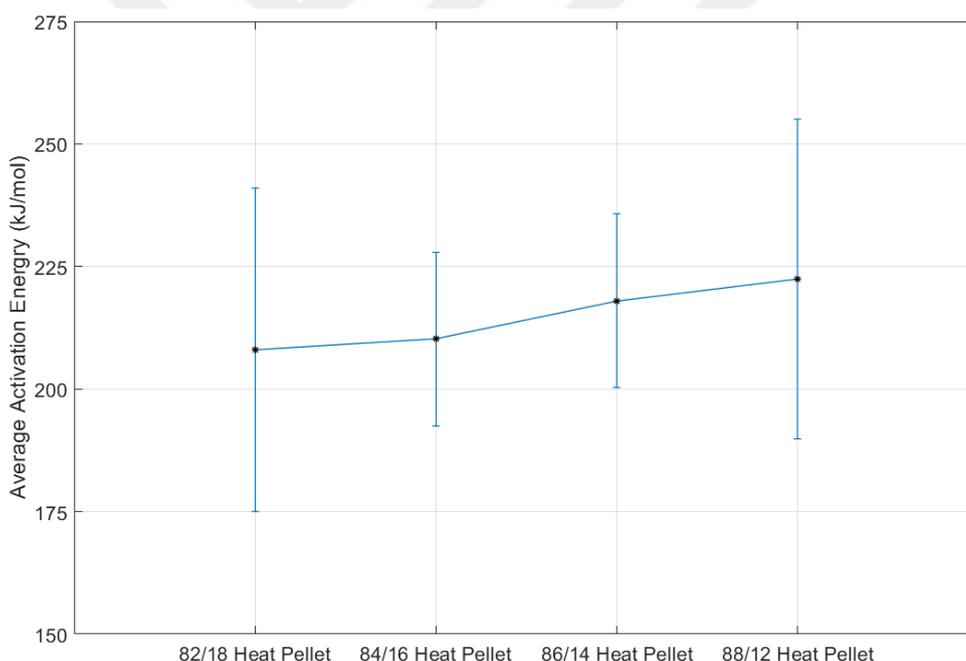
Figure 47. Average activation energies of heat pellets with different weight compositions

Figure 47 shows that with decreasing $KClO_4$ content, activation energy of thermal decomposition increases. $Fe/KClO_4$ burning process starts with the decomposition of $KClO_4$ and proceeds with Fe oxidation. As the weight composition of $KClO_4$ decreases, probability of one $KClO_4$ molecule to decompose and meet with Fe molecule decreases. Consequently, with decreasing $KClO_4$ weight composition in the heat pellet activation energy increases.

Correlation factors of activation energy in the conversion range of 0.1 – 0.4 were less than 0.98. Low correlation factors in Starink curves indicate that two or more reactions take place concurrently in that conversion range [14, 37]. In the figure below, representation of the overlapping reactions for thermal decomposition of heat pellets is given with respect to conversion.
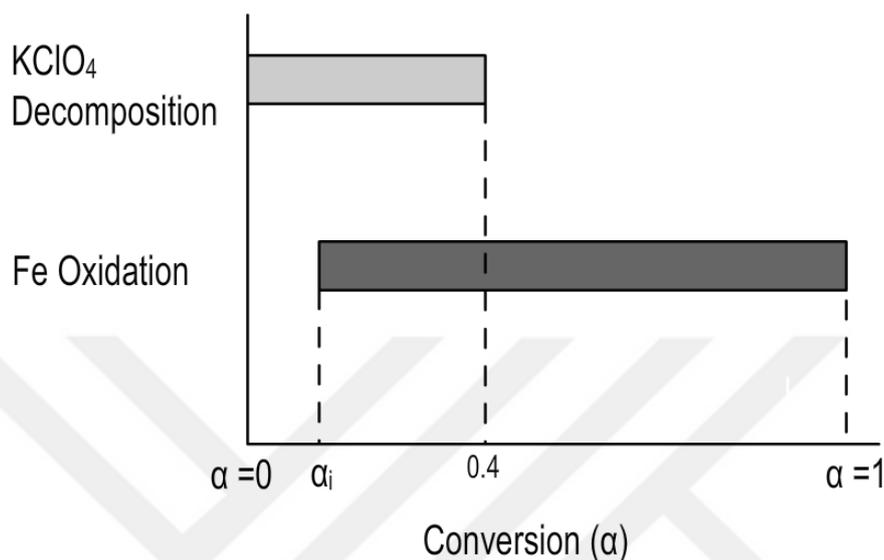
Figure 48. Stages of thermal decomposition process of heat pellet

Findings at this point suggest that while the $KClO_4$ decomposes to form oxygen, Fe oxidation starts at a certain conversion, α_i. $KClO_4$ decomposition continues until the 0.4 fraction of the products (FeO and KCl) form. After that point, decomposition ceases and the oxygen that is formed in the vicinity of Fe molecules diffuses into the Fe atoms and oxidation continues until oxygen depletes.

With the average activation energy determined, further mechanistal investigation were carried out using Malek's procedure in the next section.

4.4.2. Determination of the Reaction Model and Pre-Exponential Factor of Thermal Decomposition Process

In this section, reaction model, f(α) of the thermal decomposition of heat pellets were evaluated. With activation energy, the reaction model which best describes the thermal decomposition of heat pellets for each weight composition was determined using master plots, y(α) and z(α). y(α) and z(α) functions describes the reaction rate (dα/dt) with respect to conversion. y(α) function is also proportional to the reaction model f(α). The mathematical expression that describes the y(α) function is given

below (Equation (25)). First expression with the term of $(d\alpha/dt)_\alpha$ was used to calculate experimentally obtained thermal decomposition. Second expression $(y(\alpha)=Af(\alpha))$ was used to calculate the theoretical $y(\alpha)$ plots for reaction models given in Table 2 for comparison with experimental results. Since pre-exponential factor (A) is unknown at this point, both curves were normalized within (0-1).

$$y(\alpha) = \left(\frac{d\alpha}{dt}\right)_\alpha exp\left(\frac{E_{avg}}{RT_\alpha}\right)$$

$$y(\alpha) = Af(\alpha)$$

For all heat pellets studied, comparison of the theoretical $y(\alpha)$ plots and experimental data are given below.
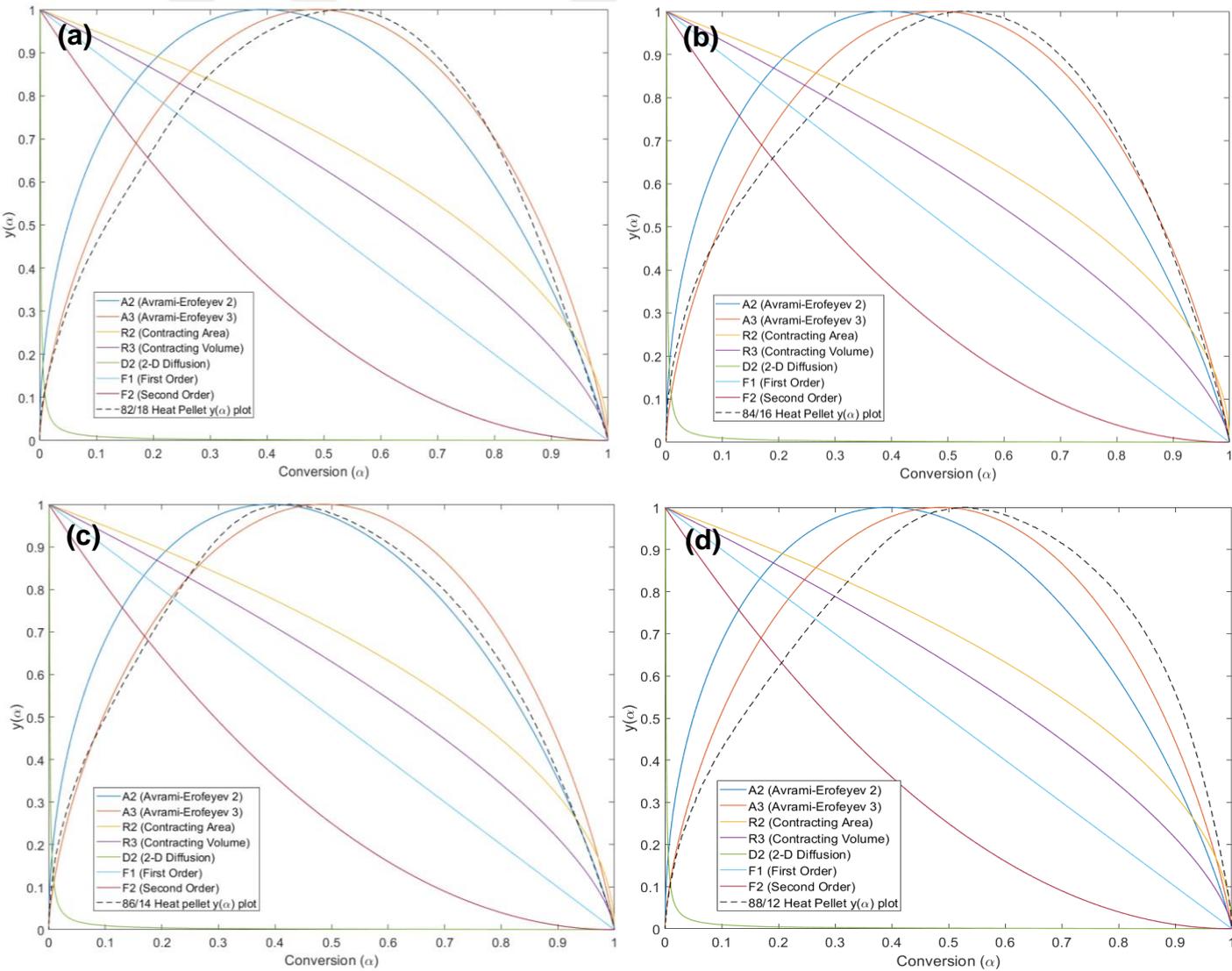

Figure 49. Plots of y(α) vs. α for theoretical reaction models and for heat pellets with different weight compositions at 5 °C/min heating rate. Heat pellets: (a) 82/18 (w:w), (b) 84/16 (w:w), (c) 86/14 (w:w), (d) 88/12 (w:w)

Regardless of the weight composition of heat pellet, y(α) master plots show resemblance with the Avrami-Erofeyev models. Avrami-Erofeyev reaction model is mainly used for describing a reaction which undergoes a nucleation process. Nucleation process is the formation of new phase at reactive sites in the lattice. Nucleation process takes place when the crystal in reacting structure has imperfections such as impurities, surfaces, edges, dislocation, cracks or point defects. These imperfections in the structure cause drop in the activation energy and therefore lets nucleation reaction start at that imperfect point. In the case of $KClO_4$ crystal structure, imperfections are caused by the impurities of Cl^- and $SO4^{-2}$ ions.

It can be seen from the mathematical expression of y(α) (Equation (25)) that y(α) function is strongly controlled by the apparent activation energy. z(α) plot is practically independent from the apparent activation energy values (Equation (26)). To compensate for the error that may come from the inaccurate result of activation energy, z(α) plot of thermal decomposition of heat pellets and nucleation models were compared.

The mathematical expression that defines z(α) function is given below. First expression with the term of $(d\alpha/dt)_\alpha$ was used to calculate experimentally obtained thermal decomposition. Second expression ($z(\alpha)=f(\alpha)g(\alpha)$) was used to calculate the theoretical z(α) plots for nucleation models (Avrami-Erofeyev) given in Table 2 for comparison with experimental results.

$$z(\alpha) = \left(\frac{d\alpha}{dt}\right)_\alpha T_\alpha^2 \left(\frac{p[(E/RT)_\alpha]}{\beta T_\alpha}\right)$$

$$z(\alpha) = f(\alpha)g(\alpha) = f(\alpha)\frac{AE}{\beta R}p\left[\left(E/RT\right)_\alpha\right]$$

Comparison of experimental data between theoretical reaction models in terms of z(α) master plot is given below.
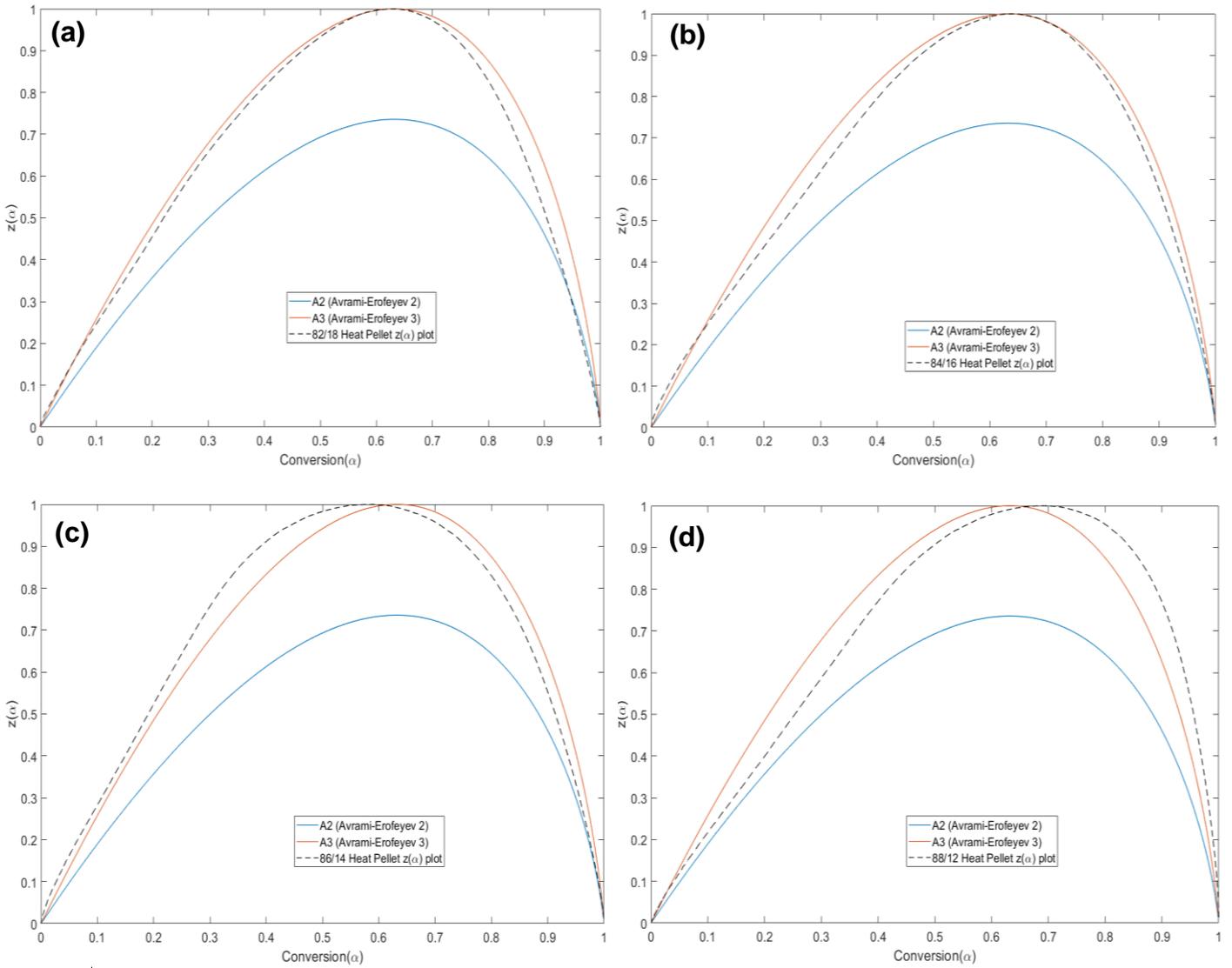
Figure 50. Plots of z(α) vs. α for theoretical reaction models and for heat pellets with different weight compositions at 5 °C/min heating rate. Heat pellets: (a) 82/18 (w:w), (b) 84/16 (w:w), (c) 86/14 (w:w), (d) 88/12 (w:w)

Figure 50 shows that although the experimental and theoretical y(α) and z(α) plots show resemblance they do not overlap. Malek et al. shows mathematically in his study that in order to select nucleation models as suitable, the conversion where the z(α) ($α_z$) should be **0.63** [59]**.** For heat pellets of 82/18 (w:w), 84/16 (w:w), 86/14 (w:w), 88/12 (w:w), $α_z$ values are **0.60, 0.65, 0.58 and 0.69** respectively. In this case, inequality of $0 < α_y < α_z$ should be checked. If this condition holds, then Śesták-Berggren's model can be used to describe the mechanism of reaction [59]. Śesták-Berggren's model (Equation ((33)) is a general form that can represent the characteristic of various reaction by adjusting its parameters (n and m) (see Table 6).

$$f(\alpha) = \alpha^m (1 - \alpha)^n \qquad \textbf{(33)}$$

To check whether $0 < \alpha_y < \alpha_z$ condition holds, α_y and α_z are determined heat pellets studied as follows.

Table 18. α_y and α_z parameters of studied heat pellets

Weight Composition of Heat Pellet (w:w)	The conversion where y(α) is maximum, α_y	The conversion where z(α) is maximum, α_z
82/18	0.51	0.60
84/16	0.51	0.65
86/14	0.42	0.58
88/12	0.52	0.69

In all cases, $0 < \alpha_y < \alpha_z$ condition holds, that is set for the eligibility of a reaction model to fit Śesták-Berggren reaction model.

Reaction model of Śesták-Berggren has parameters of m and n to be determined. To determine m and n parameters, Śesták-Berggren's reaction model expression (Equation (33)) was inserted to the general kinetic equation for non-isothermal processes (Equation (10)) and then it was linearized by taking natural algorithm (Equation (34)). Slope of this linearized form gives the value of **"n"** parameter. The intersection of the curve with ln(y(α)) axis also gives the pre-exponential factor, A. Linearity of the slope holds for conversion range of 0.5 and 0.8 (see Figure 40, Figure 41 and Figure 42) **"m"** parameter was calculated using the relation given in Equation (35).

$$\underbrace{ln\left[\frac{d\alpha}{dt}exp\left(\frac{E_{avg}}{RT}\right)\right]}_{y(\alpha)} = lnA + nln[\alpha^p(1-\alpha)] \tag{34}$$

$$p = \frac{m}{n} = \frac{\alpha_y}{1-\alpha_y} \tag{35}$$

Plots of Equation (34) for all heat pellets studied are given in figures below.

91
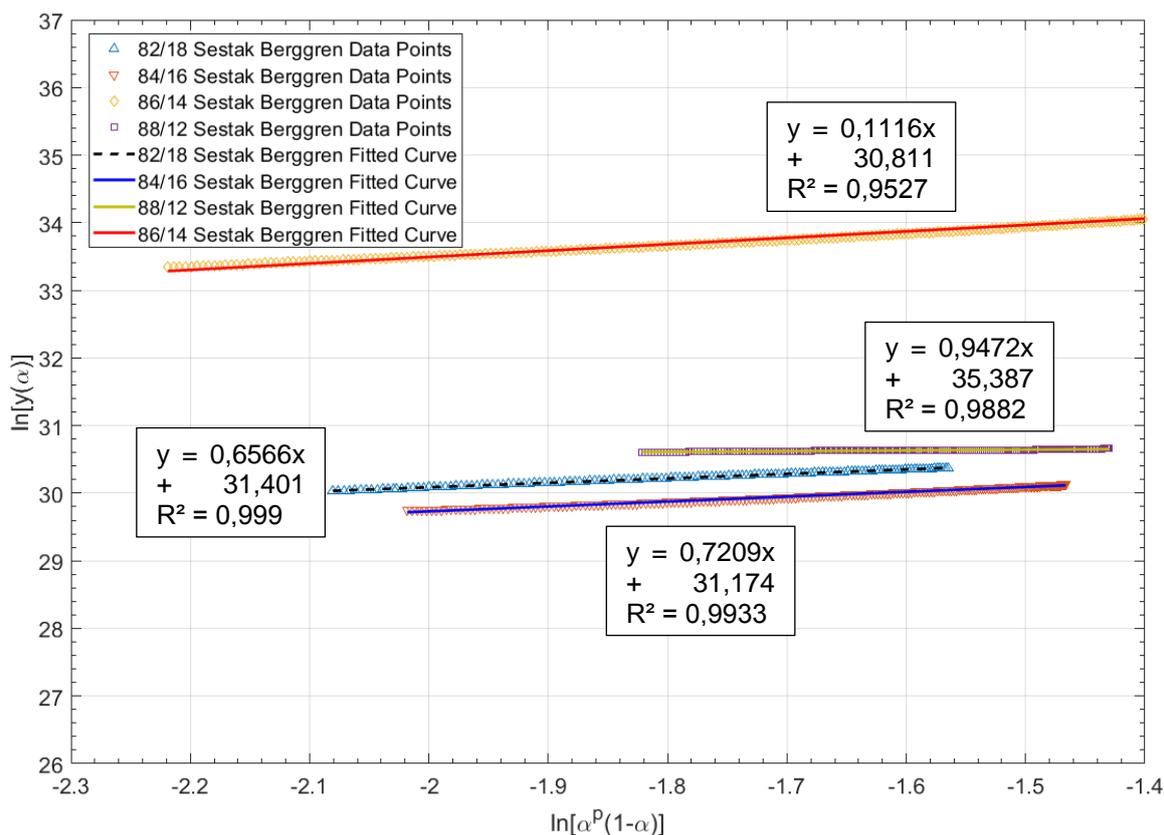
Figure 51. Experimental data and Śesták-Berggren plots for all heat pellets

The Śesták-Berggren parameters (m and n) and pre-exponential factor (A) that was calculated from the Śesták-Berggren plot is summarized in Table 19.

Table 19. Śesták-Berggren parameters and pre-exponential factor

Weight Composition of Heat Pellet (w:w)	m (Śesták-Berggren Parameter)	n (Śesták-Berggren Parameter)	Pre-exponential Factor (lnA)
82/18	0.757	0.657	31.40
84/16	0.804	0.721	31.17
86/14	0.694	0.947	35.39
88/12	0.084	0.094	30.81

Using Śesták-Berggren plot, pre-exponential factor is only calculated in the conversion range of linearity which is 0.5 and 0.8. To calculate pre-exponential factor that involved whole range of conversion or in other words thermal decomposition process, Equation (32) was used and the results were reported in Table 20.

Table 20. Calculated values of pre-exponential factor

Heat Pellet Weight Composition (w:w)	Pre-exponential Factor determined from Śesták-Berggren Plot (lnA)	Calculated Pre-exponential Factor (lnA)
82/18	31.40	30.00
84/16	31.17	30.14
86/14	35.39	32.86
88/12	30.81	32.80

To this point, all kinetic parameters (E_a, $f(\alpha)$ and A) for each weight composition heat pellet were determined. Kinetic parameters are summarized in Table 21.

Table 21. Kinetic parameters obtained for different composition of heat pellets

Heat Pellet Weight Composition (w:w)	Average Activation Energy (kJ/mol)	m (Śesták-Berggren Parameter)	n (Śesták-Berggren Parameter)	Pre-exponential Factor (lnA)
82/18	**208**	0.757	0.657	30.00
84/16	**210**	0.804	0.721	30.14
86/14	**218**	0.694	0.947	32.86
88/12	**222**	0.084	0.094	32.80

Validity of these obtained kinetic parameters is tested using COMSOL model that employs "Reaction Engineering" physics interface. Results of the comparison between model and experimental data for 82/18 (w:w) heat pellet is given below.
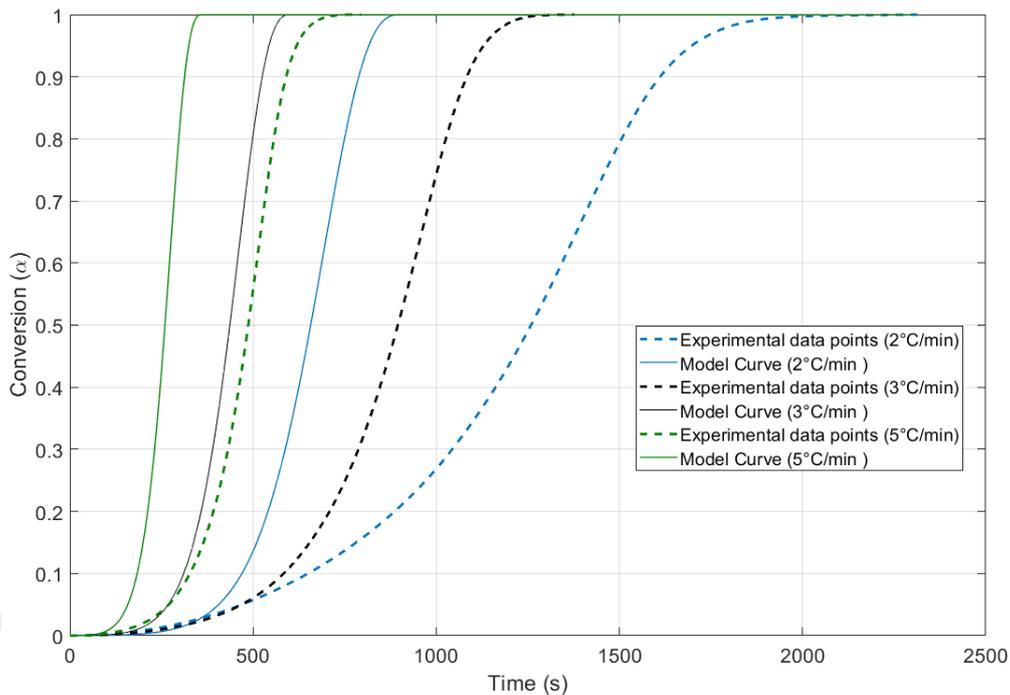
Figure 52. Comparison between time (s) vs. conversion (α) model curve and experimental data for 82/18 (w:w) heat pellet

Figure 52 shows that, conversion values of model deviate from experimental values too much. Since reaction rate of model was faster it was deduced that, either the activation energy value is too low or the pre-exponential factor is too high.

This result reveals that analytical methods (isoconversional method, Malek's procedure) used to determine kinetic parameters are prone to errors and can only produce rough estimates of kinetic parameters. Although these methods provide inaccurate results, they are needed to obtain initial values for the non-linear regression. Consequently, analytical methods are used in conjunction with a non-linear regression method. Comparison of model and experimental data was also repeated for 84/16, 86/14 and 88/12 (w:w) heat pellets as well. Results for this comparison are given in Appendix E.

The extent of distinction between model and experimental data suggests that kinetic parameters need fine-tuning before using them as parameters of reaction rate for burning simulation. In the next section, optimization procedure was carried out using the analytically obtained kinetic parameters as initial values.

4.5. Optimization of Kinetic Parameters

The optimized kinetic parameter results obtained by using the analytically calculated kinetic parameters as initial values are presented. The optimization procedure employed an iterative procedure that tried to minimize the difference between experimental and calculated conversion (α) vs. time (s) data by controlling kinetic parameters (E_a, reaction model parameters; m and n, A). This iterative procedure was created by using COMSOL Multiphysics' optimization tool (see 3.3.4).

To determine the quality of the fit, correlation coefficients (r) between calculated model and experimental data are evaluated as well. Correlation coefficient values gave insight about the obtained kinetic parameters, whether they are in the acceptable range to be used for simulation of the burning process.

The time(s) vs. conversion (α) data was obtained by non-linear regression with the optimized kinetic parameters as the initial values are shown in the same figure with experimental data. The comparison figure for 82/18 (w:w) heat pellet is given below.

Figure 53. Comparison between time(s) vs. conversion (α) model curve (calculated with optimized kinetic parameters) and experimental data for 82/18 (w:w) heat pellet

Figure 53 shows that with optimized kinetic parameters, overlapping between calculated model and experimental data were greatly improved. This improvement is

95

quantified by calculating the correlation coefficients as well. Correlation coefficients for the model and experimental data for heating rates of 2 °C/min, 3 °C/min and 5 °C/min were 0.986, 0.990 and 0.994 respectively.

The comparison figure for 84/16 (w:w) heat pellet is given below.

Figure 54. Comparison between time(s) vs. conversion (α) model curve (calculated with optimized kinetic parameters) and experimental data for 84/16 (w:w) heat pellet

Correlation coefficients for the model and experimental data for heating rates of 2 °C/min, 3 °C/min and 5 °C/min were 0.993, 0.980 and 0.991 respectively. The comparison figure for 86/14 (w:w) heat pellet is given below.
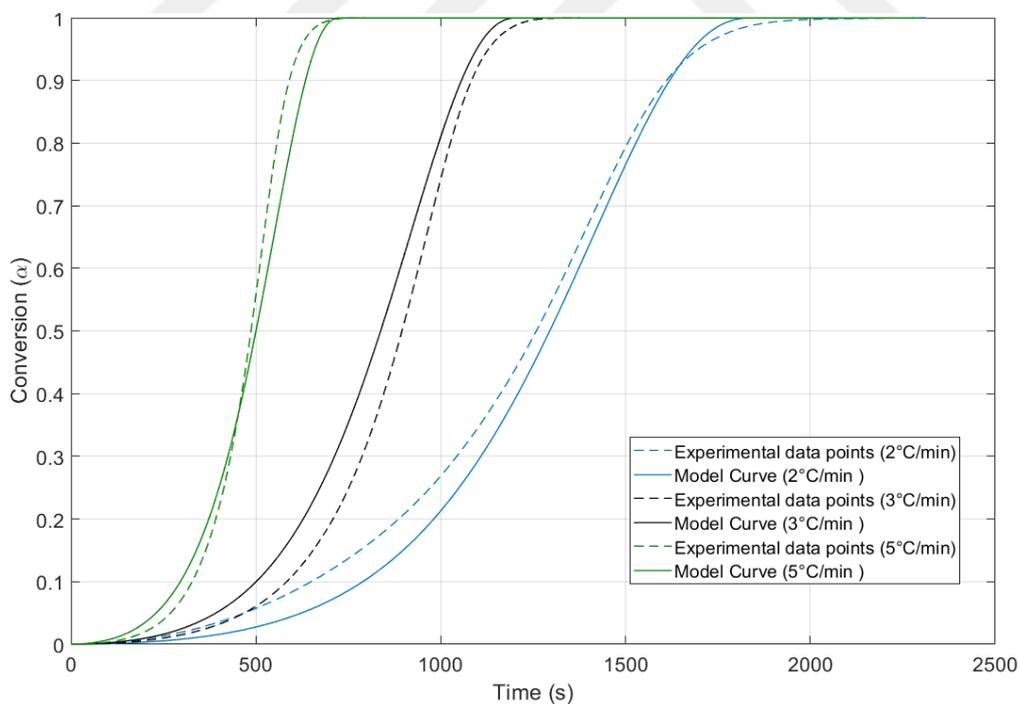
Figure 55. Comparison between time(s) vs. conversion (α) model curve (calculated with optimized kinetic parameters) and experimental data for 86/14 (w:w) heat pellet

Correlation coefficients for the model and experimental data for heating rates of 2 °C/min, 3 °C/min and 5 °C/min were 0.995, 0.982 and 0.989 respectively. The comparison figure for 88/12 (w:w) heat pellet is given below.
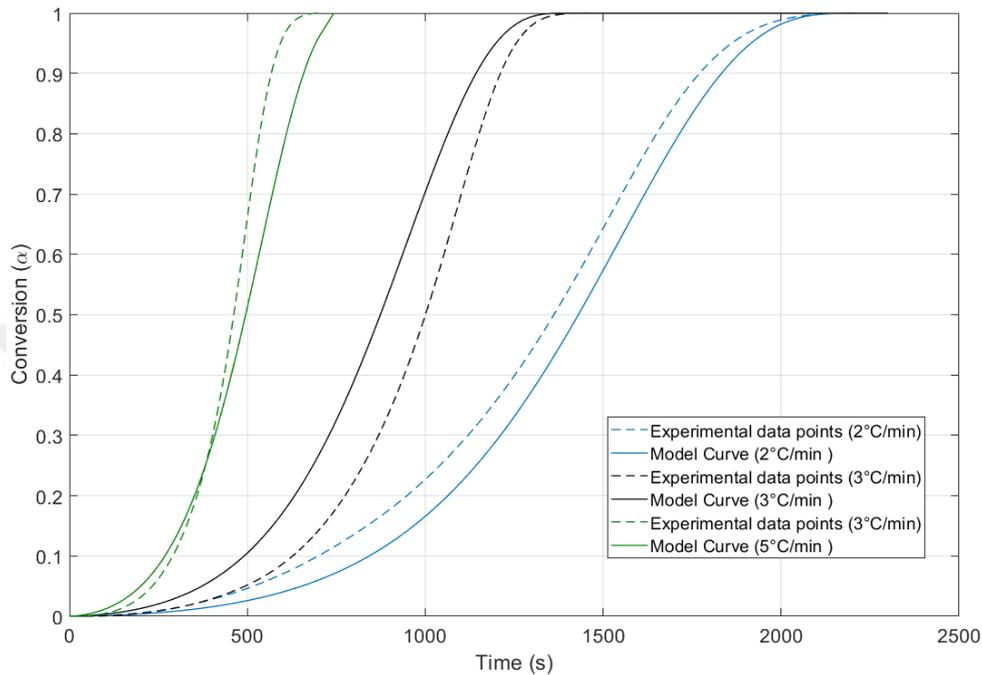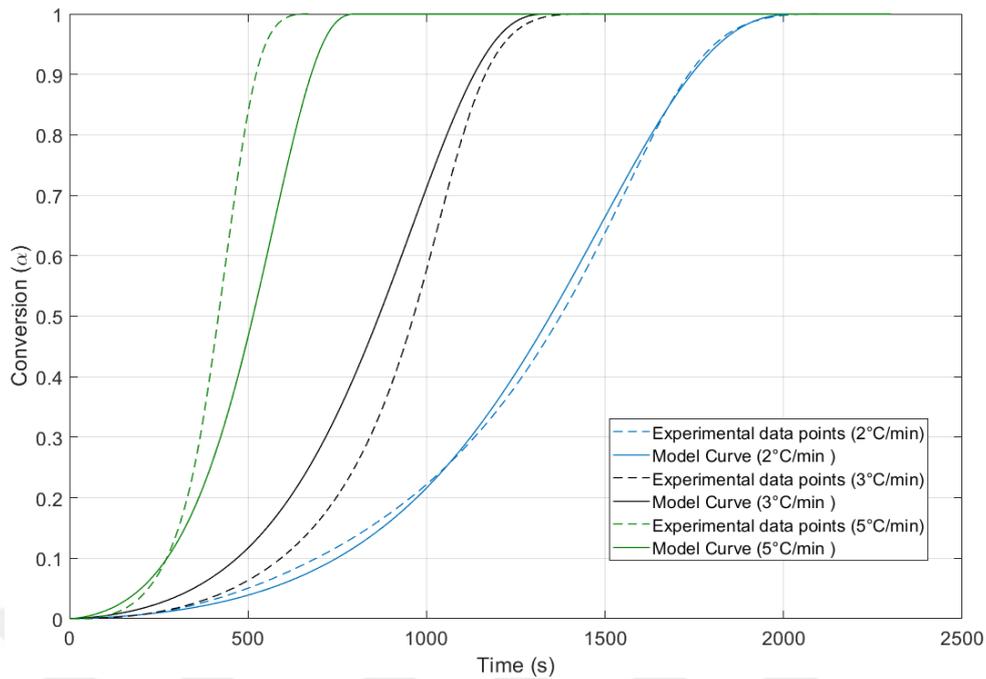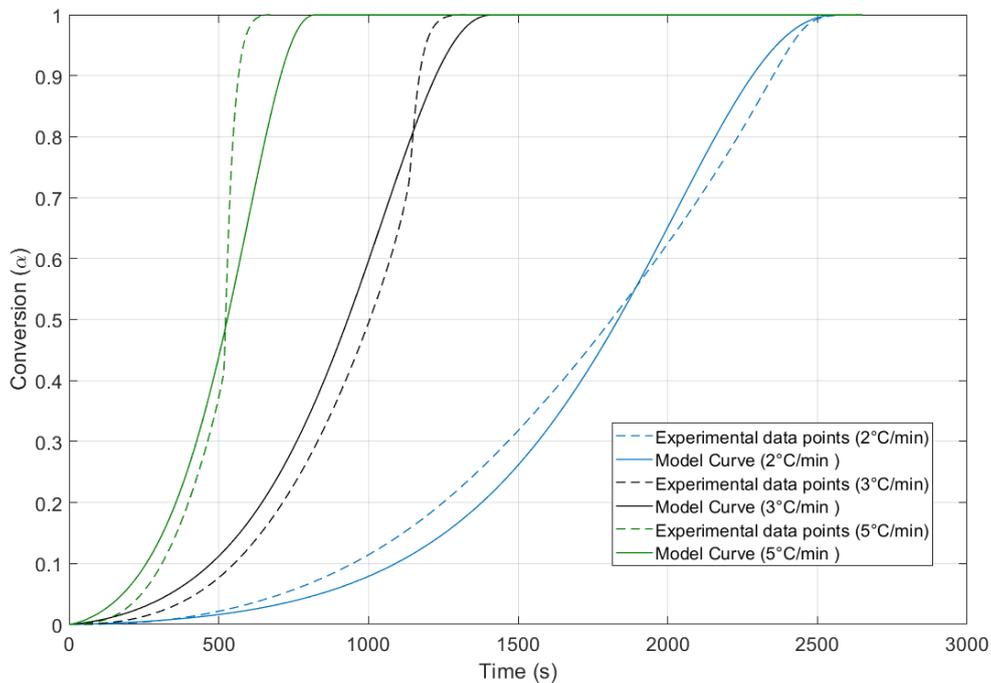

Figure 56. Comparison between time(s) vs. conversion (α) model curve (calculated with optimized kinetic parameters) and experimental data for 88/12 (w:w) heat pellet

97

Correlation coefficients for the model and experimental data for heating rates of 2 °C/min, 3 °C/min and 5 °C/min were 0.995, 0.991 and 0.989 respectively. From the results of correlation coefficient, r, it can be concluded that optimized kinetic parameters provided good fitting with model results and experimental data. Calculation time for kinetic parameter optimization of one heat pellet took about 21-22 hours with 48 iterations using a Dell T7810 Pluton workstation. Without good initial guesses obtained from analytical kinetic parameter determination methods, it would have taken too long to calculate such optimization model or the calculated parameters would have contained high error.

The results of the analytically obtained and optimized kinetic parameters are summarized in Table 22.

Table 22. Comparison of the kinetic parameters obtained by analytical methods and non-linear regression for heat pellets with weight composition range of 82/18 – 88/12

Kinetic Parameters obtained by Isoconversional Method and Malek's Procedure						Non-linear regression with COMSOL Multiphysics				
Kinetic Parameters	Heat Pellet Weight Compositions (w:w)					Kinetic Parameters	Heat Pellet Weight Compositions (w:w)			
	82/18	84/16	86/14	88/12			82/18	84/16	86/14	88/12
n(S-B parameter)	0.657	0.721	0.947	0.094	Optimization	n(S-B parameter)	0.636	0.755	0.694	0.644
m(S-B parameter)	0.757	0.804	0.694	0.084		m(S-B parameter)	0.441	0.373	0.321	0.229
E_a (kJ/mol)	208	210	218	222		E_a (kJ/mol)	215	217	223	228
ln(A)	30.0	30.1	32.8	32.8		ln(A)	29.01	29.16	30	29.77

From Table 22, it can be seen that apparent activation energy increases with decreasing $KClO_4$ content in heat pellet while pre-exponential factor relatively remains constant. Reason for increasing E_a trend is explained as: with increasing $KClO_4$ content, imperfections in the crystal structure that causes depreciation in

activation energy increases too (nucleation model). Consequently, activation energy of thermal decomposition decreases.

Reaction mechanism in solid state is mainly controlled by the structure of reactants used. For heat pellets, only the weight composition was changed. Therefore, reaction mechanism of the thermal decomposition of heat pellets should be same. Slight differences in Śesták-Berggren parameters (m and n) shows that reaction mechanism for different weight composition of heat pellets were relatively same.

Up to now, study of thermal decomposition kinetics of heat pellets used in thermal batteries was never reported. Therefore, for validation of determined kinetic parameters, simulation studies of the heat pellets to determine burn rates (cm/s) were carried out.

4.6.   Kinetic Modelling and Simulation

In this section, the burn rate results of different weight composition heat pellets were calculated using a time dependent model which was constructed using COMSOL Multiphysics. Simulation results of burn rate were compared with the experimental values in literature.

In this simulation, self-propagating combustion wave (Figure 57) was modeled. The heat source term, Q is calculated using the mass density ρ (kg/m^3), conversion α, and heat of reaction $\Delta H_{reac.}$ (kJ/mol) :

$$Q = \rho \frac{d\alpha}{dt} \Delta H \qquad (36)$$

The heat of reaction (calorific output) for this process was -413 kJ/mol Fe [3].
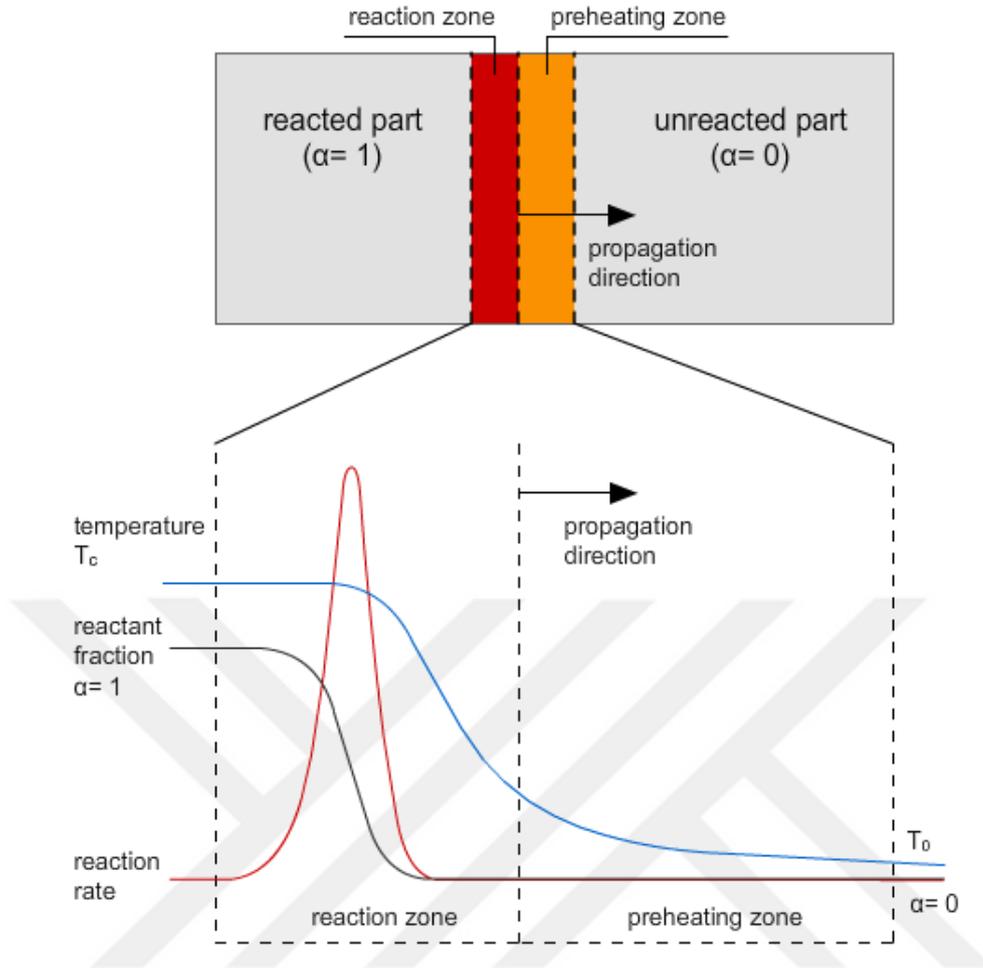
Figure 57. Combustion wave propagation

From the analysis of reaction model, dα/dt term was found to be:

$$\frac{d\alpha}{dt} = \alpha^m (1-\alpha)^n A exp\left(\frac{-E_a}{RT}\right) \tag{37}$$

where E_a is the apparent activation energy (J/mol), R is the universal gas constant (J/mol.K), A is the pre-exponential factor (s^{-1}), n and m are the Śesták-Berggren parameters.

The temperature distribution was defined by differential equation of transient heat transfer formulated based on the energy balance:

$$\frac{\partial(\rho C_p T)}{\partial t} = \frac{\partial}{\partial x}\left(k\frac{\partial T}{\partial x}\right) + Q_{reaction} \tag{38}$$

where T (K) is the temperature, ρ is the mass density (kg/m^3), C_p is the specific heat of heat pellet (J/kg.K), k is the thermal conductivity of heat pellet (W/m.K) and $Q_{reaction}$ is the exothermic heat of the pyrotechnic reaction (W/m^3).

For the concentration distribution, following differential equation of transient mass balance has been formulated:

$$\frac{\partial(c)}{\partial t} = R_c = rV \tag{39}$$

$$-r = k(\alpha)^m (1 - \alpha)^n c_0 \tag{40}$$

where c_0 is initial concentration of the limiting reactant (mol/m^3), KClO$_4$.

Solving the energy and mass balances simultaneously with the coupled independent variable of T (temperature), results of temperature and concentration distribution in heat pellets as a function of time and location is acquired. The results of temperature distribution for 82/18 heat pellet with t=0 (ms), t=t$_{final}$/2 (ms) and t=t$_{final}$ (ms) are given, respectively.

Figure 58. Temperature distribution of 82/18 (w:w) heat pellet with different stages ((a) t=0 (ms), (b) t=t$_{final}$/2 (ms) and (c) t=t$_{final}$ (ms)) of burning process

Figure 59. Temperature distribution of 84/16 (w:w) heat pellet with different stages ((a) t=0 (ms), (b) t=t_{final}/2 (ms) and (c) t=t_{final} (ms)) of burning process

Figure 60. Temperature distribution of 86/14 (w:w) heat pellet with different stages ((a) t=0 (ms), (b) t=t_{final}/2 (ms) and (c) t=t_{final} (ms)) of burning process
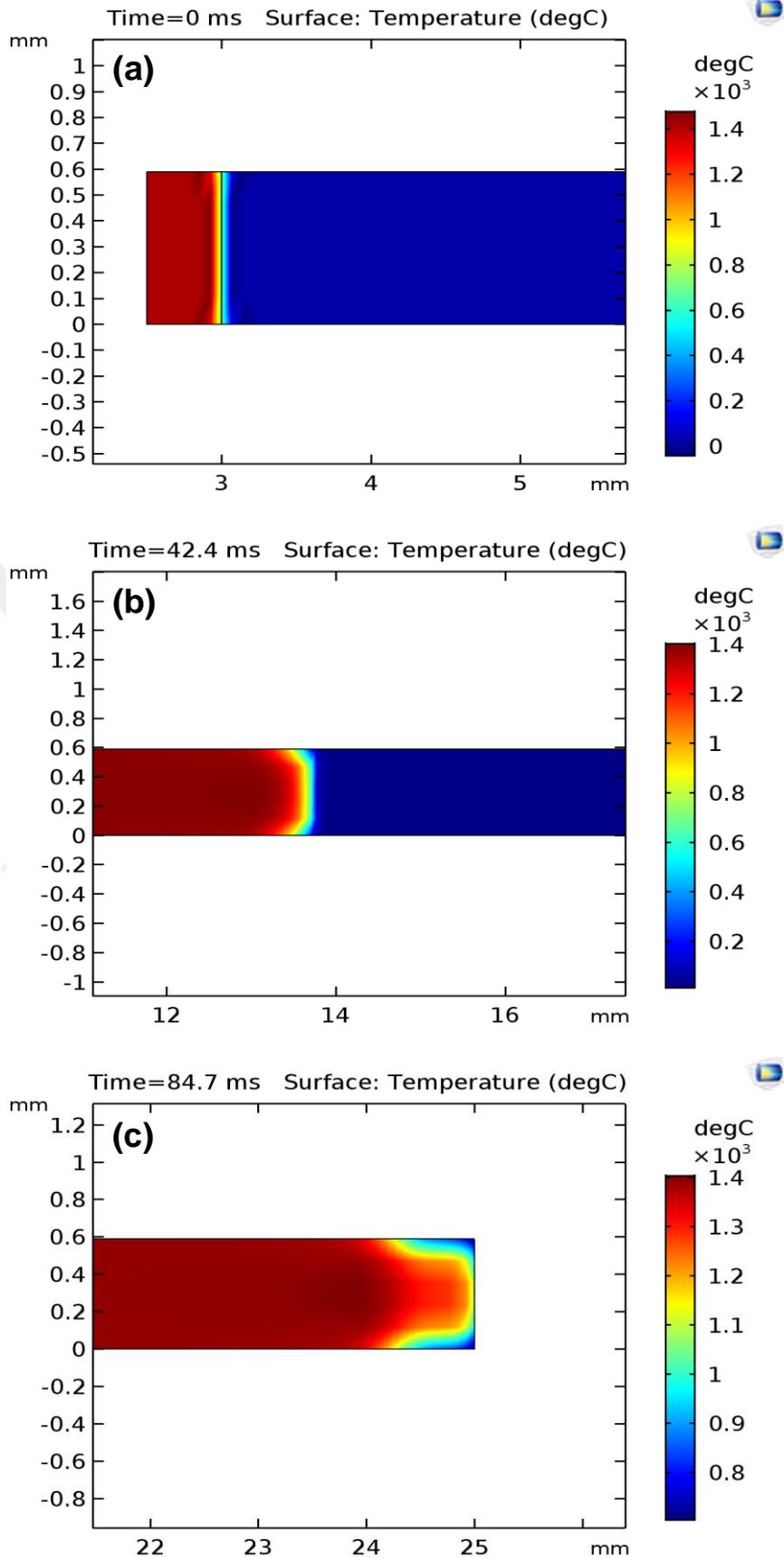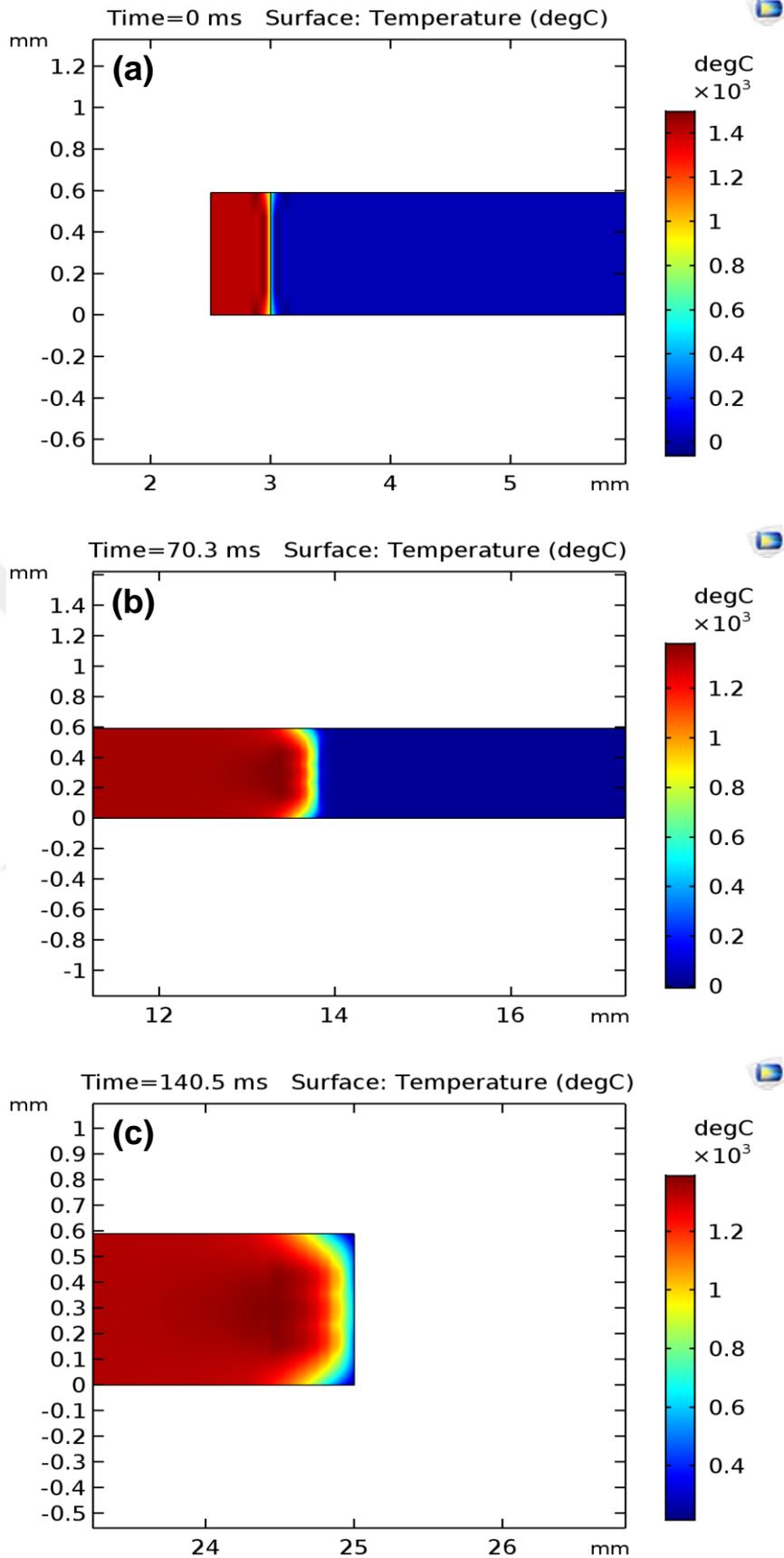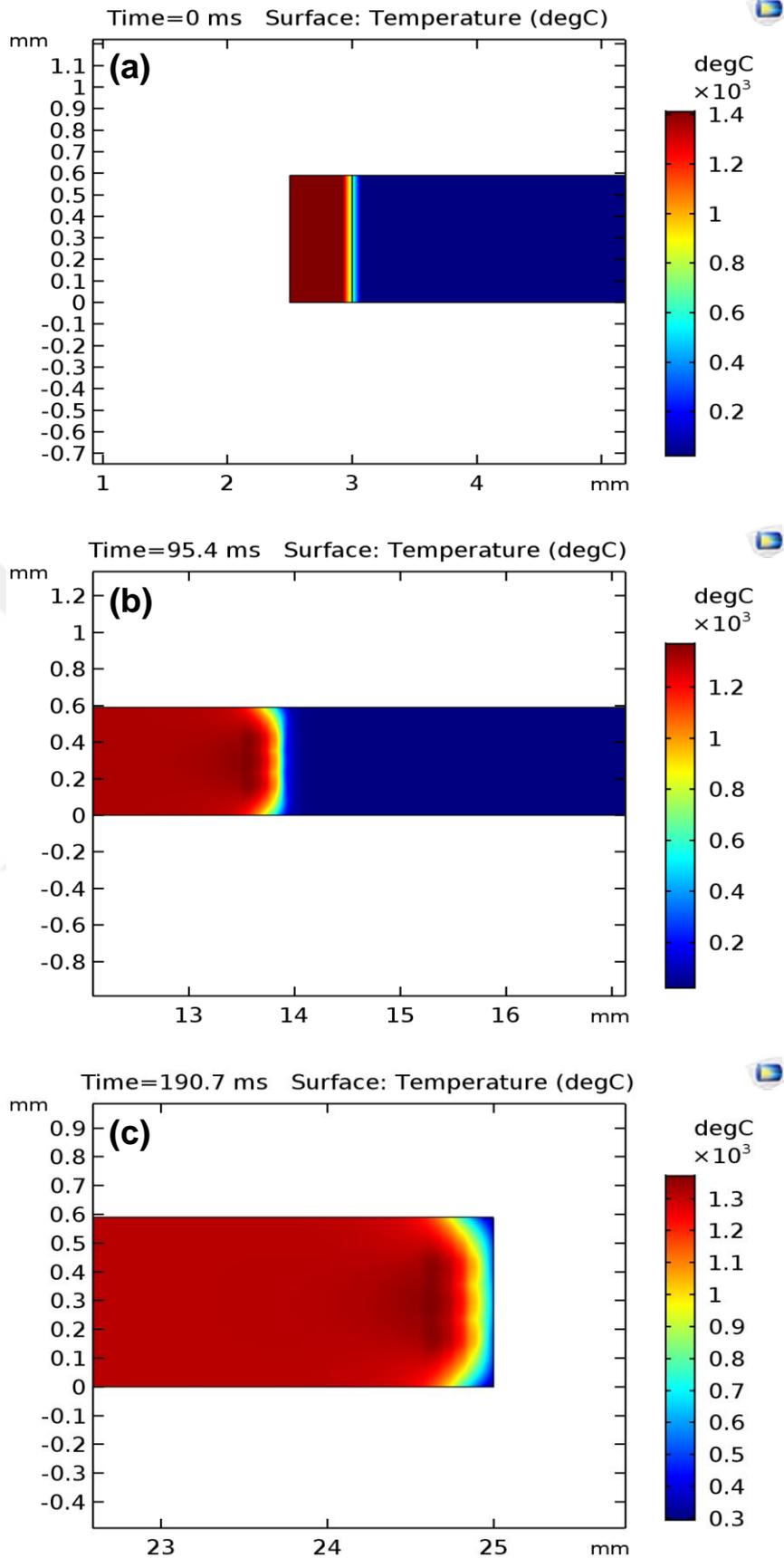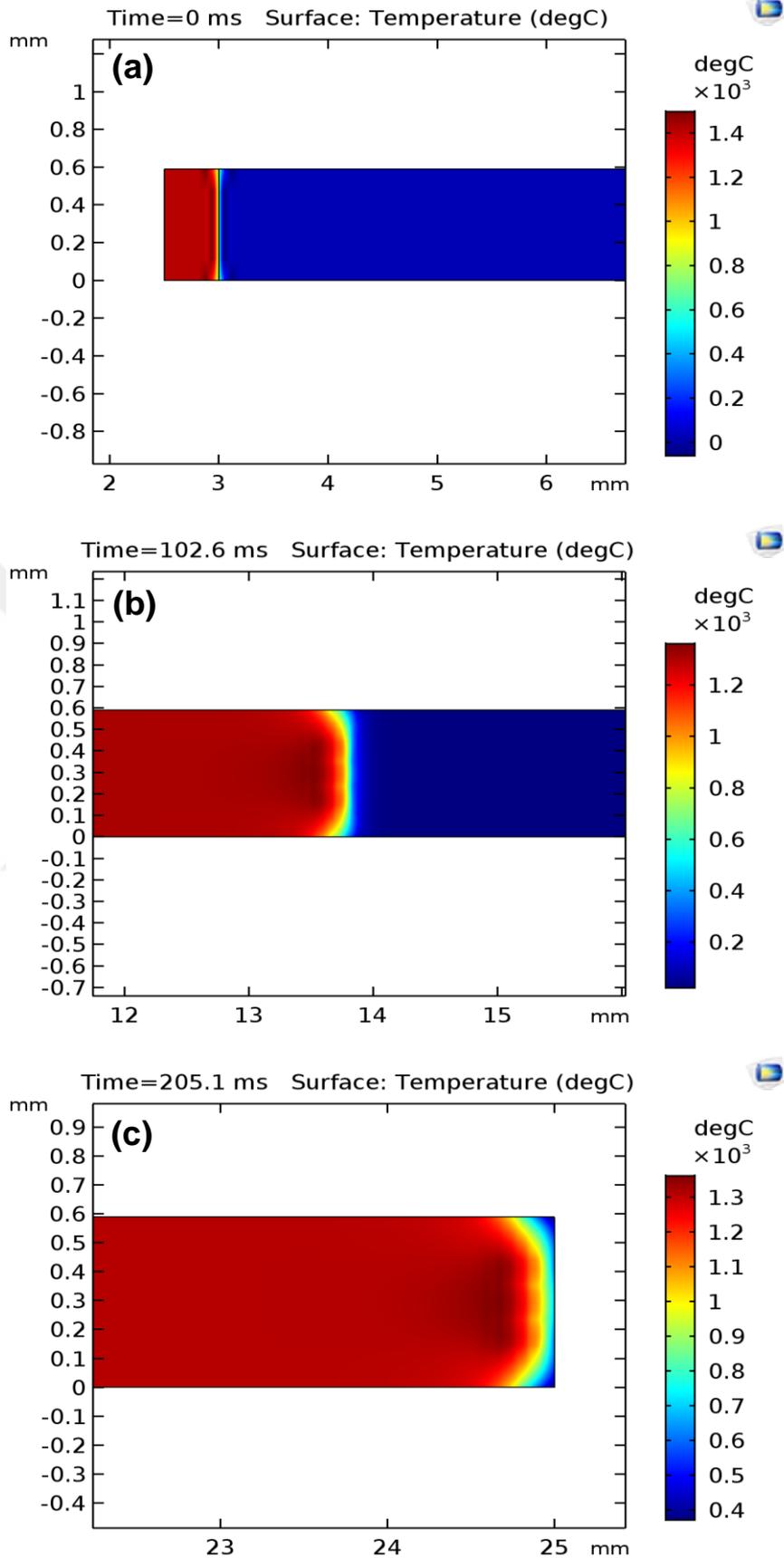
Figure 61. Temperature distribution of 88/12 (w:w) heat pellet with different stages ((a) t=0 (ms), (b) t=t$_{final}$/2 (ms) and (c) t=t$_{final}$ (ms)) of burning process

105

Time-dependent temperature distribution results were used to calculate the burn rates of heat pellets with varying weight compositions. The comparison of burn rate result of heat pellets with literature values are given in Table 23.

Table 23. Comparison of calculated and literature burn rate results for different weight composition of heat pellets

Heat Pellet Weight Composition (w:w)	Calculated Burn Rates (cm/s)	Burn Rates from Literature (cm/s) [2, 26]	Percent. Deviation from Literature (%)
82/18	26.0	22.5	15.56
84/16	15.7	15.0	4.67
86/14	11.5	10.2	12.75
88/12	10.7	9.8	9.18

The results of deviation show that there is a systematic error in burn rates. The cause for this systematic shift of burn rates to higher values is interpreted as the effect of assumption of thermal insulation on the heat pellet boundaries in simulation. In literature, burn rate values were obtained experimentally by placing heat pellets between insulators such as Min-K, quartz etc. These materials absorb some of the heat of reaction from the heat pellets causing decrease in burn rate. Apart from systematic error, calculated burn rates are in good agreement with the literature, which proves that kinetic parameters obtained by optimization are consistent (Figure 62).
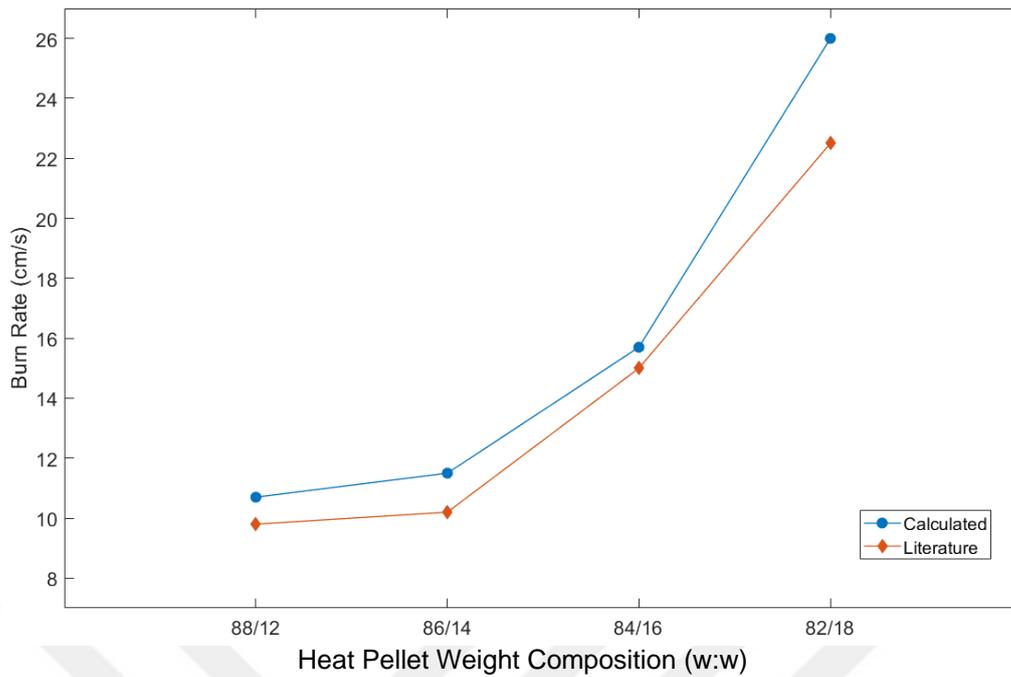
Figure 62. Comparison of calculated and literature burn rates for studied heat pellets

Both concentration of $KClO_4$ and temperature distribution in heat pellets during burning process at $t=t_{final}/2$ (Figure 63) revealed that concentration profile of the propagation has similarity with the "laminar flow" velocity profile of an incompressible fluid. This shows that heat pellet combustion wave propagation was fully developed for this simulation which is an indication of accurate simulation of burning process.
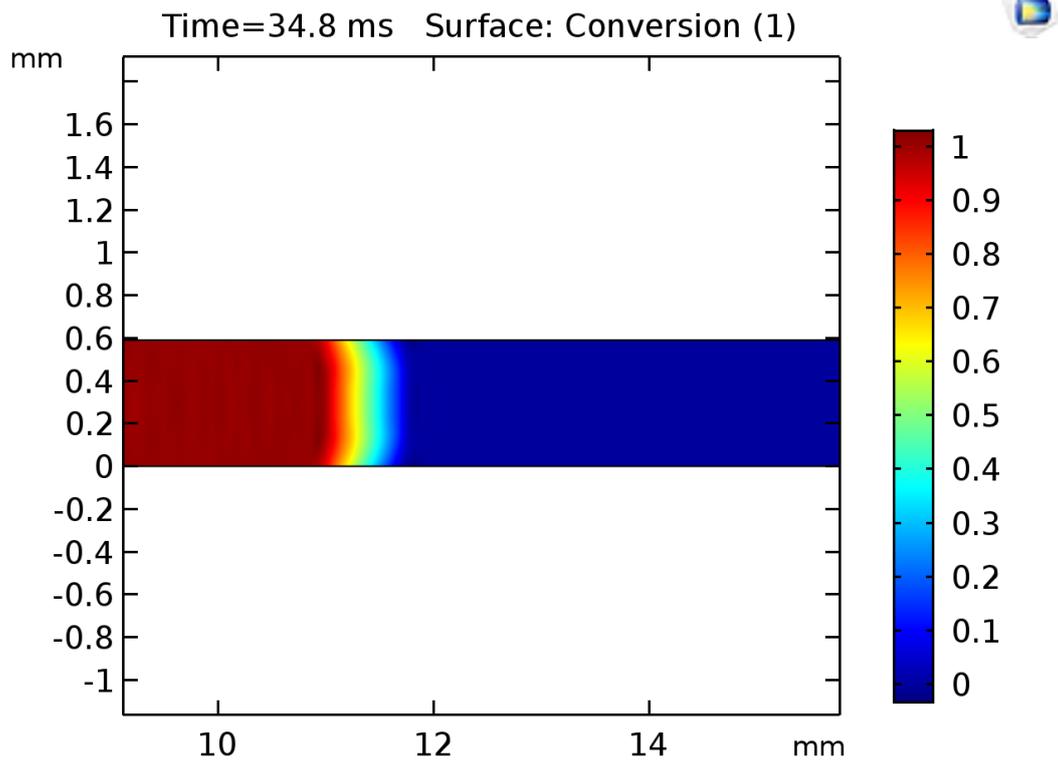
Figure 63. Conversion distribution of 82/18 heat pellet at t=t$_{final}$/2

.

5. CONCLUSIONS

In this study, kinetic parameters for heat pellets with weight compositions in the range of 82/18 – 88/12 (w:w) were determined using a complementery method which employs isoconversional and Malek's method with non-linear regression utilizing COMSOL Multiphysics's optimization tool. These kinetic parameters were used as initial values for the simulation of burning process of heat pellets. The burn rate values that were determined using simulation were compared with the literature values. The overlapping calculated burn rate values with literature values indicated that obtained kinetic parameters were accurate.

From the results of isoconversional analysis, it was seen that with increasing % content of $KClO_4$, activation energy decreases. This behavior was attributed to the increased probability of oxidation reaction with increasing % content of $KClO_4$. Isocoversional analysis also revealed that multi-step decomposition ($KClO_4$ decomposition and Fe oxidation) takes place until the overall conversion reaches 0.4.

Thermal decomposition of heat pellets was determined to follow Śesták-Berggren's model from the so called master plots, $y(\alpha)$ and $z(\alpha)$. Master plots showed that thermal decomposition mechanism can be described by nucleation model. Nucleation model is used to describe processes that take place when the crystal in reacting structure has imperfect sites. These imperfect sites become the reactive sites when the external conditions (temperature, pressure etc.) are fulfilled.

The model results computed using kinetic parameters that were obtained using isocoversional and Malek's method did not overlapped with the experimental results. Therefore, optimization routine was created in COMSOL Multiphysics that employed an iterative procedure with objective of minimizing sum of least squares between model and experimental data. Optimization procedure gave the optimal combination of reaction model, activation energy and pre-exponential factor. This showed that, determination of kinetic parameters with non-linear regression is a more robust method.

Kinetic properties of heat pellets are the most dominant parameters that controls the activation time in a thermal battery. In a case when fast power discharge is required for a thermal battery, activation time is expected to be as small as possible. For this case, kinetic parameters suggest that 82/18 (w:w) heat pellet should be selected. In the case when operation time of the thermal battery is required to be long, 88/12 (w:w) heat pellet should be selected because it release its heat of reaction more slowly.

More importantly, this study has laid foundations for thermal modelling of the ignition phase of a thermal battery.

6. REFERENCES

[1] S. Schoeffert, "Thermal batteries modeling, self-discharge and self-heating," *Journal of Power Sources,* no. 142, pp. 361 - 369, **2005**.

[2] R. A. Guidotti, J. Odinek and F. W. Reinhardt, "Characterization of Fe/KClO4 Heat Powders and Pellets," *Journal of Energetic Materials,* no. 24, pp. 271-305, **2006**.

[3] L. C. Yang, "Reaction Rate Analysis for Selected Solid-to-solid Reaction Pyrotechnic Compositions," in *48th AIAA/ASME/SAE/ASEE Joint Propulsion Conference & Exhibit*, Atlanta,Georgia, **2012**.

[4] M. Shamsipur, S. Pourmortazavi and M. Fathollahi, "Kinetic Parameters of Binary Iron/Oxidant Pyrolants," *Journal of Energetic Materials,* no. 30, pp. 97-106, **2012**.

[5] V. Klasons and C. M. Lamb, "Thermal Batteries," in *Handbook of Batteries*, **2001**, p. Chapter 21.

[6] R. A. Guidotti and P. Masset, "Thermally activated ("thermal") battery technology Part I: An overview," *Journal of Power Sources,* no. 161, pp. 1443-1449, **2006**.

[7] J. B. and K. L. Kosanke, "Control of Pyrotechnic Burn Rate," in *Second International Symposium on Fireworks*, **1994**.

[8] B. Wojciechowski and N. Rice, Experimental Methods in Kinetic Studies, Elsevier, **2003**.

[9] J. H. Van't Hoff, Etudes de Dynamique Chimique, Amsterdam, **1884**.

[10] T. E. o. E. Britannica, "Encyclopædia Britannica," [Online]. Available: https://www.britannica.com/science/activation-energy.

[11] W. Garner, Chemistry of the Solid State, **1955**.

[12] P. W. M. Jacobs and F. C. Tompkins, "Classification and theory of solid reactions," in *Chemistry of the solid state*, New York, Academic Press, **1955**.

[13] M. E. Brown, D. Dollimore and A. K. Galwey, "Reactions In the Solid State," in *Comprehensive Chemical Kinetics*, Amsterdam, Elsevier, **1980**, p. Chapter 3.

[14]   S. Vyazovkin and C. A. Wight, "Isothermal and non-isothermal kinetics of thermally stimulated reactions of solids," *International Reviews in Physical Chemistry,* vol. 17, no. 3, pp. 407-433, **1998**.

[15]   A. K. Galwey and M. E. Brown, "Application of the Arrhenius equation to solid state kinetic: can this be justified?," *Thermochimica Acta,* vol. 386, no. 1, pp. 91-98, **2002**.

[16]   J. Y. Macdonald and C. N. Hinshelwood, "The Formation and Growth of Silver Nuclei in the Decomposition of Silver Oxalate," *Journal of the Chemical Society,* vol. 127, **1925**.

[17]   A. Khawam and D. R. Flanagan, "Solid-State Kinetic Models: Basics and Mathematical Fundamentals," *Journal of Physical Chemistry,* vol. 110, pp. 17315-17325, **2006**.

[18]   S. Danali, R. Palaiah and K. Raha, "Developments in Pyrotechnics," *Defence Science Journal,* vol. 60, pp. 152-158, **2010**.

[19]   Y. Miao, C. Liping, Y. Jinyang and P. Jinhua, "Thermoanalytical investigation on pyrotechnic mixtures containing Mg-Al alloy powder and barium nitrate," *Procedia Engineering ,* vol. 45, pp. 567-573, **2012**.

[20]   L. K. and J. Kosanke, "Pyrotechnic Ignition and Propagation: A Review," in *Pyrotechnic Chemistry*, Journal of Pyrotechnic, Inc., **2004**.

[21]   T. Shimizu, "Chemical Components of Firework Compositions," in *Pyrotechnic Chemistry*, Whitewater,CO, Journal of Pyrotechnics, Inc., **2004**.

[22]   A. K. Helmy, "Prediction of Arrhenius Kinetic Constants for Zirconium Potassium Perchlorate," in *International Annual Conference, Fraunhofer Institut for Chemische Technologie, Conference 35*, **2004**.

[23]   K. Miyata, "Combustion of Boron Pyrotechnics," in *37th AIAA/ASME/SAE/ASEE Joint Propulsion Conference*, Salt Lake City, Utah, **2001**.

[24]   S. Knapp, V. Weiser, S. Kelzenberg and N. Eisenreich, "Modeling ignition and thermal wave progression in binary granular pyrotechnic compositions," *Propellants, Explosives, Pyrotechnics,* vol. 39, pp. 423-433, **2014**.

[25]   I. Bauman, D. Curic and M. Boban, "Mixing of solids in different mixing

devices," *Sadhana,* vol. 33, pp. 721-731, **2008**.

[26]   J. W. Reed, R. R. Walters, R. A. Guidotti and A. K. Jacobson, "Iron/Potassium Perchlorate Pellet Burn Rate Measurements," EG&G Mound Applied Technologies, Miamisburg, Ohio, **1995**.

[27]   J. H. McLain, Pyrotechnics and Solid State Chemistry, Philadelphia, PA: The Franklin Institute Research Laboratory, **1971**.

[28]   J. A. Conkling, Chemistry of Pyrotechnics: Basic Principles and Theory, NY: Marcel Dekker, Inc., **1985**.

[29]   L. C. Yang, "Effects of Fuel Particle Size and Impurity on Solid-to-Solid Pyrotechnic Reaction Rate," in *47th AIAA/ASME/SAE/ASEE Joint Propulsion Conference & Exhibition*, San Diego, California, **2011**.

[30]   K. Miyata and N. Kubota, "Combustion of Ti and Zr Particles with KNO3," in *Propellants, Explosives, Pyrotechnics*, **1996**, pp. 29-35.

[31]   L. J. Bement and M. L. Schimmel, A Manual For Pyrotechnic Design, Development and Qualification, Hampton, VA: NASA, **1995**.

[32]   S. Vyazovkin and C. A. Wight, "Kinetic in solids," *Annual Review of Physical Chemistry,* vol. 48, pp. 125-149, **1997**.

[33]   G. Klarčnik, J. Medved and P. Mrvar, "Differential thermal analysis (DTA) and differential scanning calorimetry (DSC) as a method of material investigation," *Materials and Geoenvironment,* vol. 57, pp. 127-142, **2010**.

[34]   G. Höhne, W. F. Hemminger and H. J. Flammersheim, Differential scanning calorimetry, Berlin: Springer-Verlag, **2003**.

[35]   F. X. Kayser and J. W. Patterson, "Sir William Chandler Roberts-Austen - His role in the development of binary diagrams and modern physical metallurgy," *Journal of Phase Equilibria,* vol. 19, no. 1, **1998**.

[36]   S. L. Boersma, "A theory of differential thermal analysis and new methods of measurement and interpretation," *Journal of American Ceramic Society,* vol. 38, p. 281, **1955**.

[37]   S. Vyazovkin, A. K. Burnham, J. M. Criado, L. Pérez-Maqueada, C. Popescu and N. Sbirrazzuoli, "ICTAC Kinetics Committee recommendations for performing kinetic computations on thermal analysis data," *Thermochimica*

Acta, vol. 520, pp. 1-19, **2011**.

[38]   J. H. Flynn, Thermal Analysis, New York: Academic, **1969**.

[39]   B. Roduit, C. Borgeat, B. Berger, P. Folly, B. Alonso, J. N. Aebischer and F. Stoessel, "Advanced Kinetic Tools For The Evaluation of Decomposition Reactions," *Journal of Thermal Analysis and Calorimetry,* vol. 80, pp. 229-236, **2005**.

[40]   D. Chen, A. Green and D. Dollimore, "DSC: the importance of baseline calibration," *Thermochimica Acta,* vol. 284, pp. 429-433, **1996**.

[41]   S. Vyazovkin, K. Chrissafis, M. L. Di Lorenzo, N. Koga, M. Pijolat, B. Roduit, N. Sbirrazzuoli and J. J. Sunol, "ICTAC Kinetics Committee recommendations for collecting experimental thermal analysis data for kinetic computations," *Thermochimica Acta,* vol. 590, pp. 1-23, **2014**.

[42]   A. Glasner and L. Weidenfeld, "Thermal Decomposition of Potassium Perchlorate," *Nature,* vol. 166, pp. 109-110, **1950**.

[43]   A. A. Jain, A. Mehra and V. V. Ranade, "Processing of TGA data: Analysis of isoconversional and model fitting methods," *Fuel,* vol. 165, pp. 490-498, **2016**.

[44]   L. A. Perez-Maqueda, J. M. Criado and P. Sanchez-Jimenez, "Combined kinetic analysis of solid-state reactions: a powerful tool for the simultaneous determination of kinetic parameters and the kinetic model without previous assumptions on the reaction mechanism," *Journal of Physical Chemistry,* vol. 110, pp. 12456-12462, **2006**.

[45]   G. Varhegyi, P. Szabo, E. Jakab and F. Till, "Least square criteria for the kinetic evaluation of thermoanalytical experiments: Examples from a char reactivity study," *Journal of Analytical and Applied Pyrolysis,* vol. 57, pp. 285-296, **2001**.

[46]   V. Mamleev, "Three model-free methods for calculation of activation energy in thermogravimetry," *Journal of Thermal Analysis and Calorimetry,* vol. 78, no. 3, pp. 1009-1027, **2004**.

[47]   A. K. Burnham and R. K. Weese, "Thermal Decomposition Kinetics of HMX," Lawrance Livermore National Laboratory, Livermore, CA, **2004**.

[48]   H. R. Pouretedal and M. Ravanbod, "Kinetic study of ignition of Mg/NaNO3 pyrotechnic using non-isothermal TG/DSC technique," *Journal of Thermal Analysis and Calorimetry,* vol. 119, pp. 2281-2288, **2015**.

[49]   M. Shamsipur, S. M. Pourmortavazi and S. S. Hajimirsadeghi, "An Investigation on Decomposition Kinetics and Thermal Properties of Copper-Fueled Pyrotechnic Compositions," *Combustion Science and Technology,* vol. 183, pp. 575-587, **2011**.

[50]   Z.-u.-d. Babar and A. Q. Malik, "Thermal Decomposition, Ignition and Kinetic Evaluation of Magnesium and Aluminium Fuelled Pyrotechnic Compositions," *Central European Journal of Energetic Materials,* vol. 12, no. 3, pp. 579-592, **2015**.

[51]   M. J. Starink, "The determination of activation energy from linear heating rate experiments: a comparison of the accuracy of isoconversion methods," *Thermochimica Acta,* vol. 404, pp. 163-176, **2003**.

[52]   H. Friedman, "Kinetics of thermal degradation of char-forming plastics from thermogravimetry- application to a phenolic resin," *Journal of Polymer Sciences Part C,* pp. 183-195, **1964**.

[53]   N. Sbirrazzuoli, Y. Girault and L. Elégant, "Simulations for evaluation of kinetic methods in differential scanning calorimetry. Part 3 - Peak maximum methods and isoconversional methods," *Thermochimica Acta,* vol. 293, pp. 25-37, **1997**.

[54]   S. Vyazovkin, K. Chrissafis, M. L. Di Lorenzo, N. Koga, M. Pijolat, B. Roduit, N. Sbirrazzuoli and J. J. Sunol, "ICTAC Kinetics Committee reccomendations for collecting experimental thermal analysis data for kinetic computations," *Thermochimica Acta,* vol. 590, pp. 1-23, **2014**.

[55]   C. Doyle , "Kinetic analysis of thermogravimetric data," *Journal of applied polymer science,* vol. 5, no. 15, pp. 285-292, **1961**.

[56]   C. Doyle, "Estimating isothermal life from thermogravimetric data," *Journal of applied polymer science,* vol. 24, no. 6, pp. 639-642, **2000**.

[57]   M. Starink, "The determination of activation energy from linear heating rate experiments: a comparison of the accuracy of isoconversion methods,"

Thermochimica Acta, vol. 404, pp. 163-176, **2003**.

[58] A. W. Coats and J. P. Redfern, "Kinetic parameters from thermogravimetric data," *Nature,* vol. 201, pp. 68-69, **1964**.

[59] J. Málek, "The kinetic analysis of non-isothermal data," *Thermochimica acta,* vol. 200, pp. 257-269, **1992**.

[60] N. Koga and H. Tanaka, "A kinetic compensation effect established for the thermal decomposition of a solid," *Journal of Thermal Analysis,* vol. 37, no. 2, pp. 347-363, **1991**.

[61] M. Kenton, J. Wilson, M. Miller, I. Yeaton, S. May, N. Elkouh and D. Bhakta, "A comprehensive, physics-based model for thermal batteries," in *44th Power Sources Conference*, Las Vages, **2010**.

[62] T. G. Voskuilen, J. C. Hewson, H. K. Moffat and S. A. Roberts, "Multi-Physics, Multi-Plateau Reaction Model for LiSi/FeS2 Batteries," in *47th Power Sources Conference*, Orlando, **2016**.

[63] D. Kim, H. Jung and S. Um, "Theoretical Analysis of the time-dependent temperature evolution for thermal runaway prevention in multi-layered LiCl-LiBr-LiF thermal batteries," *Journal of the Korean Physical Society,* vol. 55, pp. 2420-2426, **2009**.

[64] N. Eisenreich, T. S. Fischer, G. Langer, S. Kelzenberg and V. Weiser, "Burn rate models for gun propellants," *Propellants, Explosives, Pyrotechnics,* vol. 27, pp. 142-149, **2002**.

[65] G. Langer and N. Eisenreich, "Hot spots in energetic materials," *Propellants, Explosives, Pyrotechnics,* vol. 24, pp. 113-118, **1999**.

[66] A. Ambekar and J. J. Yoh, "A reduced order model for prediction of the burning rates of multicomponent pyrotechnic propellants," *Applied Thermal Engineering,* vol. 130, pp. 492-500, **2018**.

[67] J. A. Caballero and J. A. Conesa, "Mathematical considerations for nonisothermal kinetics in thermal decomposition," *Journal of Analytical and Applied Pyrolysis,* vol. 73, pp. 85-100, **2005**.

[68] S. Karpisz and S. Janas, Buoyancy force in mass measurement, Bracka: Radwag Balances and Scales.

[69] K. J. Laidler, "The Development of the Arrhenius Equation," *Journal of Chemical Education,* vol. 61, pp. 494-498, **1984**.

[70] B. L'vov, "Ups and downs in the theory of thermal decomposition of solids for 130 years," *Journal of Thermal Analysis and Calorimetry,* vol. 128, pp. 593-600, **2017**.

[71] J. Zawadski and S. Bretsznajder, "Some remarks on the mechanism of reaction of the type: solid = solid + gas," *Transactions of the Faraday Society,* vol. 34, **1938**.

[72] U. A. M. C. Headquarters, Engineering Design Handbook Military Pyrotechnic Series Part One: Theory and Application, Springfield, **1967**.

[73] L. Wachowski and B. Czajka, "Textural and catalytics properties of the FexOy/Fe-KClO4 system," *Thermochimica Acta,* no. 435, pp. 102-107, **2005**.

[74] A. A. Shidlovskiy, Principles of Pyrotechnics, American Fireworks News, **1997**.

[75] R. Furuichi, T. Ishii, Z. Yamanaka and M. Shimokawabe, "Sem observation of the thermal decomposition process of KClO4, KClO3, KBrO3, KIO4 and KIO3 in the presence of alpha-Fe2O3 and alpha-Al2O3," *Thermochimica Acta,* vol. 51, pp. 199-224, **1981**.

[76] A. M. El-Awad, "Catalytic Effect of Some Chromites on The Thermal Decomposition of KClO4," *Journal of Thermal Analysis and Calorimetry,* vol. 61, pp. 197-208, **2000**.

[77] T. R. Crompton, "High temperature thermally activated primary batteries," in *Battery Refence Book*, **2000**, pp. 1-13.

[78] P. Masset and R. A. Guidotti, "Thermal activated (thermal) battery technology Part II. Molten salt electrolytes," *Journal of Power Sources,* no. 164, pp. 397-414, **2007**.

[79] S. Vyazovkin, "Kinetic concepts of thermally stimulated reactions in solids: a view from a historical perspective," *International Reviews in Physical Chemistry,* vol. 19, no. 1, pp. 45-60, **2000**.

[80] V. Klasons and C. M. Lamb, "Thermal Batteries," in *Handbook of Batteries*, **2001**.

[81] R. A. Guidotti, J. Odinek and F. W. Reinhardt, "Characterization of Fe/KClO4 Heat Powders and Pellets," *Journal of Energetic Materials,* pp. 271-305, **2006**.

[82] B. Roduit, C. Borgeat, B. Berger, P. Folly, B. Alonso, J. N. Aebischer and F. Stoessel, "Advanced Kinetic Tools For the Evaluation of Decomposition Kinetics: Determination of thermal stability of energetic materials," *Journal of Thermal Analysis and Calorimetry,* vol. 80, pp. 229-236, **2005**.

[83] J. J. M. Órfão, "Review and evaluation of the approximations to the temperature integral," *American Institute of Chemical Engineers ,* vol. 53, no. 11, pp. 2905-2915, **2007**.

[84] T. Akahira and T. Sunose, "Method of determining activation deterioration constant of electrical insulating materials," *Res. Report Chiba Inst. Technol.,* vol. 16, pp. 22-31, **1971**.

[85] N. Sbirrazzuoli, Y. Girault and L. Elégant, "Simulations for evaluation of kinetic methods in differential scanning calorimetry. Part 3 - Peak maximum evolution methods and isoconversional methods," *Thermochimica Acta,* vol. 293, pp. 25-37, **1997**.

[86] C. Deng, J. Cai and L. Ronghou, "Kinetic analysis of solid-state reactions: Evaluation of approximations to temperature integral and their applications," *Solid state sciences,* vol. 11, pp. 1375-1379, **2009**.

[87] K. Madsen, H. Nielsen and O. Tingleff, *Methods for non-linear least squares problems,* Technical University of Denmark, **2004**.

[88] V. Kalender , "Characterization of electrolyte and pyrotechnic powders and pellets," Ankara, **2011**.

[89] J. Sestak and G. Berggren, "Study of the kinetic of the mechanism of solid-state reactions at increased temperature," *Thermochimica Acta,* vol. 3, pp. 1-12, **1971**.

[90] N. Bertrand, C. Desgranges, D. Poquillon, M. C. Lafont and D. Monceau, "Iron Oxidation at Low Temperature (260-500C) in Air and the Effect of Water Vapor," *Oxidation of Metals,* vol. 73, pp. 139-162, **2009**.

APPENDIX A – Characterization Results of Fe and KClO₄ Powders

mi micromeritics

Sample: DemirTozu129 9.11.07
Operator:
Submitter:
Bar Code:
File: C:\1340\DATA\DMTZ129.SMP

Density and Volume Table

Cycle#	Volume (cm³)	Volume Deviation (cm³)	Density (g/cm³)	Density Deviation (g/cm³)	Elapsed Time (mm:ss)	Temperature (°C)
1	2.0752	0.0004	7.8174	-0.0014	4:15	24.02
2	2.0672	-0.0076	7.8474	0.0286	5:19	24.05
3	2.0726	-0.0022	7.8271	0.0083	6:29	24.05
4	2.0718	-0.0030	7.8301	0.0113	7:40	24.07
5	2.0851	0.0103	7.7800	-0.0388	9:57	24.09
6	2.0740	-0.0009	7.8220	0.0032	11:11	24.11
7	2.0750	0.0002	7.8180	-0.0008	12:39	24.13
8	2.0718	-0.0030	7.8300	0.0112	13:50	24.14
9	2.0720	-0.0029	7.8295	0.0107	15:00	24.14
10	2.0834	0.0086	7.7863	-0.0324	17:05	24.18

Summary Data	Average	Standard Deviation
Volume:	2.0748 cm³	0.0052 cm³
Density:	7.8188 g/cm³	0.0196 g/cm³

Figure 64. Theoretical particle density result of Fe powder

Analysis date : 2018/04/12 10:55:54
Analyst   : aalkan

Meas. data:01_001-0000
Iron, Fe, 03-065-4899

Iron, Fe, 03-065-4899

Figure 65. XRD analysis of Fe Powder

MASTERSIZER 2000
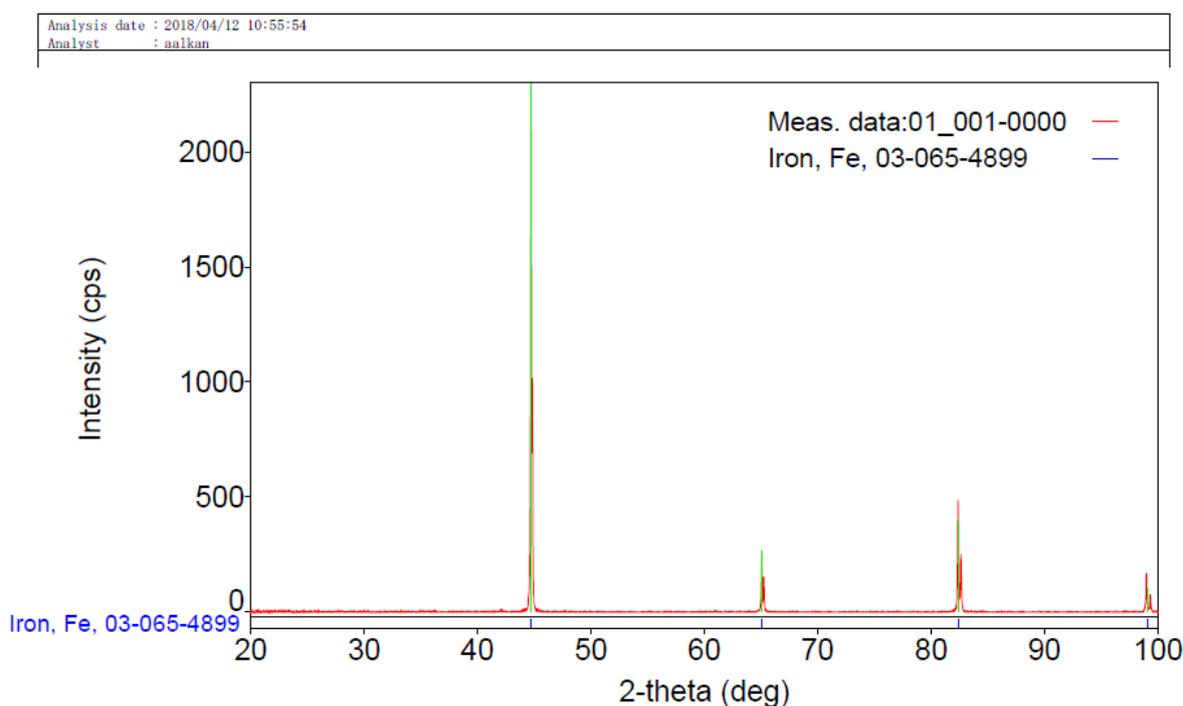
Result Analysis Report

Sample Name:
KCL04-045-0000 - Average

Sample Source & type:
Works = Isilpil

Sample bulk lot ref:
-

SOP Name:

Measured by:
fyavuz

Result Source:
Averaged

Measured:
24 Ocak 2018 Çarþamba 11:32:28

Analysed:
24 Ocak 2018 Çarþamba 11:32:29

Particle Name:
potasium per chlorate

Particle RI:
1.456

Dispersant Name:
Isoprophyl Alcohol

Accessory Name:
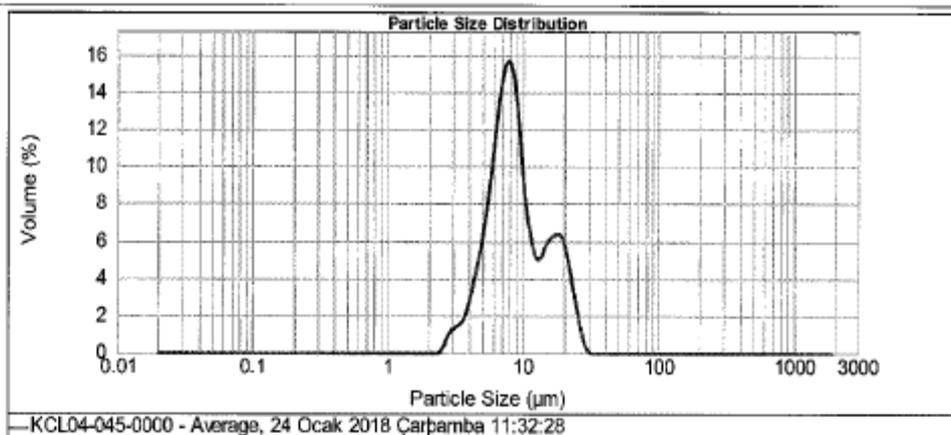Hydro 2000G (A)

Absorption:
0

Dispersant RI:
1.378

Analysis model:
Single narrow mode

Size range:
0.020 to 2000.000 um

Weighted Residual:
1.779 %

Sensitivity:
Enhanced

Obscuration:
13.13 %

Result Emulation:
Off

Concentration:
0.0125 %Vol

Specific Surface Area:
0.757 m²/g

Span:
1.640

Surface Weighted Mean D[3,2]:
7.925 um

Uniformity:
0.464

Vol. Weighted Mean D[4,3]:
10.043 um

Result units:
Volume

d(0.1): 4.964 um   d(0.5): 8.290 um   d(0.9): 18.556 um

KCL04-045-0000 - Average, 24 Ocak 2018 Çarþamba 11:32:28

Operator notes:

Figure 66. Particle size analysis result of $KClO_4$ particles

AccuPyc II 1340 V1.09   Unit 1   Serial #: 2862   Page 1

Sample: potasyum perklorat 046-0000
MB
Submitter:
Bar Code:
File: G:\124.SMP

Analysis Gas: Helium
Reported: 29.03.2018 17:15:36
Sample Mass: 4.0550 g
Temperature: 21.40 °C
Number of Purges: 20
Chamber Insert: 10 cm³

Analysis Start: 29.03.2018 16:52:13
Analysis End: 29.03.2018 17:15:28
Equilib. Rate: 0.005 psig/min
Expansion Volume: 73.9780 cm³
Cell Volume: 15.4046 cm³

Summary Report
Sample Volume
Average: 1.6038 cm³
Standard Deviation: 0.0018 cm³

Sample Density
Average: 2.5284 g/cm³
Standard Deviation: 0.0029 g/cm³

Figure 67. Theoretical particle density result of KClO₄ powder

	Spec. Values	
Assay (alkalimetric)	99.5 - 100.5	%
Insoluble matter	≤ 0.005	%
pH-value (1 %; water)	5.0 - 7.0	
Chloride (Cl)	≤ 0.003	%
Sulfate (SO₄)	≤ 0.001	%
Total nitrogen (N)	≤ 0.0005	%
Heavy metals (as Pb)	≤ 0.0005	%
Ca (Calcium)	≤ 0.005	%
Fe (Iron)	≤ 0.0005	%
Na (Sodium)	≤ 0.005	%

Corresponds to ACS

Figure 68. CoA of obtained KClO₄

APPENDIX B – Sample Calculations

Sample Calculation of Average Theoretical Density of Heat Pellets

Calculation was performed for 84/16 heat pellet:

$$\frac{100}{\frac{16}{2.54 \ g/cm^3} + \frac{84}{7.85 \ g/cm^3}} = 5.88 \ g/cm^3$$

Sample Calculation of Height of 84/16 Heat Pellet

$$\frac{d_{pellet}}{5.88 \ g/cm^3} \times 100\% = 57.5\%$$

$$d_{pellet} = 3.38 \ g/cm^3$$

$$d_{pellet} = \frac{3.92 \ g}{(\pi R_o^2 - \pi R_i^2)h_{pellet}}$$

$$h_{pellet} = 0.059 \ cm$$

APPENDIX C - Matlab Code for the Transformation of Thermal Analysis Raw Data

area.m Script

```
% Ham veri A adıyla tanımlanır. Ham verideki fazla veriler atıldıktan sonra
% A1 olarak adlandırılır.
% A1'in ilk kolonu sıcaklık verisi, ikinci kolonu
% ısı akısı verisi olmalıdır.
% bf fonksiyonu ham veriye baseline çekmek için kullanılır.
[y1,yfit]=bf(A1(:,2),'confirm',6);
figure(1);
% baseline düzeltmesi yapılmış verinin sıcaklığa karşı çizilmesi
plot(A1(:,1),y1);

% Figür üzerinden işaretleme ve iki nokta
% arası doğru oluşturma kodu
% [x,y]=ginput(2); line(x,y);

% Baseline noktaları girilecek
prompt1='x(1) değerini girin (sayının yuvarlanmadığına emin ol):';
x(1)=input(prompt1);
prompt3='y(1) değerini girin (sayının yuvarlanmadığına emin ol):';
y(1)=input(prompt3);
prompt2='x(2) değerini girin (sayının yuvarlanmadığına emin ol):';
x(2)=input(prompt2);
prompt4='y(2) değerini girin (sayının yuvarlanmadığına emin ol):';
y(2)=input(prompt4);
```

```matlab
% Girilen x ve y noktaları arasında N kadar bölme işlemi
N = 10001;
x_fine = linspace(x(1), x(2),N);
dx=x_fine(2)-x_fine(1);

% Bölünen noktaları interpolasyon ile birleştirme
% top heat flow eğrisi
% bottom baseline doğrusu
top = interp1(A1(:,1),y1,x_fine);
bottom = interp1(x,y,x_fine);

%Eğrinin altında kalan toplam alanın hesaplanması
totalarea = dx*trapz(top-bottom);

% Hesaplanan alanın taranarak gösterilmesi
figure(2);
patch([x_fine fliplr(x_fine)],[top fliplr(bottom)], 'r');

% N tane fraksiyon için ayrı ayrı eğrinin altında kalan alanın
% hesaplanması


%Baseline fonksiyonunun tanımlanması
x=x';y=y';
Baselinefit = fit(x,y,'poly1');
Coeff = coeffvalues(Baselinefit);
Bfunction = @(x) Coeff(1)*x+Coeff(2);

% Baseline'ın başladığı ve bittiği veri noktasının işaretlenmesi
for i=1:1:length(A1)
    if A1(i,1) == x(1)
    Tinitial = i;
    end
    if A1(i,1) == x(2)
    Tfinal = i;
    end
end

% fBottom için vektör oluşturulması
controlmatrix = zeros(Tfinal-Tinitial,1);
for n=Tinitial:1:Tfinal
    controlmatrix(n-Tinitial+1,1)= A1(n,1);
end

% Sıcaklık aralığının hesaplanması
Ti= x(2)-x(1);

% Data noktası sayısı
NT=Tfinal-Tinitial;

%dT
dT=Ti/NT;

fTop = zeros(NT,1);
fBottom =zeros(NT,1);

for m= Tinitial:1:Tfinal-1
    %linspace yerine interp1'de kullanılabilir
```

123

```matlab
    fTop((2*(m-Tinitial+1))-1:(2*(m-Tinitial+1)),1)                      = ...
linspace(y1(Tinitial,1),y1(m+1,1),2);
    fBottom((2*(m-Tinitial+1))-1:(2*(m-Tinitial+1)),1)                   = ...
linspace((Bfunction(controlmatrix(1))),(Bfunction(controlmatrix(m-
Tinitial+2))),2);
    fArea(m-Tinitial+1,1) = dT*trapz(fTop-fBottom);
    Conversion (m-Tinitial+1)=fArea(m-Tinitial+1)/totalarea;


end


Conversion = Conversion';
figure(3);
[n,m]=size(controlmatrix);
controlmatrix=controlmatrix(1:n-1,1);
plot(controlmatrix(:,1),Conversion(:,1))
```

bf.m Script

```matlab
function [ycorr,yfit] = bf(y,varargin)
def_method  = 'spline';
def_avgpts  = 3;


method = [];
avgpts = [];
pts    = [];
confirm = false;
for n = 2:nargin,
    f = varargin{n-1};
    if ischar(f),
        if strcmpi(f,'confirm'),
            confirm = true;
        else
            method = f;
        end
    elseif isnumeric(f) && numel(f) == 1,
        avgpts = f;
    elseif isnumeric(f) && numel(f) > 1,
        pts = f;
    elseif isempty(f),
        continue
    else
        error ('  Invalid input argument!')
    end
end
if isempty(method),    method = def_method;        end
if isempty(avgpts),    avgpts = def_avgpts;        end
dimy = size(y);
lst = dimy(1);
newdimy = [dimy(1),prod(dimy(2:end))];
y = reshape(y,newdimy);
x = 1:lst;
if isempty(pts),
    interactive = true;
else
    interactive = false;
end
if interactive || confirm,
    bffig = figure;
else
```

```matlab
        bffig = 0;
end
ok = false;
while ~ok,
    if interactive,
        plot(x,real(y(:,1)))
        set(bffig,'Name','Baseline Fit - Select points')
        fprintf(['\n  Now  select  baseline  points  to  fit  by  positioning
cursor,',...
            '\n   and selecting points with mouse button or key press.',...
            '\n Press Enter key when done.\n'])
        [a,b] = ginput;                             %#ok
        pts = round(a.');
    end
    pts = sort(pts);
    pts(diff(pts)==0) = [];          % delete duplicate points
    if pts(1)~=1,       pts = [1,pts];           end     %#ok
    if pts(end)~=lst,   pts = [pts,lst];         end     %#ok
    npts = numel(pts);
    pss = zeros(npts,2);
    pss(:,1) = pts - floor(avgpts/2);
    pss(:,2) = pss(:,1) + avgpts;
    pss(pss < 1) = 1;
    pss(pss > lst) = lst;
    yavg = zeros([npts,newdimy(2)]);
    for n = 1:npts,
        yavg(n,:) = mean(y(pss(n,1):pss(n,2),:),1);
    end
    yfit = interp1(pts,yavg,x,method);
    if size(yfit,1) ==1,
        yfit = shiftdim(yfit,1);     % make yfit a column if it is a row
vector
    end
    if confirm,
        interactive = true;
        figure(bffig)

plot(x,real(y(:,1)),'b',x,real(yfit(:,1)),'r',pts,real(yavg(:,1)),'ob')
        set(bffig,'Name','Baseline Fit - Verify baseline')
        answer = input('  Do you want to redo fit and reselect baseline
points?[N] ','s');
        if isempty(answer),     answer = 'n';    end
        if strcmpi(answer,'y'),
            ok = false;
        else
            ok = true;
        end
    else
        ok = true;
    end
end
if any(findobj('Type','figure')==bffig),
    close(bffig),                    % close figure if it exists
end
ycorr = y - yfit;
ycorr = reshape(ycorr,dimy);
yfit = reshape(yfit,dimy);
```

APPENDIX D – Results of Repeatability Analysis

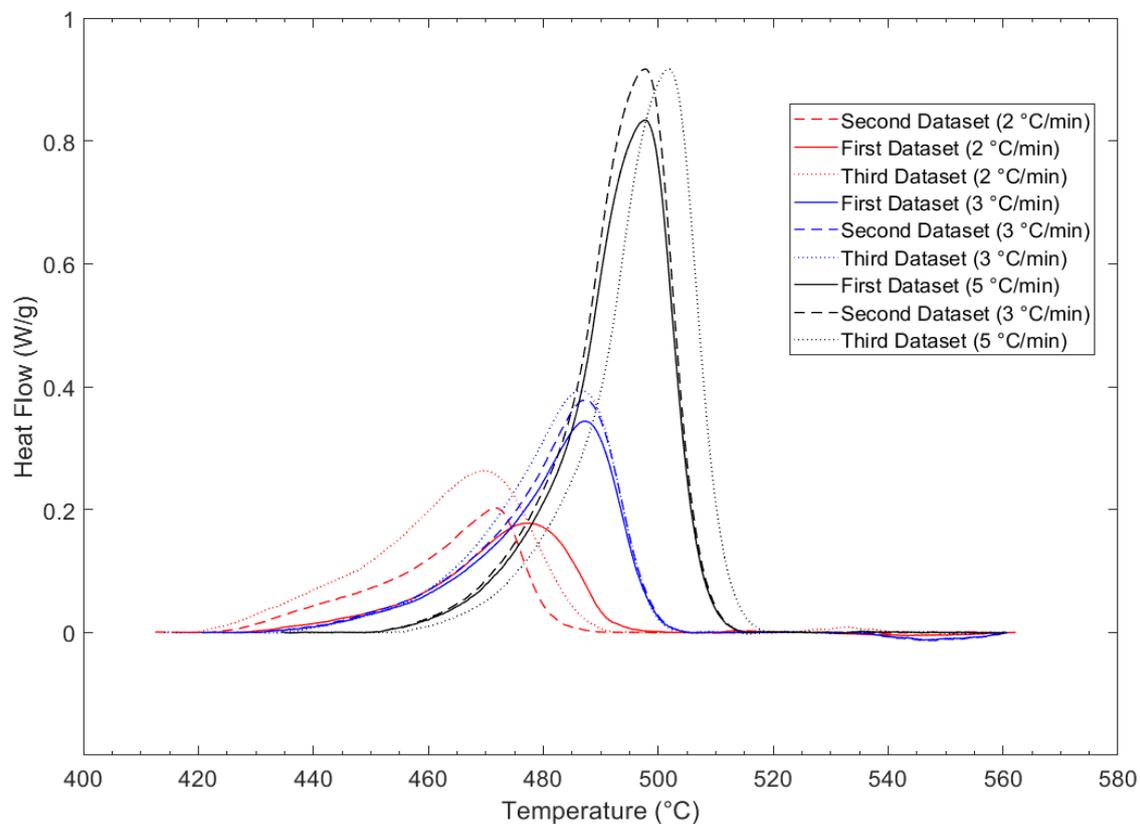*Repeatability Analysis Result for 84/16 (w:w) Heat Pellet:*

Figure 69. Repeatability of heat flow data for 84/16 heat pellet thermal decomposition
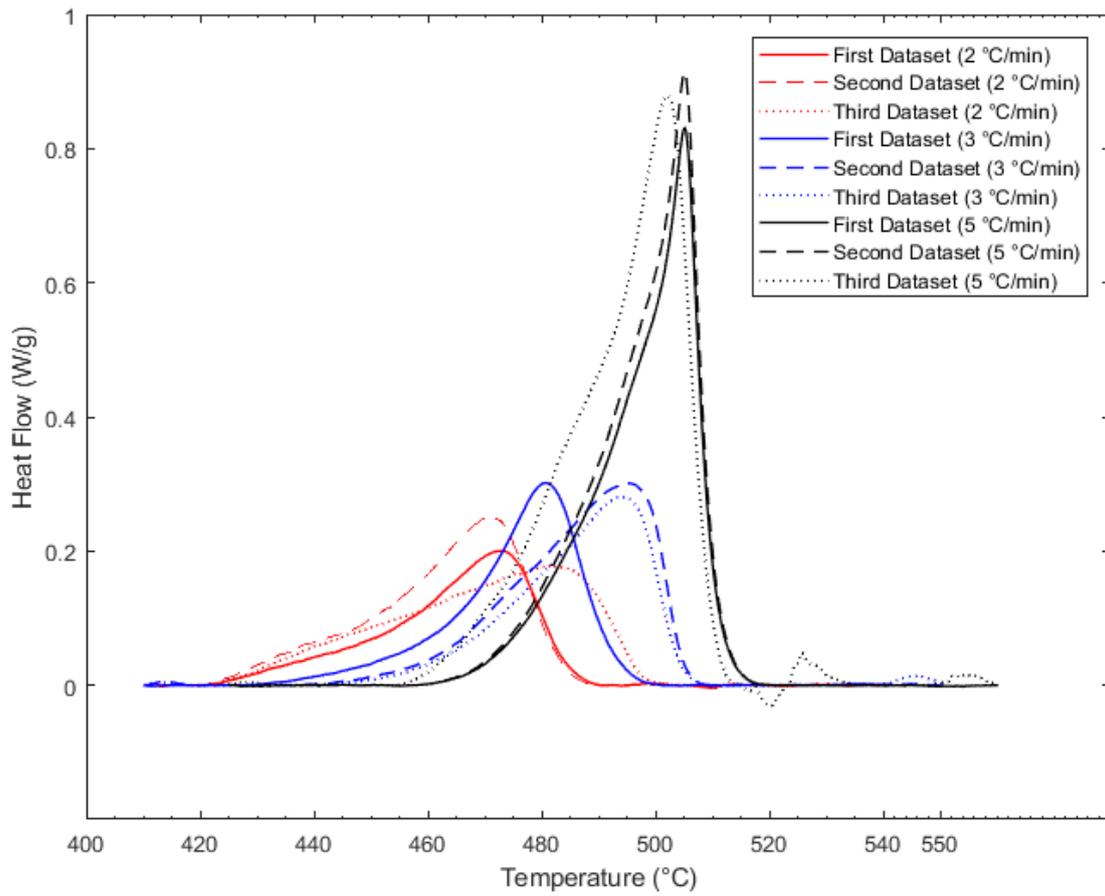
Figure 70. Repeatability of heat flow data for 86/14 heat pellet thermal decomposition
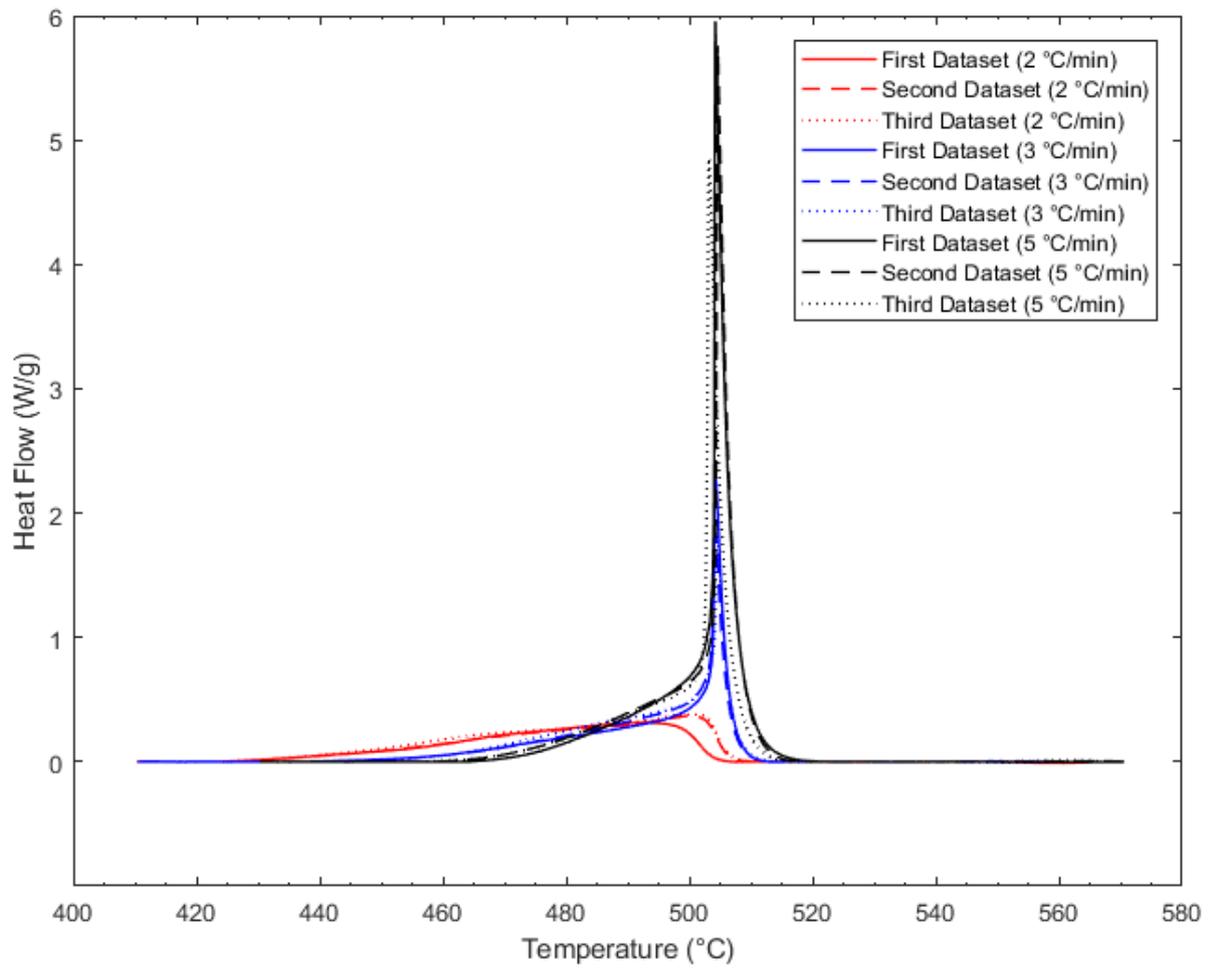
Figure 71. Repeatability of heat flow data for 88/12 heat pellet thermal decomposition

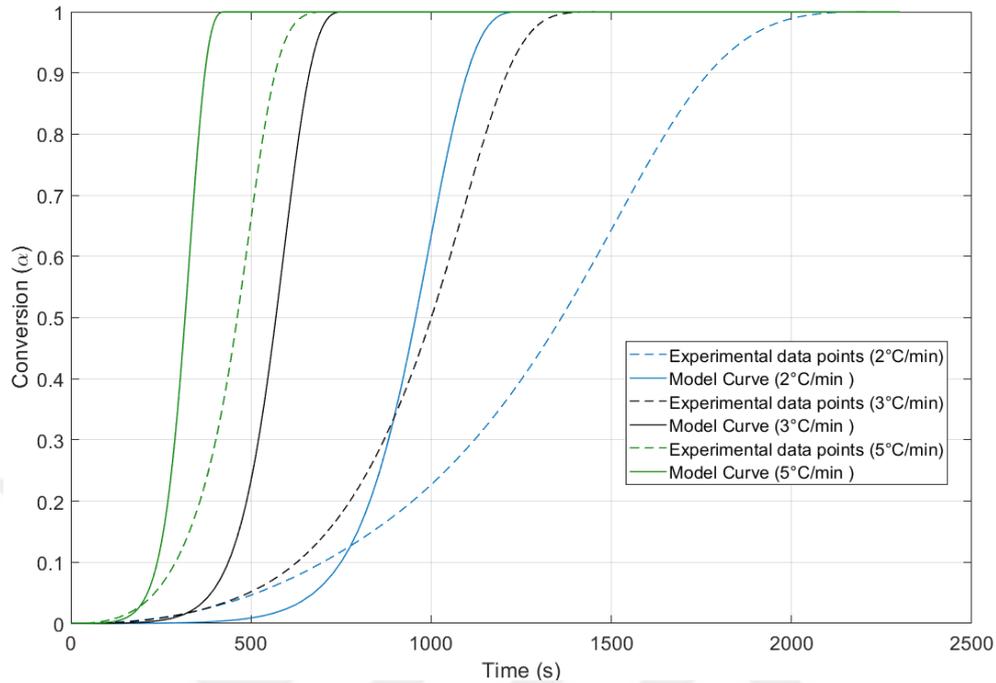## APPENDIX E – Comparison of Model and Experimental Conversion Curves

Figure 72. Comparison between time (s) vs. conversion (α) model curve and experimental data for 84/16 (w:w) heat pellet
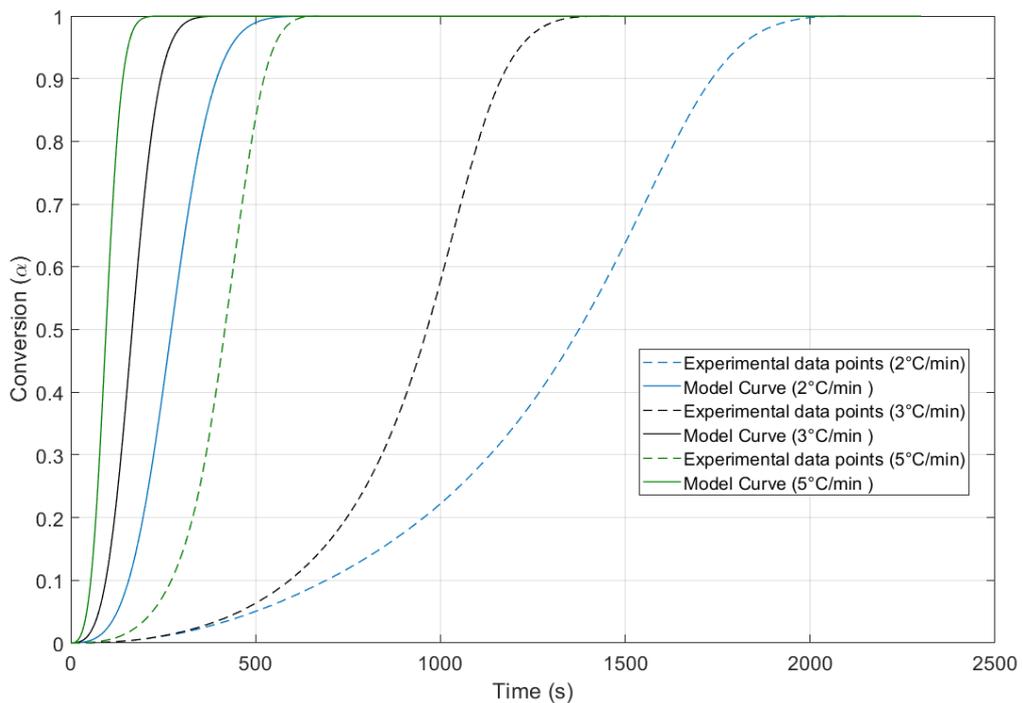

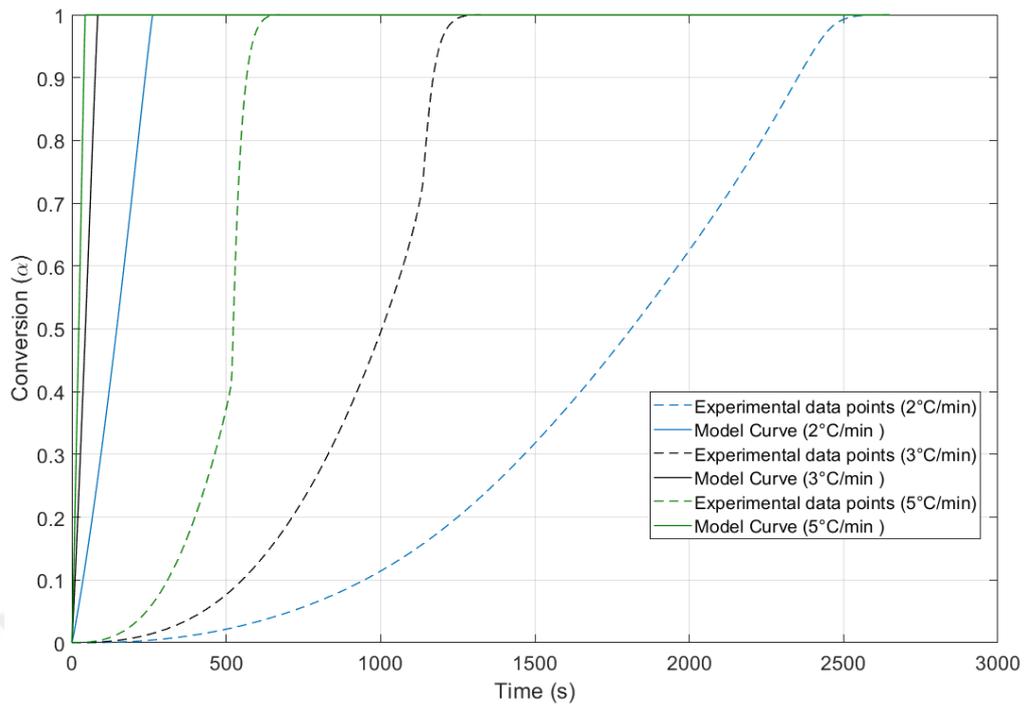**Figure 73. Comparison between time (s) vs. conversion (α) model curve and experimental data for 86/14 (w:w) heat pellet**

Figure 74. Comparison between time (s) vs. conversion (α) model curve and experimental data for 88/12 (w:w) heat pellet

CURRICULUM VITAE

Credentials

Name, Surname : Anıl Alkan

Place of Birth : YENİMAHALLE/ANKARA

Marital Status : Married

E-mail : anil.alkan@tubitak.gov.tr

Address : Ata Mah. Lizbon Cad. 79/15 Çankaya/ANKARA

Education

- **High School :** Gölbaşı Anatolian High School
- **BSc. :** Hacettepe University Chemical Engineering
- **MSc. :** Hacettepe University Chemical Engineering

Foreign Languages

- **English :** YDS – 91,25/100

Work Experience

- The Scientific and Technological Research Council of Turkey (TÜBİTAK) Defense Industries Research and Development Institute (SAGE) – Research Engineer (10.08.2015 – ongoing)

Areas of Experiences

- Thermal batteries, simulation and modelling, material characterization, kinetic analysis, non-linear optimization, thermal analysis, electrochemical analysis.

Projects and Budgets

-

Publication

-

Oral and Poster Presentations

-

HACETTEPE UNIVERSITY
GRADUATE SCHOOL OF SCIENCE AND ENGINEERING
THESIS/DISSERTATION ORIGINALITY REPORT

Date: 11/06/2018

Thesis Title / Topic: DETERMINATION OF THERMAL DECOMPOSITION KINETICS FOR Fe/KClO$_4$ BINARY MIXTURES UTILIZING ANALYTICAL AND NUMERICAL METHODS

According to the originality report obtained by myself/my thesis advisor by using the *Turnitin* plagiarism detection software and by applying the filtering options stated below on 29/05/2018 for the total of 109 pages including the a) Title Page, b) Introduction, c) Main Chapters, d) Conclusion sections of my thesis entitled as above, the similarity index of my thesis is 9 %.

Filtering options applied:
1. Bibliography/Works Cited excluded
2. Quotes included
3. Match size up to 5 words excluded

I declare that I have carefully read Hacettepe University Graduate School of Sciene and Engineering Guidelines for Obtaining and Using Thesis Originality Reports; that according to the maximum similarity index values specified in the Guidelines, my thesis does not include any form of plagiarism; that in any future detection of possible infringement of the regulations I accept all legal responsibility; and that all the information I have provided is correct to the best of my knowledge.

I respectfully submit this for approval.

11.06.2018

Date and Signature

Name Surname:	ANIL ALKAN
Student No:	N14121028
Department:	Chemical Engineering
Program:	Masters with Thesis
Status:	☒ Masters ☐ Ph.D. ☐ Integrated Ph.D.

ADVISOR APPROVAL

APPROVED.

_____
(Title, Name Surname, Signature)

Prof. Dr. Selma Mutlu